The Thesis Committee for Jeffrey Robert Stewart

Certifies that this is the approved version of the following thesis:

Pipe Fractional Flow through Branching Conduits

APPROVED BY

SUPERVISING COMMITTEE:

Supervisor:

Mukul M. Sharma

Anand S. Nagoo

Pipe Fractional Flow

through Branching Conduits

by

Jeffrey Robert Stewart, B.S.

Thesis

Presented to the Faculty of the Graduate School of

The University of Texas at Austin

in Partial Fulfillment

of the Requirements

for the Degree of

Master of Science in Engineering

The University of Texas at Austin

August 2015

Dedication

To my late grandfather O. Phillip Kent.

Acknowledgements

First, I would like to thank Dr. Mukul M. Sharma and Dr. Anand S. Nagoo for their guidance and mentorship over the past two years. In addition to this work, I can say confidently that I have also gained a solid fundamental knowledge in multiphase flow and scientific computing. Their guidance is also greatly appreciated in matters outside of this academic pursuit. I have learned a great deal about professionalism, especially in a research and industry setting.

Additionally, I would like to extend my sincere gratitude to the members of the Joint Industry Project (JIP) on Hydraulic Fracturing and Sand Control for their financial support and technical suggestions. Having industry experts' insights into my project helped to keep this work relevant and applicable to industry.

Finally, I would like to thank my colleagues, family and friends. Eric, Manolis, Hisanao, Scott, Ruth, Roy, Wynn, Michael, Jake, Andrew, Juan Diego, Caesar and the others I have failed to mention, thank you. I would like to extend a heartfelt thank you to my parents, Richard and Carol, my brother and his partner, Ben and Chris, and my grandmother Marjorie, for their continued support in my education.

August 2015

Abstract

Pipe Fractional Flow

through Branching Conduits

Jeffrey Robert Stewart, M.S.E.

The University of Texas at Austin, 2015

Supervisor: Mukul M. Sharma

In the field of multiphase flow, the so-called phase splitting problem is a recurrent topic of discussion. In a branching conduit, it is of practical importance to know *a priori* how the phases split. Over the years, a variety of models have been developed to predict this and describe the physics involved. Despite this wealth of knowledge, little connection has been made between this question and fluid flow in networks. How phases split is determined by the system of equations solved, and no physics is incorporated to determine the phase split.

To address this issue, a novel formulation of a multiphase network has been devised and validated against data and existing solutions, as well as compared to existing software. Additionally, current phase-splitting models have been discussed and compared. A new phase-splitting model based on a conservation-of-momentum approach is discussed and compared to branched-flow data. In building and validating this new model, a database of

branched-flow experiments containing over 5000 data points from multiple laboratories has been gathered and systematized. This model has been incorporated into the existing network model to serve as additional equations when boundary conditions are unknown, and also to validate solutions found by the solver to ensure it is feasible.

From this study, it was found that some current network solvers commercially available can arrive at inaccurate solutions. Moreover, such solvers can use an unorthodox approach to solve network problems and does not explicitly solve for Kirchhoff's laws. This issue is compounded by solution non-uniqueness—especially in networks with a high degree of looping. It is shown here that convergence is largely dependent on the initial guess. The phase splitting equation developed shows the degree of phase splitting at a junction varies primarily with branch configuration, pressure, void fraction, and flow rate. Current phase-splitting equations tend to exaggerate the phase split at a branch. In order to obtain the most exaggerated phase split, a vertical side-branch orientation should be used with a high mass takeoff.

Table of Contents

List of Tables

List of Figures

Chapter 1: Introduction

1.1 Research Motivation

Multiphase flow is a central topic in petroleum engineering. In production engineering, wells that produce below the bubble point exhibit complex behavior. A functioning model of the vertical lift performance is needed to describe the production behavior of a well. Additionally, such models are needed in surface facilities to design new installations, as well as monitor existing ones. These models must be robust as input parameters can vary widely. High pressures and flow rates can be observed during initial production, and low pressures and flow rates can be seen after reservoir decline. Other effects such as water cut, GOR, and inclination can combine to create discontinuities that are difficult to predict. Such a model has been formulated in previous works, and opportunities to expand on this have been explored in this work.

One pertinent subtopic in the field of multiphase flow is flow in pipe networks. While pipe networks are commonly encountered in the oil and gas industry, their applications are even more common outside of industry. The chemical process industry, nuclear industry, and water treatment industries are just a few that rely on network simulators to characterize the flow conditions in a network. For example, recycle streams in the process industry are often used, which require an iterative approach to solve as the mass balances are implicitly defined.

This requires a workflow that can solve the system of equations that are manifest in the often complex topology of the network. Elements from graph theory are necessary

to convert the set of pipes and intersections into a well-defined set of equations. Next, the system of equations needs to be solved so that all equations are satisfied. Finally, the solution needs to be vetted. It is common knowledge that the solution of a system of nonlinear equations is dependent on the initial guess, so an adequate initial guess is necessary to arrive at the correct solution. Many methods to solve such non-linear problems and to help validate the solution have been explored as well.

Despite the complexity in multiphase networks, little thought has been put into the physics of phase splitting at an intersection in networks. Indeed, as quoted by Dr. Lahey, "Experienced engineers have developed the attitude that the only way to analyze the division is to avoid it" (Lemonnier & Hervieu, Theoretical modelling and experimental investigation of single-phase and two-phase flow division at a tee-junction, 1991). Nonetheless, the field of branched flow in multiphase flow has been extensively studied, but outside the context of fluid flow in networks. The motivation for these studies is often in loss-of-coolant accidents in nuclear reactors, where the phase split needs to be known *a priori*, or in branched pipes that are often used as economical separators. Here, the lighter phase is preferentially split into the branch from the main pipe. To address these issues, researchers have developed a sundry of models to describe the phase-splitting behavior. These range from empirical, mechanistic, phenomenological (flow regime), and probabilistic models. In the context of multiphase fluid networks, these models can fall short of the rigor necessary, as the input parameters often fall outside of the range characterized by the model. Despite the disconnect between the fields of network fluid flow and branched flow, the same physics that describes the phase split in loss-of-coolant

accidents and in branched pipes is the same physics present at pipe intersection in a network. Hence, combining the two fields can be beneficial to network models. If one boundary condition is unknown for a given network, one phase splitting equation can be added to compensate. Also, a phase-splitting equation can be used to further validate solutions to network simulations. Currently, phase splitting in networks is determined implicitly via the mathematical satisfaction of system of equations of mass and momentum balances and auxiliary equations. If the phase split at an intersection calculated from a network simulator differs significantly from the phase split determined by the phase splitting equation, this could be a sign of a non-unique solution that is not the true, physical solution of the problem at hand.

1.2 Research Objectives

In light of the issues discussed above, there were three main objectives in this study:

1. Develop a workflow to describe the network in a mathematical context.
2. Characterize the system of equations necessary to make the network simulation well posed.
3. Develop a numerical method to satisfy the system of equations posed by the network simulation.
4. Develop a phase splitting model that can be used in network simulations.

1.3 Review of Chapters

Chapter 1 introduces the topics discussed in this study. Chapter 2 gives a review of the current state of the art in multiphase fluid networks and in multiphase flow bifurcation. The

related models are described in earnest and branched flow experimental data is described in this chapter. Chapter 3 develops the formulation in the multiphase network solver developed in this work. Chapter 4 presents the validation of the network solver with published data and solution sets, as well as comparisons to existing commercial simulators. Chapter 5 presents the development and motivation of the phase-splitting model in this work and compares it to existing data. Chapter 6 gives the conclusions and suggests for future work on this topic.

Chapter 2: Literature Review

This chapter presents all relevant background information that forms the foundation of this work, as well as presenting other models that have traditionally been used to solve for flow in pipe networks, as well as describing phase splitting at a pipe branch.

2.1 GRAPH THEORY

Before looking into the numerical methods used to solve for fluid flow in pipe networks, it is important to understand how one can efficiently describe a pipe network in a systematic mathematical description. Any network can be described by a *graph*, which is comprised of a combination of *branches* and *nodes*. A *directed graph* is a graph whose branches have a directionality associated with them. A directed graph can be mathematically described using an adjacency matrix, where each column represents a branch in the graph, and each row represents a node in the graph. An entry of -1 indicates that the branch is directed away from the node, and an entry of 1 indicates the branch is directed towards the node.

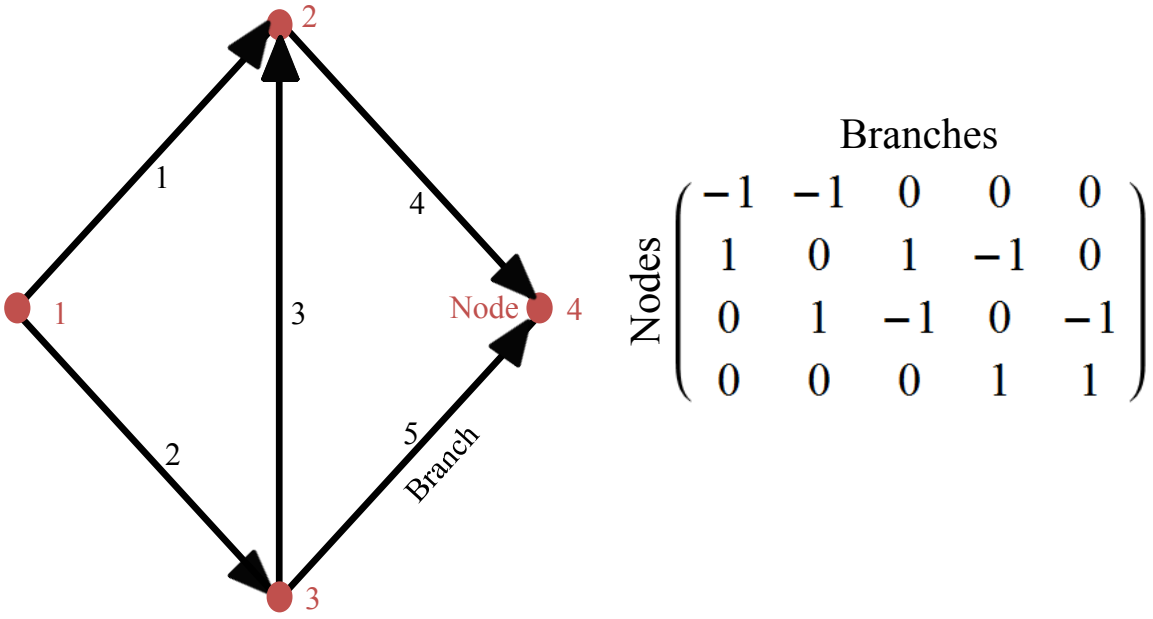

Figure 2.1: Example of a directed graph and its corresponding incidence matrix

Figure 2.1 shows the translation from a directed graph to an incidence matrix. From it, one can quickly determine where each branch originates and terminates, and which nodes are connected to which branches. Each row also conveniently represents each mass balance equation in a given network.

2.2 Network Analysis

As in electrical circuits, the two main physical laws that govern fluid flow in pipe networks are Kirchhoff's first and second laws; also known as Kirchhoff's node and loop laws, respectively (Nagoo A. S., 2003). Kirchhoff's first law states that the sum of the flow rates at a node is zero (mass is conserved), and Kirchhoff's second law states that the sum of the pressure changes around a loop is zero (each node has only one pressure). For these laws, it can be shown that there are $N_n - 1$ mass balance equations, and $N_b - N_n + 1$ loop

equations. There are only $N_n - 1$ linearly independent mass balance equations because an overall mass balance can be applied to the entire network (Dolan & Aldous, 1993). There are $N_b - N_n + 1$ loop equations as this is the number of independent loops in any given graph (Dolan & Aldous, 1993). A simple way to explain this is that in a tree (a graph with no loops), there are $N_n - 1$ branches ($N_b = N_n - 1$). With the addition of another branch to the graph, there will be one loop formed. Hence, each additional branch over $N_n - 1$ represents one loop ($N_b = N_n - 1 + N_\ell \rightarrow N_\ell = N_b - N_n + 1$). For a more rigorous proof, see *Networks and Algorithms* by Dolan and Aldous (Dolan & Aldous, 1993).

Given these two laws, a certain number of input parameters need to be known *a priori* in order to have the problem be well-posed. While other network problems exist, especially when designing pipe networks where there are additional variables like pipe diameter and length, this work focuses on networks where the only unknowns are pressures, and each phase's flow rate. In this case, $N_p N_n + 1$ boundary conditions need to be specified, where N_p is the number of phases, N_n is the number of nodes. This will be shown later in the analysis of primary dependent variables and independent equations in Chapter 3.

2.3 MULTIPHASE NETWORK SOLVERS

2.3.1 Hardy Cross Method

The oldest and most widely used method for analyzing pipe networks is the Hardy Cross method (Jeppson, 1976). In the pre-computer age, the Hardy Cross method offered

the advantage that each equation could be solved individually instead of simultaneously with all other equations. While this was an advantage in the absence of computers, the Hardy Cross method converges much slower than other methods.

The Hardy Cross method is based on the Newton-Raphson method. For an equation $\boldsymbol{F}$, a Taylor series can be expanded around a point x such that:

$$\mathbf{0} = \boldsymbol{F}(\boldsymbol{x}) = \boldsymbol{F}(\boldsymbol{x^m}) + (\boldsymbol{x} - \boldsymbol{x^m})\boldsymbol{F'}(\boldsymbol{x^m}) + (\boldsymbol{x} - \mathbf{x^m})^{\mathbf{2}}\frac{\mathbf{F''(\xi)}}{\mathbf{2}} + \cdots \qquad (2.1)$$

where $\boldsymbol{F}$ is a continuous, differentiable function being satisfied, m is the iteration number, x is the variable being solved, and ξ is a value which lies between x and x^m. The Newton-Raphson method truncates equation (2.1) after the linear term. This leads to a numerical error that is proportional to the square of the error in the previous iteration. Rearranging the remaining terms in (2.1) and solving for x:

$$x^{m+1} = x^m - \alpha\frac{F(x^m)}{F'(x^m)} \qquad (2.2)$$

where the step size, α, has been included and is unity for the traditional Newton-Raphson method. The above equation can then be used iteratively such that $F(x^m) \to 0$. The Hardy Cross method uses this equation, where $F = \sum_l K_b Q_b^n$, and K_b is the hydraulic resistance, Q_b is the volumetric flowrate, n is an exponent which depends upon the frictional loss term decided (2 for Darcy-Weisbach, and 1.852 for Hazen-Williams), and the summation is for all pipes around one loop, and hence is satisfying Kirchhoff's second law. Also, instead of solving for Q, The Hardy Cross method solves for ΔQ, which is a correction applied to the previous iteration's flow rate. Hence, $\Delta Q \to 0$ as $F \to 0$. Consequently, equation (2.2) reduces to:

$$\Delta Q = -\frac{F_l}{\frac{dF_l}{d\Delta Q}} = -\frac{\sum_l K_b Q_b^n}{n\sum_l |K_b Q_b^{n-1}|} = -\frac{\sum_l h_f}{n\sum_l |\frac{h_f}{Q_b}|} \quad (2.3)$$

Using equation (2.3), one can arrive at the proper flow rates necessary to satisfy Kirchhoff's laws. The following steps are implemented:

1. An initial guess is chosen for all flow rates in the network, and all hydraulic resistances are determined. Note that the initial guesses must satisfy the mass balances at each node.
2. Compute the sum of the head loss in the first loop, and calculate $-\frac{\sum_l h_f}{n_i \sum_l |\frac{h_f}{Q_i}|}$.
3. Repeat step 2 for all loops.
4. Repeat steps 2 and 3 until all ΔQs are arbitrarily small.

2.3.2 Linear Theory Method (LTM)

LTM is a quasi-Newton method that offers many advantages over the Hardy Cross method. It takes less iterations to arrive at a solution, and it requires no initialization (Wood & Charles, 1972). To do this, LTM linearizes the nonlinear Kirchhoff's second law equations using the following transformation:

$$K'_{b,i} = K_b Q_{b,i-1}^{n-1} \quad (2.4)$$

Where K_i is the hydraulic resistivity, Q is the volumetric flow rate, n is the exponent, j is the iteration number, and K'_j is the modified hydraulic resistivity. From this relationship, the pressure drop can be related to the flow rate by:

$$\Delta P_{b,i} = K'_{b,i} Q_{b,i} \quad (2.5)$$

where $\Delta P_{b,i}$ is the pressure drop in branch b for iteration i. For the first iteration, $Q_{i,j-1}^{n-1} = 1$. Next iterations then depend upon the previous iteration's flow rate for computation. To set up a well-posed system of equations, the ℓ loop equations are combined with $n-1$ node equations. This yields the same number of independent equations as unknowns.

Number of unknowns	Unknown	Description
N_b	ΔP_b	Pressure drop in branch
N_n	P_n	Pressure at node
N_b	u_b	Velocity in branch
N_b	ρ_b	Density in branch
$\boldsymbol{3N_b + N_n}$		**Total**

Table 2.1: Primary dependent variables in a single-phase network

Number of equations	Equation	Description
$N_n - 1 = N_b - N_\ell$	$\sum_{b=1}^{b_{adj,n}} dir_b \rho_b u_b A_b = \dot{m}$	Mass Balance around node, where $b_{adj,n} \subset b \mid b\ adjacent\ to\ n$
N_b	$\frac{\Delta P_b}{\Delta L} = \frac{f_d \rho_b u_b^2}{2D_H} + \rho_b g sin(\theta)$	Momentum balance
N_ℓ	$\sum \Delta P_{loop} = 0$	Kirchhoff's second law
N_b	$\rho_b = f(P,T)$	EOS density calculation
$N_b - N_\ell$	$\Delta P_b = P_n - P_{(n-1)}$	Definition of pressure drop
1	$P_n = constant$	Pressure boundary condition
$\boldsymbol{3N_b + N_n}$		**Total**

Table 2.2: Independent equations in a single-phase network

From the formulation given in Table 2.1 and Table 2.2, a $N_b \times N_b$ matrix can be constructed, where the first $N_n - 1$ rows comprise the mass balance constraints at each node, and the last N_ℓ equations are the loop equations (Kirchhoff's second law). It should be noted that one variable needs to be specified, which in LTM is typically the pressure at a node. After this matrix has been constructed, a simple linear system $\boldsymbol{Ax = b}$ can then be

solved. $\boldsymbol{A}$ is the $b \times b$ matrix described above, $\boldsymbol{x}$ is the vector of pressure drops in each branch, and $\boldsymbol{b}$ is a vector comprised of the constants to satisfy Kirchhoff's laws (e.g., the first $N_n - 1$ entries are the external demands at the node, and the last $N_b - N_n + 1$ entries are to satisfy the loop equations). To illustrate this, the linear system of equations that would characterize the LTM approach to solving the graph in Figure 2.1 would be:

$$\begin{pmatrix} -K_1' & -K_2' & 0 & 0 & 0 \\ K_1' & 0 & K_3' & -K_4' & 0 \\ 0 & K_2' & -K_3' & 0 & -K_5' \\ 1 & -1 & -1 & 0 & 0 \\ 0 & 0 & 1 & 1 & -1 \end{pmatrix} \begin{pmatrix} \Delta P_1 \\ \Delta P_2 \\ \Delta P_3 \\ \Delta P_4 \\ \Delta P_5 \end{pmatrix} = \begin{pmatrix} Q_{n=1} \\ Q_{n=2} \\ Q_{n=3} \\ 0 \\ 0 \end{pmatrix} \tag{2.6}$$

where the first three rows are the mass balance relationships for nodes 1-3, and the last two rows are the loop equations for the two independent loops in the graph (comprised of branches 1, 2 and 3, and branches 3, 4 and 5). More information on the formulation of the loop equations is presented in Chapter 3. In order to arrive a solution, the following steps are followed:

1. Equation (2.6) is solved for $\Delta \boldsymbol{P_{b,i}}$ (the pressure drops).
2. Equation (2.5) is solved for $\boldsymbol{Q_{b,i}}$.
3. Equation (2.4) is solved for $K_{b,i}'$ using the new values of $\boldsymbol{Q_{b,i}}$ and $\boldsymbol{K_b}$.
4. Equation (2.6) is solved, and the above steps are repeated until $\boldsymbol{Q_{b,i}}$ and $\boldsymbol{Q_{b,i-1}}$ reach the convergence criteria.

Adewumi and Mucharam proposed LTM to solve two-phase flow in networks by using Beggs- and Brill's two-phase flow model (Mucharam, Leksono & Adewumi, 1990). The authors gave an algorithm and code written in FORTRAN. While the formulation

works for Beggs- and Brill's two-phase model, it works due to the explicit definition of the given two-phase friction multiplier and the explicit definition of void fraction. Therefore these calculations could be made explicitly in the algorithm rather than solved simultaneously in another computation scheme.

2.3.3 Newton-Raphson Method

The last numerical method used to solve pipe network problems that will be discussed is the Newton-Raphson method. While a succinct explanation of the Newton-Raphson method is given in equations (2.1) and (2.2), the method needs to be extended to systems larger than one-equation, one-unknown. In matrix form, equation (2.2) becomes:

$$\boldsymbol{x}^{m+1} = \boldsymbol{x}^{m} - \alpha \frac{f(\boldsymbol{x}^{m})}{f'(\boldsymbol{x}^{m})} = \boldsymbol{x}^{m} - \alpha \boldsymbol{J}_{\boldsymbol{f}}^{-1}(\boldsymbol{x}^{m}) f(\boldsymbol{x}^{m}) \tag{2.7}$$

where $\boldsymbol{x}$ is the solution vector, $f(\boldsymbol{x}^{m})$ is the function vector (which is zero when all equations are satisfied), and $\boldsymbol{J}_{\boldsymbol{f}}^{-1}(\boldsymbol{x}^{m})$ is the inverse of the Jacobian matrix. The Jacobian is defined as the matrix of all first-order partial derivatives of the system of equations:

$$\boldsymbol{J}_{\boldsymbol{f}}(\boldsymbol{x}) = \frac{d\boldsymbol{f}}{d\boldsymbol{x}} = \begin{bmatrix} \frac{\partial \boldsymbol{f}}{\partial x_1} & \cdots & \frac{\partial \boldsymbol{f}}{\partial x_n} \end{bmatrix} = \begin{bmatrix} \frac{\partial f_1}{\partial x_1} & \cdots & \frac{\partial f_1}{\partial x_n} \\ \vdots & \ddots & \vdots \\ \frac{\partial f_n}{\partial x_1} & \cdots & \frac{\partial f_n}{\partial x_n} \end{bmatrix} \tag{2.8}$$

While this method is perhaps the most common numerical method that a modeler might use, it offers many advantages over the Hardy Cross method and LTM. Firstly, it is more extensible to problem sets where the numbers of equations and unknowns are different from that of a single-phase, incompressible fluid. Secondly, while its convergence

may be slightly slower than LTM (due to the calculation *and inversion* of the Jacobian), both have quadratic convergence. One drawback when compared to LTM is the selection of the initial condition, which can heavily influence the solution found. This will be discussed in more detail in the following sections.

As the Newton-Raphson method forms the basis of the numerical method chosen in this work, further review is necessary.

2.3.3.1 Newton step selection

A subtopic of particular interest when using Newton's method is the selection of a step size, α. The traditional Newton-Raphson method uses a value of unity, as that ensures quadratic convergence to the solution set. This, however, is true only under certain circumstances. These circumstances are due to the selection of the initial point, but if a function is not continuous or differentiable in the region of interest, it may lead to additional complications. In the particular case of an initial guess being far from the solution, it is often not advisable to choose a step size of unity, especially when a function is particularly oscillatory and the quadratic convergence is not readily apparent.

To accomplish this, a line search is used. While an exact value for α can be find to minimize $f(\boldsymbol{x}^m)$, it is often undesirable to spend further computational resources to arrive at an exact value that only serves as the starting point for the next iteration. To account for this, a backtracking algorithm is often used. Starting at the Newton step, alpha is decremented an arbitrary number of times, and usually decreased by ½ at each evaluation.

If the newly calculated functional value is less than a pre-determined fraction of the Newton step (usually ½ again), then that value of α is chosen.

$$f\left(\boldsymbol{x} - \alpha \boldsymbol{J}_{\boldsymbol{f}}^{-1}(\boldsymbol{x}^m) f(\boldsymbol{x}^m)\right) \leq f(\boldsymbol{x}) - \alpha c m; m = \left(\boldsymbol{J}_{\boldsymbol{f}}^{-1}(\boldsymbol{x}^m) f(\boldsymbol{x}^m)\right)^T \nabla f \qquad (2.9)$$

Equation (2.9) gives the so-called Armijo-Goldstein condition to test whether a value of unity for the step size should be chosen or not (Armijo, 1966).

Using a line search can drastically reduce the number of iterations in the Newton-Raphson method. The following example illustrates how important a line search can be for rapid convergence:

$$f(x, y) = e^{x+3y-0.1} + e^{x-3y-0.1} + e^{-(x-0.1)}$$

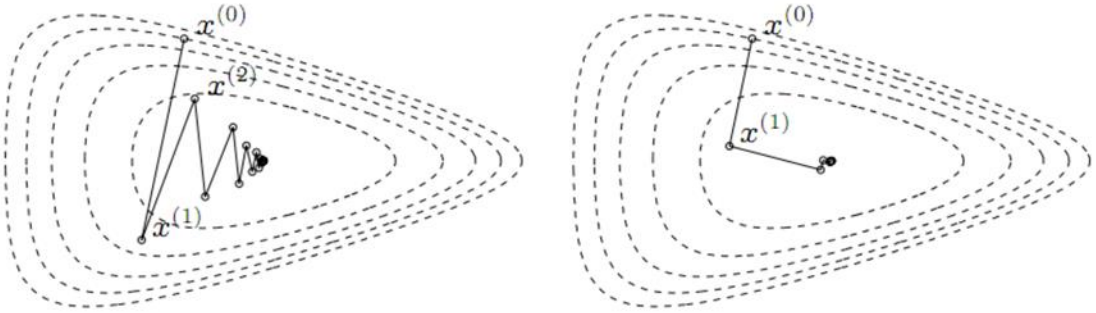

Without line search With line search

Figure 2.2: Graphical comparison of Newton-Raphson method with and without a line search (Abbeel, 2012)

Figure 2.2 shows how the Newton-Raphson method without the line search oscillates until reaching the solution, whereas with the line search the solution is found much quicker.

2.3.3.2 Importance of the initial guess

As stated previously, an accurate initial guess is crucial to the convergence, especially when a function has multiple solutions. One simple example to illustrate this is found in "Cubics, chaos, and Newton's Method" by Thomas Dence (Dence, 1997). Dence shows that for the function:

$$f(x) = x^3 - 2x^2 - 11x + 12 \tag{2.10}$$

x converges to different roots for small changes in initial guesses.

Initial Guess	Root Found
2.35287527	4
2.35284172	-3
2.35283735	4
2.352836327	-3
2.352836323	1

Table 2.3: Sensitivity on initial guess for sample function (Dence, 1997)

Table 2.3 shows that for changes as small as 0.000000004 in the initial guess, Newton's method can converge to different roots.

2.4 THE MANIFOLD PROBLEM

Often times the quality of the external mass influx and outflux in multiphase networks is not well known, which causes the number of unknowns to be greater than the number of knowns. When this occurs, an additional equation needs to be specified. This problem has been extensively studied, and is often called the "manifold problem," "flow

bifurcation problem," or the "phase-splitting problem." Review papers have been written by Azzopardi (Azzopardi, Two Phase Flow in Junctions, 1986), (Azzopardi & Hervieu, Phase Separation at Junctions, 1994), (Azzopardi, Phase Separation at T Junctions, 2000), by Lahey (Lahey, Current Understanding of Phase Separation Mechanisms in Branching Conduits, 1986), and Muller (Muller & Riemann, 1991).

2.4.1 Introduction to the Manifold Problem

The manifold problem exists when multiphase flow occurs at a pipe junction. Typically, three pipe junction configurations are seen: the side-arm junction, the symmetric impacting junction, and the asymmetric impacting junction. Figure 2.3, below, shows how these configurations look. Typically, the three pipes that are in the junction are called the inlet, denoted with a subscript 1, the outlet, denoted with a subscript 2, and the branch, denoted with a subscript 3.

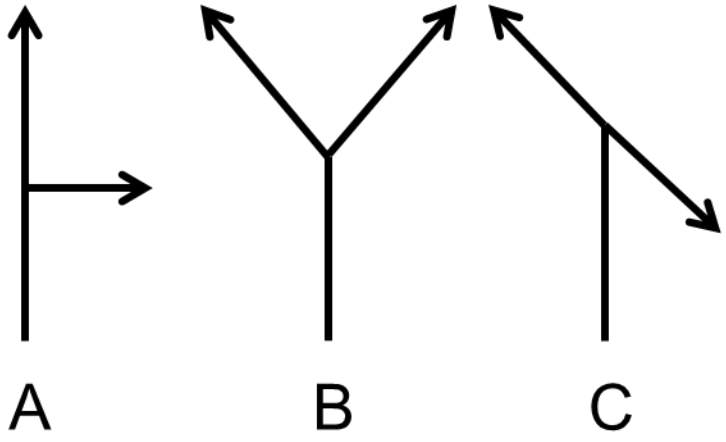

Figure 2.3: A) Side-arm junctions, B) Symmetric impacting junctions, C) Asymmetric impacting junctions.

In order to specify fully a pipe junction, five angles must be specified: three inclinations with respect to horizontal, and two azimuths from each branch to the inlet, as seen in Figure 2.4. Typically, phase splitting is exaggerated as the inclination of the branch, Inc_3, is increased towards 90° and as the azimuth of the branch, Az_3, is increased towards 180°. This is because the lighter phase tends to segregate on top of the heaver phase, and the lighter phase has less inertia than the heavier phase, which means the lighter phase can be diverted into the branch easier.

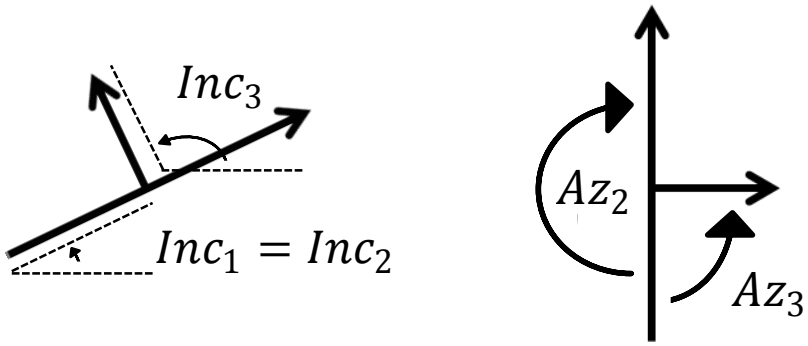

Figure 2.4: Figure of the three inclinations (Inc_1, Inc_2, Inc_3) and two azimuths (Az_1, Az_2) needed to specify a pipe junction.

2.4.2 Practical Applications of the Manifold Problem

The manifold problem has many applications in industry. In the nuclear industry, loss-of-coolant accidents can occur, where water can evaporate and leak out of reactors. Other fluids can be used which are composed of multiple phases. Here, the quality is unknown and hence another equation is necessary. In addition, pipe junctions can be used as in situ separators. The configuration of a pipe junction can exaggerate the phase split, splitting the lighter phase preferentially into the branch. Moreover, gas or water injection

in the oil and gas industry often has pipe junctions that split flow into various different wells, which are controlled by adjustable chokes. This also constitutes a practical example of the manifold problem in oil and gas.

2.4.3 Manifold Models

As the manifold problem has been extensively studied, several models have been developed to predict the extent of phase splitting that occurs at a pipe junction. These models are based on a variety of approaches: empirical, mechanistic, phenomenological (flow-pattern based), probabilistic, and computational fluid dynamics (CFD). The difficulties in modeling the phase splitting at pipe junctions has been a continuing source of frustration for modelers, and many have proposed a collection of existing models to accommodate the entire range of data (Riemann, Brinkmann, & Domanski, 1988) (Lahey, Current Understanding of Phase Separation Mechanisms in Branching Conduits, 1986). A brief review of these is presented below.

2.4.3.1 Empirical Approaches

One of the first and simplest models was developed in 1982 by Zetzmann (Zetzmann, 1982). Zetzmann's approach was to model air-water mixtures in side-arm tees and Ys. The diameter ratio (d_1/d_3) was varied between 1 and 2, and the takeoff (m_3/m_1) was varied between 0 and 1. Zetzmann developed three equations—each for a distinct range of takeoff—and fit these equations with two fitting parameters.

These equations are:

For $0 \leq \frac{m_3}{m_1} \leq 0.12$,

$$\frac{x_2}{x_1} = b * \left\{ Exp\left(-4 \left(\frac{m_3}{m_1} \right)^{1.75} \right) - 0.147 * \left(\frac{m_3}{m_1} \right) * \left(1 - \frac{m_3}{m_1} \right) \right\} \tag{2.11}$$

$$\frac{x_3}{x_1} = \frac{a\left\{ 1 - \left(\frac{x_2}{x_1} \right) * \left(1 - \frac{m_3}{m_1} \right) \right\}}{\frac{m_3}{m_1}} \tag{2.12}$$

For $0.12 \leq \frac{m_3}{m_1} \leq 0.5$,

$$\frac{x_2}{x_1} = b * \left\{ Exp\left(-4 \left(\frac{m_3}{m_1} \right)^{1.75} \right) - 0.147 * \left(\frac{m_3}{m_1} \right) * \left(1 - \frac{m_3}{m_1} \right) \right\} \tag{2.13}$$

$$\frac{x_3}{x_1} = a * \left\{ 15.64 \left(\frac{m_3}{m_1} \right)^{0.75} e^{-2.75\left(\frac{m_3}{m_1} \right)} - 2 \left(\frac{m_3}{m_1} \right) \left(1 - \frac{m_3}{m_1} \right) \right\} \tag{2.14}$$

And for $0.5 \leq \frac{m_3}{m_1} \leq 1$,

$$\frac{x_2}{x_1} = \frac{1}{1 - \frac{m_3}{m_1}} * \left[1 - \left(\frac{m_3}{m_1} \right) \left(\frac{x_3}{x_1} \right) \right] \tag{2.15}$$

$$\frac{x_3}{x_1} = a * \left\{ 15.64 \left(\frac{m_3}{m_1} \right)^{0.75} e^{-2.75\left(\frac{m_3}{m_1} \right)} - 2 \left(\frac{m_3}{m_1} \right) \left(1 - \frac{m_3}{m_1} \right) \right\} \tag{2.16}$$

For equations (2.11) through (2.16), a and b are fitting parameters based on diameter and branch azimuth.

$\frac{d_2}{d_3}\left(\frac{mm}{mm}\right)$	$Azimuth, \phi_3$ (deg)	a	b
100/50	90	0.8	1.0
50/24	90	1.35	0.75
50/24	45	1.4	0.8
50/50	90	1.05	0.9
24/24	90	1.05	0.9
24/24	45	0.9	0.98
50/50	45	0.9	0.98

Table 2.4: Parameters used in Zetzmann's Empirical Relationships (Lahey, Current Understanding of Phase Separation Mechanisms in Branching Conduits, 1986).

The key insight that Zetzmann relies on for his relationship is that as takeoff increases, the phase split goes towards unity, meaning that the outlet quality tends towards the inlet quality.

Seeger et. al. developed three empirical relationships for branch azimuths of 0 (horizontal), 90 (upward), and -90 (downward) degrees in the case of low pressure, gas-water flow (Seeger, Reimann, & Muller, 1985). For upward branches, the authors use the relation:

$$\frac{x_3}{x_1} = \eta^{-0.8} \tag{2.17}$$

Where $\eta = \frac{G_3}{G_1}$ and $G_i = \frac{m_i}{A_i}$. (2.17) is valid for $\eta > 0.15$. It is noted that total phase separation results in an exponent of -1, and upward side arms exaggerate the phase split when compared to horizontal branches. For horizontal side arms, the authors propose:

$$\frac{x_3}{x_1} = 5\eta - 6\eta^2 + 2\eta^3 + a\eta(1-\eta)^b \tag{2.18}$$

Where $b = 4$ and a is a flow-regime dependent parameter. For downward branches, the authors propose:

$$\frac{x_3}{x_1} = 5\eta - 6\eta^2 + 2\eta^3 + a\eta(1-\eta)^b \tag{2.19}$$

However, the parameter η is altered such that:

$$\eta = \frac{\frac{G_3}{G_1} - \frac{G_{3,max}}{G_1}}{\left(1 - \frac{G_{3,max}}{G_1}\right)}; G_{3,max} = 0.52\rho_l^{0.5}\left(\sigma g\left(\rho_l - \rho_g\right)\right)^{0.25} \tag{2.20}$$

And $b = 3 + 2.2\tanh\left(0.5(G_1 - 3000)\right)$, and a remains the same as in the side-arm case. For Seeger's empirical correlations, all terms are in SI units.

It should be noted that these equations are only valid for conditions present in the experimental setup. These are for low pressures ($P < 1MPa$), inlet mass fluxes between $500 \leq G_1 \leq 7000\frac{kg}{m^2 s}$, and equal diameter branches.

2.4.3.2 Phenomenological Approaches

One of the most well-known models is from Azzopardi and Whalley, who developed an equation to describe the phase splitting of annular and churn flows

(Azzopardi & Whalley, The Effect of Flow Patterns on Two-Phase Flow in a 'T' Junction, 1982). Their model postulates that in annular flow, a “region of influence” exists, whereby increasing withdrawal increases the region of influence. This region is characterized by an angle, θ^*, where $\theta^* = 0$ for $\frac{m_3}{m_1} = 0$, and $\theta^* = 2\pi$ for $\frac{m_3}{m_1} = 1$. This angle defines the section of pipe from which the heavier phase is removed.

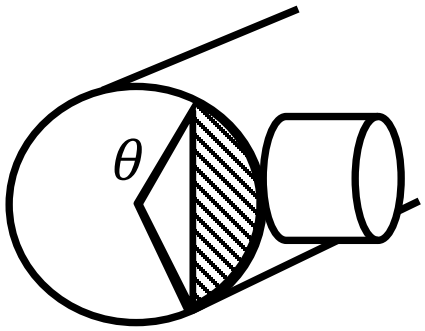

Figure 2.5: Depiction of Region of Influence (shaded) in Azzopardi's annular flow model.

If one assumes that the gas mass flux is uniform over the cross-sectional area, then the ratio of gas removed to the total gas flow rate is:

$$\frac{x_3}{x_1}\frac{m_3}{m_1} = \frac{1}{2\pi}(\theta - \sin(\theta) \tag{2.21}$$

where θ is the zone of influence for the gas. To determine the liquid flow rate, the following equation is solved:

$$m_3(1 - x_3) = \frac{\pi}{180}\int_{\phi-\frac{\theta^*}{2}}^{\phi+\frac{\theta^*}{2}} r\Gamma(\phi')d\phi' \tag{2.22}$$

where $\Gamma(\phi')$ is the liquid flow rate per unit length around the circumference of the pipe, and θ^* is the liquid zone of influence. Consequently, one must know the axial distribution of the liquid flow rate to solve equation (2.22). If one assumes that the flow rate is uniform around the pipe's circumference, as in the case of vertical flow or in high flow rate horizontal pipes, equation (2.22) reduces to:

$$m_3(1-x_3) = \frac{2\pi r\Gamma\theta^*}{360} = \frac{m_1(1-x_1)(1-E_1)\theta^*}{360} \tag{2.23}$$

where E_1 is the entrained liquid fraction. It was found, though, that the liquid is withdrawn from a larger region than the gas. Hence the authors introduced a correction to account for this ($\theta^* = 1.2\theta\left(\frac{D_3}{D_1}\right)^{0.4}$). The resulting equation from combining equations (2.21) and (2.23) is:

$$\frac{x_3}{x_1} = \frac{1}{2\pi}\frac{1}{\frac{m_3}{m_1}} * \left\{\frac{5}{3}\pi\left(\frac{d_1}{d_3}\right)^{0.4} * \left[\frac{m_3}{m_1} * \frac{1-x_3}{(1-x_1)(1-E_1)}\right] - \sin\left(\frac{5}{3}\pi\left(\frac{d_1}{d_3}\right)^{0.4} * \left[\frac{m_3}{m_1} * \frac{1-x_3}{(1-x_1)(1-E_1)}\right]\right)\right\} \tag{2.24}$$

where all degrees are in radians, x is the mass fraction for a given branch, and E_1 is the liquid entrainment for the inlet.

While this model works well for low takeoffs, it has been shown to predict poorly at high takeoffs (Lahey, Current Understanding of Phase Separation Mechanisms in Branching Conduits, 1986). Moreover, this method only works in side-arm configurations, meaning that its extensibility is limited. The model also lacks a physical basis. While it may seem intuitive that the fluids closest to the outlet are the first to be withdrawn, there

are multiple hypotheses that could explain takeoff. It has been shown that in cases of obstructed flow, which is the case in the manifold problem, that slip can be exaggerated, which alters the radial distribution of fluids in the conduit (Kawahara, Sadatomi, Matsuo, & al., 2011). Moreover, one needs to know the radial and azimuthal distributions of the liquid film in order to properly use the model.

Smoglie et. al. developed a phase splitting model to be used for stratified flow (Smoglie & Reimann, Flow Through a Small Pipe at the Top of a Large Pipe with Stratified Flow., 1983) (Smoglie, Reimann, & Muller, Two-Phase Flow Thorugh Small breaks in a Horizontal Pipe with Stratified Flow, 1986). Smoglie investigated horizontal side-arms with diameter ratios much less than 1 ($\frac{d_3}{d_1} \ll 1$). The authors hypothesized that if the gas-liquid interface is high above or below the branch entrance that only one phase can enter the branch. The branch quality is hence described as:

$$x_3 = \left[\frac{1.15}{1+\left(\frac{\rho_l}{\rho_g}\right)^{0.5}}\right]^{\left(1+C\frac{h}{h_b}\right)} \left[1-\frac{1}{2}\frac{h}{h_b}\left(1+\frac{h}{h_b}\right)\left(\frac{1.15}{1+\left(\frac{\rho_l}{\rho_g}\right)^{0.5}}\right)^{\left(1-\frac{h}{h_b}\right)}\right]^{0.5} \tag{2.25}$$

where h is the interface level, h_b is the critical interface level where entrainment begins, and C is a constant depending on liquid or gas entrainment. $C = 1$ for $\frac{h}{h_b} \leq 0$ and $C = 1.09$ for $\frac{h}{h_b} > 0$. The critical interface level can be determined by:

$$h_b = \frac{K}{\left(g\rho_b\left(\rho_l - \rho_g\right)\right)^{0.2} m_{3b}^{-0.4}} \tag{2.26}$$

Where $K = 0.69$ for liquid entrainment and $K = 0.75$ for gas entrainment, and ρ_b is the continuous phase density. In this formulation, $h = 0$ corresponds to a liquid level that is at the center of the branch's entrance, and hence is positive for gas entrainment and negative for liquid entrainment. While the model shows good agreement with the data presented, it should be noted that the validity of the model is restricted to air-water stratified flow where $\frac{h_b}{D_3} > 1$ (Smoglie, Reimann, & Muller, Two-Phase Flow Thorugh Small breaks in a Horizontal Pipe with Stratified Flow, 1986).

Shoham, Brill and Taitel developed a model for horizontal side arms for stratified wavy and annular flow patterns (Shoham & Taitel, 1987). The authors model these flow patterns by including centripetal, inertial, and gravity forces. In annular flow, the centripetal force dominates and in stratified-wavy flow, the inertial and gravity forces dominate. The model shows reasonable agreement with the experimental data presented by the authors. Shoham later extended this model to branch inclinations other than horizontal, collecting data with branch inclinations ranging from $-60°$ to $35°$ (Shoham, Ashton, & Penmatcha, 1996).

Arirachakaran developed a model to describe slug flow in side-arm branches that idealized a slug as one stratified flow section followed by a fully-liquid body (Arirachakaran, 1990). The author used an existing phase-splitting model to describe the phase split of the gas-rich stratified flow region, and used a model based on the "dam break" concept. Dam break is a field of study in fluid dynamics where one wall of a pool

is removed and the resulting flow is described. The total phase split is then described as the weighted average of the phase split of each component of the flow.

Lemmonier and Hervieu use a two-dimensional approach to describe the bubble flow regime (Lemonnier & Hervieu, 1991). The authors argue that such two-phase flows can be described by the superposition of two single-phase flows. The model assumes that the bubbles are non-interacting and no mass transfer occurs between phases. The models described the data from the authors quite well, and the model also predicts the recirculation zones at the branch entrance as seen experimentally. Clearly, at higher void fractions this model will become more inaccurate as bubbles coalesce and the assumption of non-interacting bubbles does not apply.

2.4.3.3 Probabilistic Approach

Azzopardi and Baker sought to extend the region-of-influence approach to other flow regimes by approaching the problem from a probabilistic rather than physical standpoint (Azzopardi & Baker, Two-phase flow in a 'T' junction. The effect of flow pattern in vertical upflow., 1981). The probability of a phase entering a branch would clearly be a function of the takeoff, the momentum of each phase, pressures, etc. A generalized expression for this is:

$$m_3(1-x_3) = \int_{\phi-\frac{\theta^*}{2}}^{\phi+\frac{\theta^*}{2}} \int_0^R P(r',\phi')\,\rho_l u_l r' * (1-\alpha(r'))r' dr' d\phi' \qquad (2.27)$$

where $P(r', \phi')$ is the probability function for the heavier phase entering the branch, ρ_l is the density of the heavier phase, u_l is the volume flux of the heavier phase, θ^* is the region of influence, and α is the void fraction radial profile (Lahey, Current Understanding of Phase Separation Mechanisms in Branching Conduits, 1986). It should be noted that equation (2.24) can be derived from equation (2.27) by using the correct closure relationship for $P(r', \phi')$. To illustrate this, the authors used the case of bubbly flow as a case study. They hypothesized that the probability function could be described by:

$$P(r', \phi') = A \frac{\rho_g u_g^2(r)}{\rho_l u_l^2(r)} \tag{2.28}$$

where $u_g^2(r)$ is the velocity profile of the gas phase and $u_l^2(r)$ is the velocity profile of the liquid phase. Furthermore, the authors used the approximation that the gas velocity profile was twice the *average* liquid velocity ($\overline{u_l}$). This reduces equation (2.28) to:

$$P(r', \phi') = 4A \frac{\rho_g \overline{u_l}^2}{\rho_l u_l^2(r)} \tag{2.29}$$

Combining equations (2.27) and (2.29), and using the identity $r(\phi') = \frac{Rcos\left(\frac{\theta}{2}\right)}{\cos(\phi')}$, and assuming power-law relationships $\left(\frac{1}{n}\ and \frac{1}{m}\right)$ for the liquid velocity profile and the void fraction profile:

$$m_3(1-x_3) = \frac{4n^2 A \rho_g \overline{u_l}}{m^2(n+1)(2n+1)} \int_{\phi-\frac{\theta^*}{2}}^{\phi+\frac{\theta^*}{2}} \int_{r(\phi')}^{R} \left[\frac{r'}{\left(1-\frac{r'}{R}\right)^{\frac{1}{n}}} \right] \times \left[2m^2 - (m+1)(2m+1)\bar{\alpha}\left(1-\frac{r'}{R}\right)^{\frac{1}{m}} \right] dr' d\phi' \tag{2.30}$$

While equation (2.30) can be integrated analytically in the radial direction, it should be noted that it must be numerically integrated in the ϕ' direction. Also, in order to eliminate the variable θ^*, equation (2.30) must be solved simultaneously with the equation:

$$\frac{x_3 m_3}{x_1 m_1} = \frac{1}{2\pi}(\theta^* - \sin(\theta^*)) \tag{2.31}$$

which is a continuation of the "region of influence approach. In solving equations (2.30) and (2.31), the authors assumed that the liquid velocity profile can be approximated by $n = 7$, and that the average void fraction was negligible. They also used the value $A = 20$ as a fitting parameter.

A probabilistic approach's chief advantage is its ability to use some key insights into the problem to determine a relationship for the manifold problem. This means that the physics can be incorporated into the model without having an exact equation. However, it can be readily seen that this comes at the expense of multiple fitting factors and some less-than-realistic assumptions (for example, gas velocity is twice the liquid velocity). Moreover, one needs to know local data on the liquid and void fraction radial profiles in order to have a tractable profile. As seen in Nagoo's thesis, gas profiles can change readily from core-peaking to wall-peaking as a function of multiple parameters that may not be

taken into account (Nagoo A. , 2013). For instance, low gas volume fluxes tend toward wall-peaking profiles and high gas volume fluxes tend toward core-peaking. Conversely, high liquid volume fluxes tend towards wall-peaking profiles and low liquid volume fluxes tend toward core-peaking.

2.4.3.4 Computational Fluid Dynamics (CFD)

Kalcach-Navarro and Lahey similarly proposed a two-fluid CFD approach with mass and momentum conservation equations for each phase (Kalcach-Navarro, Lee, Lahey, & Drew, 1990). The authors used a $k-\epsilon$ model for turbulence, and interfacial momentum transfer is handled using a drag coefficient.

Issa and Oliveira formulated a three-dimensional CFD approach to the manifold problem, using a two-fluid approach for dispersed flow (Issa & Oliveira, 1993). The authors used a finite-volume computation and an unstructured mesh. The model successfully describes data from Popp and Sallet, but a deviating trend can be seen as the void fraction increases and the assumption of dispersed flow becomes increasingly inaccurate (Popp & Sallet, 1983).Also, the model predicts the formation of eddies as is commonly seen experimentally (Issa & Oliveira, 1993).

2.4.3.5 Mechanistic & General Models

El-Shaboury, Soliman, and Sims conducted air-water experiments in horizontal impacting tees for a wide range of flow regimes (El-Shaboury, Soliman, & Sims, 2007). The authors proposed wall shear coefficients for their data, and develop a momentum balance for impacting tees. The authors assumed that inlet flow was fully-developed, and imposed the condition that at equal flow rates of air and water, for 50 percent takeoff, that the phase split must be identical. This makes sense for equal-sided impacting tees as the

momentum change to enter either branch is equal and opposite. The consequence of this model is that it is only applicable for impacting tees.

A general model was developed by Saba and Lahey based on the gas-phase conservation of momentum and assuming homogeneous flow (Saba & Lahey, The Analysis of Phase Separation Phenomena in Branching Conduits, 1984) (Saba & Lahey, Phase Separation Phenomena in Branching Conduits, 1981). As this model is of similar origin to the model proposed in this work, more attention to detail will be given to this model.

The authors described the manifold problem as a system of five equations and five unknowns. The variables of interest are:

Variable	Symbol
Inlet quality	x_1
Pressure change from branch to inlet	ΔP_{1-3}
Pressure change from run to inlet	ΔP_{1-2}
Inlet mass flux	G_1
Run mass flux	G_2
Branch mass flux	G_3
Run quality	x_2
Branch quality	x_3

Table 2.5: Variables of interest in the Saba-Lahey model

Four of the equations are then well known:

1. Overall mass balance

2. Lighter phase mass balance
3. Mixture momentum balance for the run
4. Mixture momentum balance for the branch

As in the problem's formulation only three variables are specified, it is therefore necessary to derive a fifth equation to have a well-posed problem. The authors proposed a momentum balance for the branch of the lighter phase. They justified this by recognizing that the inertia of the lighter phase had been hypothesized to be one of the deciding factors that contributes to phase splitting.

The first two equations are straightforward:

$$G_1 A_1 = G_2 A_2 + G_3 A_3 \tag{2.32}$$

$$x_1 G_1 A_1 = x_1 G_2 A_2 + x_1 G_3 A_3 \tag{2.33}$$

Equation (2.32) is the overall mass balance at the junction and equation (2.33) is the lighter phase mass balance at the junction. The next two equations are the momentum balances for the mixture for the run and the branch:

$$\Delta P_{1-2} = P_1 - P_{1j} + (\Delta P_{1-2})_j + P_{2j} - P_2 \tag{2.34}$$

$$\Delta P_{1-3} = P_1 - P_{1j} + (\Delta P_{1-3})_j + P_{3j} - P_3 \tag{2.35}$$

where P_1 is the pressure at the beginning of the inlet, P_{1j} is the pressure at the inlet just before the bifurcation occurs, P_{2j} is the pressure just after the bifurcation in the run, P_{3j} is the pressure just after the bifurcation in the branch, and P_2 and P_3 are the pressures at the end of the run and branch respectively. The pressure drop in the closed conduits are found using existing two-phase pressure drop correlations (the authors use a homogeneous two-

phase multiplier to approximate wall shear). The pressure change at the junction for the run is described as:

$$(\Delta P_{1-2})_j = P_{1j} - P_{2j} = \frac{K_{1,2}}{2}\left(\frac{G_2^2}{\rho_{H,2}} - \frac{G_1^2}{\rho_{H,1}}\right) \tag{2.36}$$

where $K_{1,2}$ is an empirical pressure recovery coefficient:

$$K_{1,2} = 0.11 + \frac{5}{\left(\frac{G_1 D_1}{\mu_{L1}}\right)^{0.17}} \tag{2.37}$$

Equation (2.36) suggests that the pressure change in the run is due only to inertial forces (convective acceleration/deceleration), and that no wall shear or hydrostatic forces are at play. ρ_{Hi} is the so-called homogeneous density where:

$$\rho_{Hi} = \frac{1}{\frac{1}{\rho_l} + x_i\left(\frac{1}{\rho_g} - \frac{1}{\rho_l}\right)} \tag{2.38}$$

The homogeneous density is the mixture density if no slip exists between the two phases. Equation (2.37) suggests that the transport coefficient that determines the pressure change in the run is dependent on the inlet, superficial liquid Reynold's number ($\frac{G_1 D_1}{\mu_{L1}}$).

Next, the authors describe the pressure drop between the branch and the inlet as the combination of an irreversible and reversible pressure change:

$$(\Delta P_{1-3})_j = (\Delta P_{1-3})_{j,rev} + (\Delta P_{1-3})_{j,irr} \tag{2.39}$$

$$(\Delta P_{1-3})_{j,rev} = \frac{\rho_{H3}}{2}\left(\frac{G_3^2}{\rho_{H3}^2} - \frac{G_1^2}{\rho_{H1}^2}\right) \tag{2.40}$$

$$(\Delta P_{1-3})_{j,irr} = \frac{K_{1,3}}{2}\frac{G_1^2}{\rho_l}(1-x_1)^2\left[1+\frac{C_{1,3}}{X_{tt}}+\frac{1}{X_{tt}^2}\right] \tag{2.41}$$

From equation (2.40), it is readily seen that the reversible pressure change at the junction is simply a convective acceleration term. A few terms in equation (2.41) need to be defined. $K_{1,3}$ is the wall-shear transport coefficient (friction factor) in a tee junction, given by:

$$K_{1,3} = [1.18 + \left(\frac{m_3}{m_1}\right)^2 - 0.8\left(\frac{m_3}{m_1}\right)](\frac{A_1}{A_3}) \tag{2.42}$$

Note that equation (2.41) describes the momentum lost to wall shear at the junction, and hence has a similar form to a closed-conduit wall shear term. $C_{1,3}$ is an empirical drift-flux term that describes the velocity profile of a two-phase flowing mixture, and $C_{1,3} = 1$ indicates a uniform velocity profile. As the authors assume homogeneous flow, this term can be written as:

$$C_{1,3} = \left[\left(\frac{\rho_l}{\rho_g}\right)^{0.5} + \left(\frac{\rho_g}{\rho_l}\right)^{0.5}\right] \tag{2.43}$$

X_{tt} is the Martinelli parameter, which is a term defined as:

$$X_{tt} = \left[\frac{\left(\frac{\partial P}{\partial z}\right)_{fric,l}}{\left(\frac{\partial P}{\partial z}\right)_{fric,g}}\right]^{0.5} \approx \left(\frac{x_i}{1-x_i}\right)\left(\frac{\rho_l}{\rho_g}\right)^{0.5} \tag{2.44}$$

The Martinelli parameter is the square root of the ratio of the frictional pressure gradient of the liquid to the frictional pressure gradient of the gas. The approximation given in equation (2.44) is valid for sufficiently high Reynolds number.

The gas-phase conservation of momentum for steady state can be written as:

$$\overbrace{-s_2\frac{dP}{dz}}^{Body\ Force} \quad \overbrace{-s_2\rho_2 g sin(\theta)}^{Hydrostatic\ Force} \quad \overbrace{-\tau_i}^{Interfacial\ Shear} \quad \overbrace{-\tau_w}^{Wall\ Shear} = \overbrace{s_2\rho_2 u_2\frac{du_2}{dz}}^{Convective\ Acceleration} \tag{2.45}$$

These terms can be expanded such that:

$$P_1 - P_3 = \overbrace{s_2\rho_{g,1} g sin(\theta) L_j}^{Hydrostatic\ Force} + \overbrace{\frac{\rho_{g,1}}{2}\left(\left\langle\left\langle u_{g,3}\right\rangle\right\rangle^2 - \left\langle\left\langle u_{g,1}\right\rangle\right\rangle^2\right)}^{Convective\ Term} + \overbrace{\frac{K_{1,3}\rho_{g,1}}{2}\left(\left\langle\left\langle u_{g,1}\right\rangle\right\rangle^2\right)}^{Wall\ Shear} + \overbrace{\frac{3}{4}\rho_{g,1} L_j {u_r}^2 \frac{C_D}{d}}^{Interfacial\ Shear} \tag{2.46}$$

Where L_j is the characteristic length from the inlet to the branch for the gas, $\left\langle\left\langle u_{g,i}\right\rangle\right\rangle$ is the *in situ* velocity of the gas phase in the ith pipe, u_r is the slip velocity between the two phases, and $\frac{C_D}{d}$ is the interfacial drag term.

$$L_j = 2.81 D_3 \left[e^{-0.12}\left(\frac{1-x_1}{x_1}\right)^{0.15}\left(\frac{\rho_{g,1}}{\rho_{l,1}}\right)^{0.5}\right]\left[\left(\frac{G_3}{G_1}\right)^{(1-x_1)^3}\right][(1-x_3)^3] \tag{2.47}$$

L_j can also be described as the average length traveled by the gas phase that splits into the branch. The *in situ* velocity as defined by the authors is:

$$\left\langle\left\langle u_{g,i}\right\rangle\right\rangle = \frac{G_i x_i}{\rho_{g,i} S_{g,i}} \tag{2.48}$$

Where $S_{g,i}$ is the volume fraction of the gas in the ith branch, which the authors define using the drift-flux relation:

$$S_{g,i} = \frac{x_i}{C_0\left[x_i + \frac{\rho_{g,i}}{\rho_{l,i}}(1 - x_i)\right] + \frac{\rho_{g,i} V_{Gji}}{G_i}} \tag{2.49}$$

where C_0 is the concentration parameter, which is an empirical drift-flux term defined as:

$$C_0 = 1.4 - 0.4\left(\frac{\rho_{g,i}}{\rho_{l,i}}\right)^{0.5} \tag{2.50}$$

and V_{Gji} is the drift-velocity of the gas ($\left\langle\left\langle u_{g,i}\right\rangle\right\rangle - u_{m,i}$), which the authors define as:

$$V_{Gji} = 2.5\left[\frac{(\rho_{l,i} - \rho_{g,i})\sigma}{\rho_1} g\right]^{0.25} \sin(\theta_3) \tag{2.51}$$

where σ is the surface tension and θ_3 is the inclination from vertical of the branch, and ρ_1 is the mixture density at the inlet. The slip velocity is defined as:

$$u_r = \frac{u_{m,i}(C_0 - 1) + V_{Gji}}{1 - S_{g,i}} \tag{2.52}$$

where $u_{m,i}$ is the mixture velocity (volumetric flux) being defined as ($\frac{G_i x_i}{\rho_{g,i}} + \frac{G_i(1-x_i)}{\rho_{l,i}}$). The interfacial drag term is defined as:

$$\frac{C_D}{d} = 54.9\left[\frac{\rho_{g,1}}{\rho_{l,1}} S_{g,1}\left(1 - S_{g,1}\right)^2 + \left(1 - S_{g,1}\right)^3\right], (m^{-1}) \tag{2.53}$$

where it should be noted that the constant 54.9 is in units of inverse meters. These five equations must be solved simultaneously in order to determine the phase split, as the branch's quality is implicitly defined in these equations.

Lahey, Hwang and Soliman expand the approach of Lahey and Saba for junction configurations to impacting tees and wyes (Lahey, Soliman, & Hwang, Phase separation in impacting wyes and tees, 1989) (Lahey & Hwang, A Study on Phase Separation

Phenomena in Branching Conduits, 1986). By examining the mean length of the lighter phase in branch configurations other than side-arm configurations, they make the model extensible to far more junctions found in industry. The authors then compare this model to existing data and see that the model fit 95 percent of the data to within ± 25 percent.

2.4.4 Other Studies on the Manifold Problem

Outside of model development, many other studies have been carried out to determine the experimental characteristics of the manifold problem. These studies have been carried out under a variety of circumstances, and often measure only the variables of interest in the given study, omitting other desirable parameters.

Reimann, Brinkman, and Domanski conducted an exhaustive study of side-arm tees in upward, horizontal and downward branch orientations (Riemann, Brinkmann, & Domanski, 1988). The authors conducted experiments for air-water and steam-water systems, varying inlet quality, flow rates, branch diameters, pressures and takeoff. In all, over 2000 data points were taken. The experimenters noted several experimental difficulties associated with the manifold problem, particularly when $\frac{d_3}{d_1} \ll 1$. While the experimenters would have liked to conduct experiments from 0 to 100 percent takeoff, they noted the difficulty in doing tests with high takeoffs with small side-arm diameters, and suggested that a choking mechanism occurred.

Davis and Fungtamasan investigated void fraction and transient effects in vertical tees (Davis & Fungtamasan, 1990). In their investigation, the authors conclude that the wall shear in their two-phase, air-water mixture was tantamount to single phase flow,

suggesting that single phase friction factors can be used in two-phase flow. Additionally, the authors concluded that the length required to re-establish steady state flow after a transient effect increases with an increase in Reynolds number, and the length tends to decrease with average void fraction. The authors include all flow rates, qualities, pressures and volume fractions.

Abu-Mulaweh, et. al. conducted experiments in two-phase, air-water flow in horizontal tee-junctions for slug flow (Abu-Mulaweh, Al-Halhouli, Hammad, & al., 2008). The primary purpose of the article was educational, but the authors also proposed wall shear coefficients that fit their data. The authors reported flow rates, qualities, and pressures but omit volume fraction data.

Katsaounis conducted experiments for side-arm tees with both horizontal and vertical branch orientations (Katsaounis, 1987). Katsaounis observed higher phase splitting in the vertical branch configuration, which makes sense as the split is exaggerated by the effect of gravity. Katsaounis also compared visually-obtained void fraction estimates to existing correlations. The author proposed a *vena contracta* in order to make pressure drop models more accurate.

Chapter 3: Multiphase Pipe Network Formulation

The first step in a robust calculation algorithm for any network solver is to convert the graphical representation of the network into a consistent set of mass balance equations, which satisfies Kirchhoff's first law. Next, to satisfy Kirchhoff's second law, a systematic method is needed in order to identify a set of independent loops present in a network. While visual inspection might be sufficient in small networks that are not well-connected, this task becomes increasingly difficult and error-prone in larger, more connected networks.

3.1 Fundamental Loop Matrix

In any connected graph, the number of linearly independent loops is $N_b - N_n + 1$, where N_b is the number of branches and N_n is the number of nodes (Dolan & Aldous, 1993). A set of loops are said to be linearly independent if the resulting hydraulic potential equations ($\sum \Delta P = 0$) are independent. One systematic way to identify a set of linearly independent loops is to use Kirchhoff's idea of the spanning tree (Dolan & Aldous, 1993). A spanning tree can be defined as a subgraph that contains all nodes in a graph and is also a tree. If one knows a spanning tree of a particular network, a simple algebraic manipulation of the incidence matrix yields a set of linearly independent loop equations. It is also of note to mention that the selection of spanning tree effects which loops are chosen. This means that two spanning trees of a particular network will result in two separate sets of equations.

To illustrate this, consider the network in Figure 2.1. The following two spanning trees result in two loop equations:

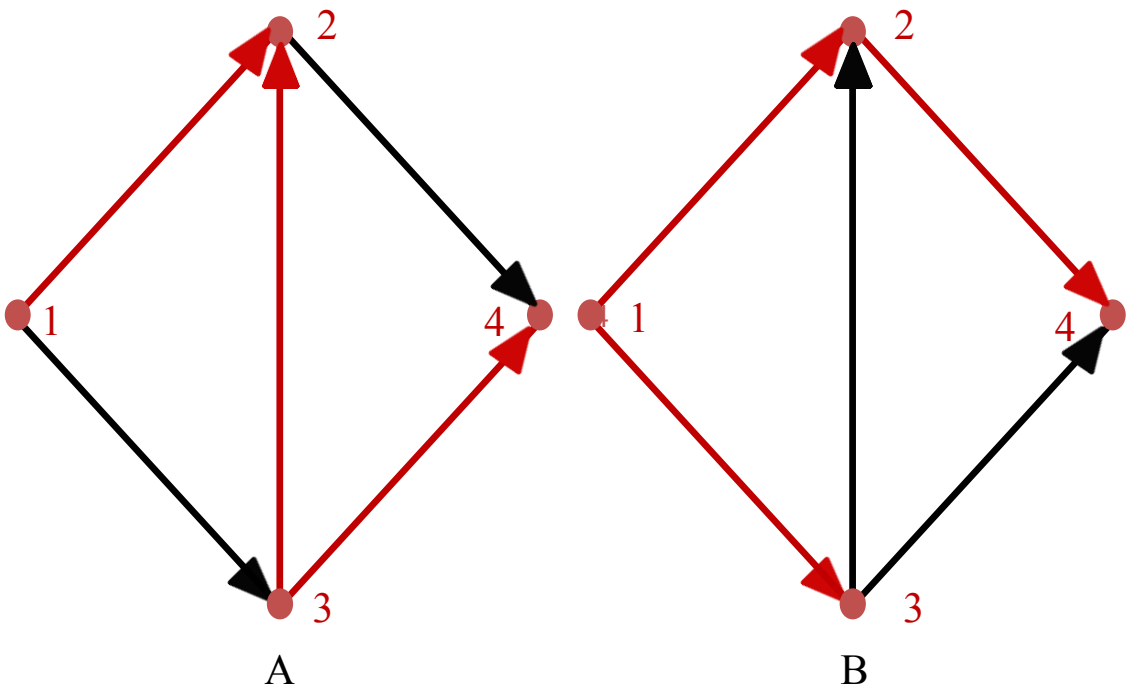

Figure 3.1: Two spanning trees constructed for the graph presented in Figure 2.1. Graph A shows a depth-first spanning tree whereas graph B shows a breadth-first spanning tree.

As will be seen later, the spanning tree chosen in graph A will result in the loops {1, 2, 3} and {2, 3, 4} and the spanning tree in graph B will result in the loops {1, 2, 3} and {1, 2, 3, 4}. While the selection of spanning tree, and hence loop equations, may seem trivial, the selection has implications in the numerical scheme to solve network problems. Knowing this, then which spanning tree is best?

There are a myriad of algorithms present to generate a spanning tree in a graph. Three popular methods are the depth-first search, breadth-first search, and the minimum-weighted tree. It should be noted that the directionality of a network is ignored when constructing these spanning trees.

3.1.1 Depth-First Search

The principal idea behind the depth-first search is to penetrate a graph as deeply as possible before fanning out to other vertices (Dolan & Aldous, 1993). When a search can go no further into a graph, the search must backtrack, and hence it is also called a backtrack search. This can be illustrated in a simple graph:

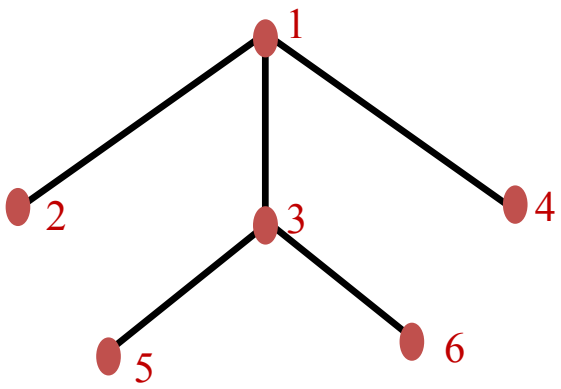

Figure 3.2: Sample graph

From Figure 3.2, a depth-first search starting at node 1 will first go to node 2, but at node 2, the search must return to the first as node 2 is not adjacent to any other nodes. The search then proceeds to node 3. Next, the search goes to node 5, but as node 5 is not adjacent to any other nodes, the search must backtrack again to 3. The search then proceeds to node 6, and then the search backtracks to the first node again, where node 4 is discovered and the search is over. This approach is also called last-in, first out, as the last node discovered is the first node that is left in a search. A more rigorous formulation can be found in *Networks and Algorithms* by Dolan & Aldous (Dolan & Aldous, 1993).

Returning to the example graph in Figure 2.1, we can similarly construct a depth-first search in this graph. The resulting spanning tree can be found in graph A in Figure 3.1. The convention used in this work is to always visit the lowest-number adjacent node in all searches. As seen in this example, no backtracking is necessary, and the spanning tree $\{1 \rightarrow 2, 2 \rightarrow 3, 3 \rightarrow 4\}$ is constructed.

3.1.2 Breadth-First Search

Another algorithm commonly used is the breadth-first search, where the goal is to fan out to as many vertices as possible before penetrating into the graph (Dolan & Aldous, 1993). In Figure 3.2, a breadth-first search starting at the first node would first find nodes 2, 3, and 4. Then, the search proceeds to node 2, but as the only adjacent node is node 1, and it has already been discovered, the search proceeds to node 3. Next, nodes 5 and 6 are discovered and the search is over. Note that when vertices are laid out into levels, as in Figure 3.2, the breadth-first search must complete each level before proceeding to the next one.

The breadth-first search for Figure 2.1 can be found in graph B in Figure 3.1. Starting at node 1, the algorithm first discovers nodes 2 and 3 ($\{1 \rightarrow 2, 1 \rightarrow 3\}$), then at node 2, only node 4 remains undiscovered, so the final branch is ($\{2 \rightarrow 4\}$). Hence, the final spanning tree is $\{1 \rightarrow 2, 1 \rightarrow 3, 2 \rightarrow 4\}$.

3.1.3 Minimum-Weighted Spanning Tree

A third method to find a spanning tree in a given graph is the use of a minimum-weighted spanning tree. The principal idea behind this spanning tree is the sum of the branch numbers is the lowest of all other spanning trees in a given graph. A simple algorithm presented is derived by Kruskal and is used in the work by Nagoo on gas

transmission lines (Nagoo A. S., 2003). Instead of a search algorithm, a spanning tree is constructed by choosing the lowest-numbered branches in a graph first, and proceeding to add branches to the tree that have larger numbers. If a lower-numbered branch would cause the tree to contain a loop, then it is omitted and a higher-numbered branch is chosen. The minimum-weighted spanning tree for our sample graph in Figure 2.1 would then be:

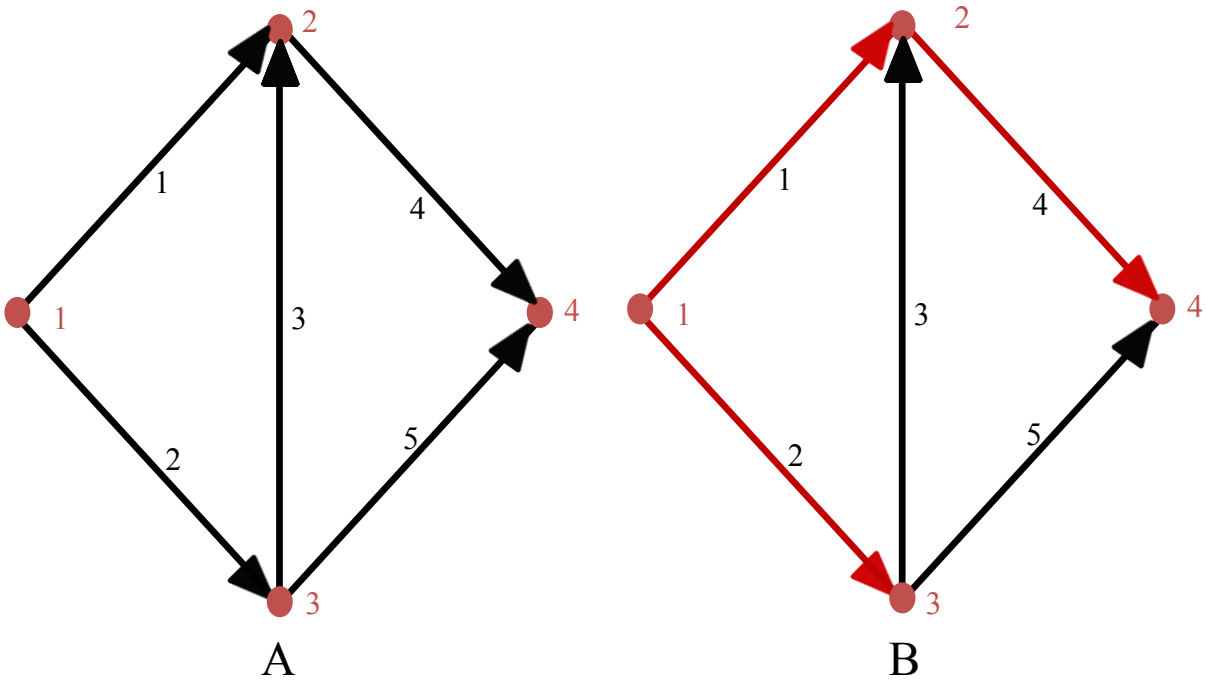

Figure 3.1: Sample graph (A) and its minimum-weighted spanning tree (B)

After examining these three spanning tree algorithms, it should also be noted that each spanning tree has a set of branches that are not included in the tree. These branches are referred to as *chords*. When a chord is added to a spanning tree, a loop is formed.

3.1.4 Transforming a Spanning Tree into Loop Equations

For a given graph, the fundamental loop matrix (set of linearly independent loops) is defined as:

$$\boldsymbol{F_\ell} = [-(\boldsymbol{A_t^{-1}A_c})'|\boldsymbol{I_{b-n+1}}] \tag{3.1}$$

Where $\boldsymbol{F_\ell}$ is the fundamental loop matrix, $\boldsymbol{A_t^{-1}}$ is the submatrix of the tree branches, $\boldsymbol{A_c}$ is the submatrix of chord branches, and $\boldsymbol{I_{b-n+1}}$ is the identity matrix of size ℓ (the number of loops in the graph) (Nagoo A. S., 2003).

To find $\boldsymbol{A_t}$ and $\boldsymbol{A_c}$, consider the same sample graph as in the previous section. As shown in Figure 2.1, the graph can be represented by an incidence matrix. This matrix, however, is not full-rank. The rank is one less than the number of nodes. Therefore, a reduced incidence matrix is defined to obtain a full-rank matrix. In this case, the reduced incidence matrix is:

$$A_r = \begin{bmatrix} -1 & -1 & 0 & 0 & 0 \\ 1 & 0 & 1 & -1 & 0 \\ 0 & 1 & -1 & 0 & -1 \end{bmatrix} \tag{3.2}$$

It should be noted that the omitted row from the incidence matrix can be obtained from (3.2) by multiplying the sum of all rows by -1. To obtain $\boldsymbol{A_t}$ and $\boldsymbol{A_c}$, A_r is permuted such that the tree branch columns are on the left and the chord columns are on the right. For the three algorithms presented in this work, $\boldsymbol{A_t}$ and $\boldsymbol{A_c}$ are:

Algorithm	A_t	A_c
Depth-First	$\begin{bmatrix} -1 & 0 & 0 \\ 1 & -1 & 0 \\ 0 & 1 & -1 \end{bmatrix}$	$\begin{bmatrix} -1 & 0 \\ 0 & -1 \\ 1 & 0 \end{bmatrix}$
Breadth-First	$\begin{bmatrix} -1 & -1 & 0 \\ 1 & 0 & -1 \\ 0 & 1 & 0 \end{bmatrix}$	$\begin{bmatrix} 0 & 0 \\ -1 & 0 \\ 1 & -1 \end{bmatrix}$
Minimum-Weighted	$\begin{bmatrix} -1 & -1 & 0 \\ 1 & 0 & -1 \\ 0 & 1 & 0 \end{bmatrix}$	$\begin{bmatrix} 0 & 0 \\ -1 & 0 \\ 1 & -1 \end{bmatrix}$

Table 3.1: Spanning trees and their tree-branch and chord matrices

Then, the fundamental loop matrix can be calculated by using (3.1). It should be noted that this matrix then needs to be permuted so that the columns are in the original order. For example, the result for the depth-first search is:

$$\boldsymbol{F}_{\boldsymbol{\ell}} = \begin{bmatrix} -1 & 1 & 0 & 1 & 0 \\ 0 & 1 & -1 & 0 & 1 \end{bmatrix} \tag{3.3}$$

(3.3) must be permuted such that the columns are in the original order as the reduced incidence matrix:

$$\boldsymbol{F'}_{\boldsymbol{\ell}} = \begin{bmatrix} -1 & 1 & 1 & 0 & 0 \\ 0 & 0 & -1 & 1 & 1 \end{bmatrix} \tag{3.4}$$

(3.4) shows that the two loops identified from the depth-first search are $\{1 \rightarrow 2, 2 \rightarrow 3, 1 \rightarrow 3\}$ and $\{2 \rightarrow 3, 2 \rightarrow 4, 3 \rightarrow 4\}$, where ± 1 indicates the directionality.

3.1.5 Selection of loops

The selection of loops in a graph can be critical when solving the system of equations in a multiphase flow solver. As will be explained later, selecting the smallest loops in a graph helps to reduce the number of nonzero entries in the Jacobian matrix, which increases the stability of the solver. Graphically speaking, this occurs when two chords are adjacent to a common node. When this occurs, one loop will then be a subgraph of the other loop, which results in one loop that is larger than necessary. This can be accounted for in a depth-first search by including a check at the end of the algorithm ensuring that no two chords have a common node.

3.2 ANALYSIS OF EQUATIONS VS. UNKNOWNS

Now that the equations for both Kirchhoff's first and second laws have been identified, it is necessary to compare the number linearly independent equations with the primary dependent variables. In single-phase flow, this is rather trivial, and the list can be seen in Table 2.1.In multiphase flow, additional variables need to be taken into account. In a multiphase network, the following primary dependent variables are present when no interphase transport of components is considered:

Number of unknowns	Unknown	Description
N_B	$\Delta P_{b,m}$	Mixture pressure drop in branch
N_n	$P_{n,m}$	Mixture pressure at node
N_b	$u_{b,m}$	Mixture volume flux (velocity) in branch
$N_p N_b$	$s_{b,i}$	Phase saturation in branch
$N_p N_b$	$f_{b,i}$	Phase fractional flow in branch
$N_p N_b$	$\rho_{b,i}$	Phase density in branch
$\boldsymbol{2N_b + 3N_p N_b + N_n}$		**Total**

Table 3.2: Primary dependent variables in a multiphase network

Note that in the multiphase network, there are $3N_P N_b - N_b$ extra variables than in the single-phase system. While the first three variables are the same as in the single-phase system, the last three should be defined. The phase saturation ($s_{b,i}$), which is also referred to as void fraction in a wide array of publications, can be defined as:

$$s_{b,i} = \frac{L^3 \; of \; i}{L^3 of \; V_{local}} \tag{3.5}$$

Note that this is the same definition given in Nagoo's thesis (Nagoo A. , 2013). Put qualitatively, $s_{b,i}$ is the fraction of a control volume in a branch that is occupied by phase

i at a given instant. In this work, and in the field of averaged-flow, the saturation that is of primary interest is the time- and area-averaged value, that is:

$$\langle\langle s_{b,i}\rangle\rangle = \frac{\int\int s_{b,i} dA dt}{\int dA \int dt} = \frac{L^3 \; of \; i}{L^3 of \; V_{branch}} \tag{3.6}$$

However, the brackets are often omitted for brevity and to eliminate clutter.

The second variable, phase fractional flow ($f_{b,i}$), can be defined as:

$$f_{b,i} = \frac{\langle u_{b,i}\rangle}{\langle u_{b,m}\rangle} \tag{3.7}$$

Where $\langle u_{b,i}\rangle$ is the area-averaged phase velocity and $\langle u_{b,m}\rangle$ is the area-averaged mixture velocity. This is also known as no-slip holdup or input concentration or delivered concentration, but is referred to as fractional flow in this work. The final variable is the component's density, which is the same as in single-phase networks but allows for additional components.

The same number of equations need to be included to have a well-conditioned problem.

Number of equations	Equation	Description
N_b	$\sum_{i=1}^{Nphases} f_{b,i} = 1$	Fractional flow unity equation
N_b	$\sum_{i=1}^{Nphases} s_{b,i} = 1$	Saturation unity equation
$(N_p - 1)N_b$	$s_{b,i} = f(f_{b,i})$	Saturation – fractional flow relationship
$N_p(N_n - 1)$ $= N_p(N_b - N_\ell)$	$\sum_{b=1}^{b_{adj,n}} dir_b \rho_{b,i} f_{b,i} u_{b,m} A_b = x_{n,i} m_i$	Mass Balance relationship around node, where $b_{adj,n} \subset b \mid b\ adjacent\ to\ n$
N_b	$\frac{\Delta P_{b,m}}{\Delta L} = \tau_w + \rho_{b,m} g sin(\theta) - \frac{\sum G_i \Delta\left(\frac{G_i}{\rho_i s_i}\right)}{\Delta L}$	Mixture momentum balance
$N_p N_\ell$	$\sum_{b=1}^{b_\ell} s_{b,i} \Delta P_b = 0$	Kirchhoff's second law
N_b	$\rho_{b,m} = \sum_{i=1}^{Nphases} s_{b,i} * \rho_{b,i}$	Definition of mixture density
$N_p N_b$	$\rho_{b,i} = f(P, T)$	EOS density calculation
$N_b - N_\ell$ $= N_n - 1$	$\Delta P_{b,m} = P_{n,m} - P_{(n-1),m}$	Definition of pressure drop
$\boldsymbol{2N_b + 3N_pN_b + N_n - 1}$		**Total**

Table 3.3: Independent equations to solve the multiphase network problem

While the first two equations are straightforward, the third deserves a bit more explanation. As shown in Nagoo's thesis, the basic tenant of the work is that the saturation of a phase can be described as a function of the phase's fractional flow. The function used to express

this depends on the flow characteristics. For example, the simplest one is the no-slip relationship, which states:

$$s_{b,i} = f_{b,i} \tag{3.8}$$

Simply put, this relationship states that the *in situ* phase velocities are equal to their phase volume fractions, implying there is no slip between phases. Of course, this type of flow occurs only under limited circumstances, and hence is not applicable in most situations. A review of existing volume fraction/fractional-flow relationships can be found in Woldesemayat and Ghajar (Woldesemayat & Ghajar, 2007). This work incorporates the same relationships present in Nagoo (Nagoo A. , 2013).

The next two equations are the conservation of mass and momentum equations, respectively. The conservation of mass equation is quite straightforward: there are N_P mass balances per node less the one overall mass balance (assuming single-component phases with no mass transfer). The conservation of momentum equation becomes increasingly more complicated with the addition of another phase. While there are several multiphase flow closure relationships for conservation of momentum, this work uses those employed by Nagoo, and assumes a mixture model for the wall shear term (Nagoo A. , 2013). The final term, the inertial or convective acceleration term, deserves additional discussion.

To account for changes in density, two density models are used. For incompressible fluids, density is assumed to be constant or changing by a set compressibility factor. The form of this equation is:

$$\rho_{b,i} = \rho_{b,io} e^{(P_b - P_{io})K} \tag{3.9}$$

Where $\rho_{b,io}$ is the reference density for the given phase, P_b is the branch's pressure, P_{io} is the reference pressure (usually atmospheric), and K is the compressibility factor, in units of inverse pressure. Equation (3.9) is especially important in oils where the compressibility can change the density appreciably. For gases, the ideal gas law can be used alone or with the gas deviation factor, Z. This equation is:

$$\rho_{b,i} = \frac{P_b M_w}{ZRT} \tag{3.10}$$

Where M_w is the average molecular weight, Z is the gas deviation factor, R is the gas constant, and T is the temperature. To calculate Z, the Dranchuk-Kassem equation is used (Dranchuk & Abu-Kassem, 1975). This equation takes the form:

$$\begin{aligned} Z = 1 &+ \left(0.3265 - \frac{1.07}{T_r} - \frac{0.5339}{T_r^3} + \frac{0.01569}{T_r^4} - \frac{0.05165}{T_r^5}\right)\rho_r \\ &+ \left(0.5475 - \frac{0.7361}{T_r} + \frac{0.1844}{T_r^2}\right)\rho_r^2 \\ &+ 0.1056\left(-\frac{0.7361}{T_r} + \frac{0.1844}{T_r^2}\right)\rho_r^5 \\ &+ 0.6134(1 + 0.721\rho_r^2)\left(\frac{\rho_r^2}{T_r^3}\right)e^{-0.721\rho_r^2} \end{aligned} \tag{3.11}$$

where $\rho_r = 0.27\left(\frac{P_r}{ZT_r}\right)$, T_r is the reduced temperature ($T_r = T/T_{pc}$), P_r is the reduced pressure ($P_r = P/P_{pc}$). The pseudo-critical values for pressure and temperature are defined here as:

$$T_{pc} = \begin{cases} 157.5 + 336.1S_G & |S_G < 0.55 \\ 170.491 + 307.344S_G & |0.55 \leq S_G \leq 1.7 \end{cases} \tag{3.12}$$

$$P_{pc} = \begin{cases} 690.0 - 31.0S_G & |S_G < 0.55 \\ 709.64 - 58.718S_G & |0.55 \leq S_G \leq 1.7 \end{cases} \tag{3.13}$$

where S_G is the specific gravity of the gas. These equations come from the American Gas Association and work done by Hankinson et. al. (Saleh, 2002) (Hankinson, Thomas, & Phillips, 1969).

As this work takes the averaged-flow approach, there remains only one momentum balance for the entire mixture. The consequence of this is that another equation set must be specified in order to have a well-conditioned system. Two-fluid systems have the benefit of having an additional momentum equation for each phase, which leads to a formulation not unlike the single-phase formulation, albeit with the need for two boundary conditions instead the one needed in single-phase flow. The extra set of equations in this work comes from Kirchhoff's second. This equation can be written as:

$$\sum_{b=1}^{b_\ell} s_{b,i} \Delta P_b = 0 \tag{3.14}$$

Equation (3.14) expands upon Kirchhoff's second law by stating that sum of pressure changes *for each phase* is zero around a loop. As shown in Nagoo's work, a phase's pressure can be defined as:

$$P_i = s_i P_m \tag{3.15}$$

where P_i is the phase's pressure and P_m is the mixture pressure (Nagoo A. , 2013). A phase's individual pressure is often moot in averaged-flow formulations, and indeed is relevant only in decoupled (segregated) flows (Nagoo A. , 2013). However, equation (3.14)

is still a logical stipulation and extension of Kirchhoff's second law as only one mixture pressure can be present in one location, and likewise a phase can have only one individual pressure in one location. With this stipulation, the variables are balanced by the equations and the system is well conditioned.

One last point in this formulation is the complexity that loops cause. While here we see that loops complicate the degrees-of-freedom analysis, we will also see how loops complicate the numerical stability and solution space of the multiphase network problem. Indeed, conventional flow simulation software and even an eager engineer can evaluate a network *without loops*, as the mass balances solve the direction of flow in each branch *a priori*.

3.3 PROGRAM DESIGN

In order to systematize the workflow of solving multiphase flow in networks, an executable program has been written in C++. This program can be broken into three main components: input, computation, and output. A more in-depth explanation of the input and output can be found in Appendix B. The computational portion will be explained more here.

After reading all data from the input file, first the loops in the network are identified, taking care to select the small loops. This work uses Intel's MKL linear algebra library to invert the reduced tree incidence matrix using an armadillo shell. With all necessary information, the program then sets up all the equations in the Newton-Raphson solver. This work uses the globally-converging Newton-Raphson method presented in *Numerical Recipes in C++*, second edition (Press, 2002). This solver uses preconditioning and partial

pivoting to increase both stability and computation time. Figure 3.3, below, shows a flowchart for the program.

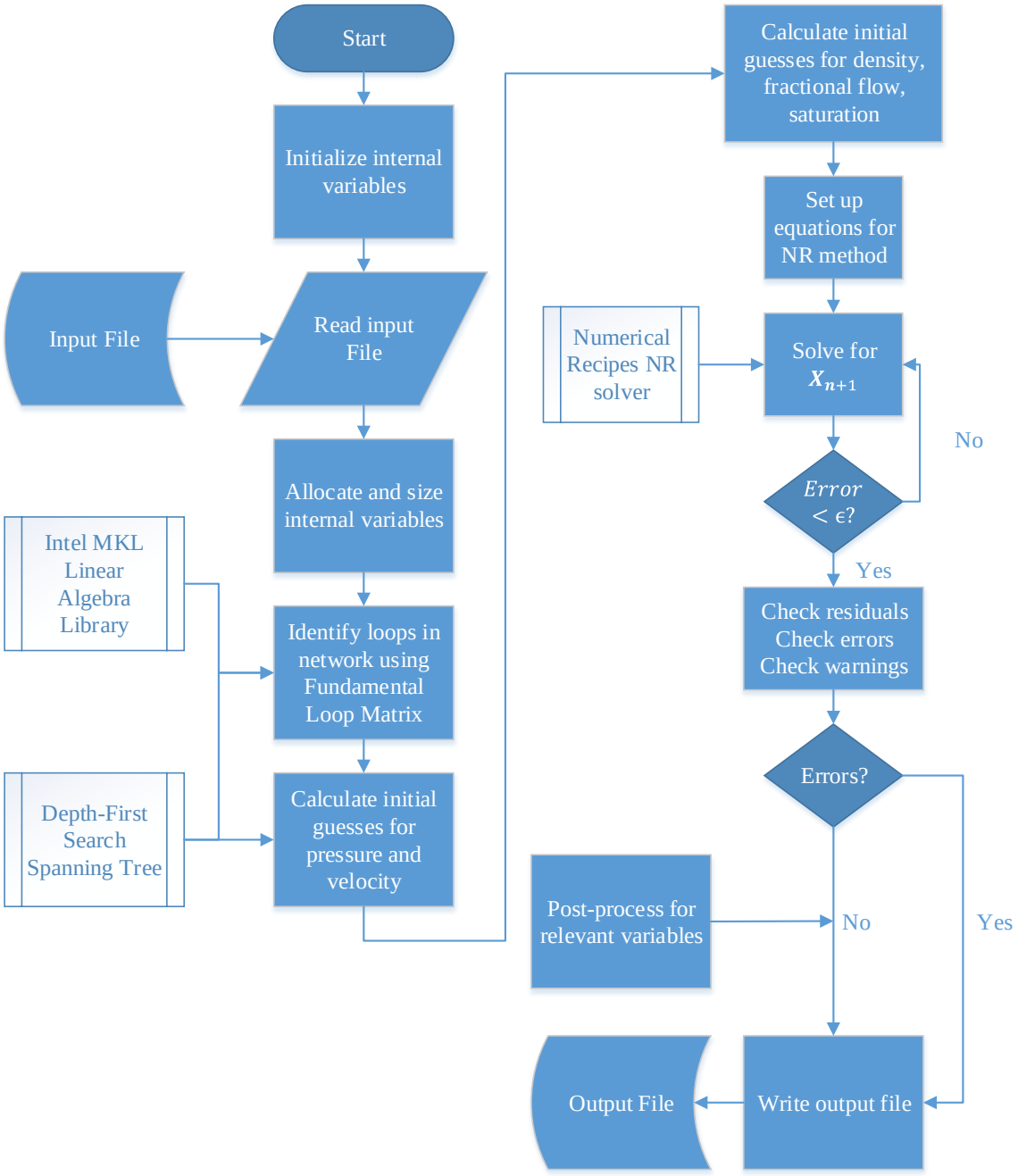

Figure 3.3: Flowchart of multiphase network solver

As the initial guesses are crucial in Newton-Raphson methods, it is important to have a systematic approach to having accurate initial guesses. For pressure, one simple method is to initialize all node pressures to the pressure given as a boundary condition. While this is a viable strategy in simpler networks, it is untenable in larger and more complicated ones. To address this, the program asks the user for an additional pressure guess at another node. With the length of each branch known, this gives an implied pressure gradient that can be applied to the network at large, via the spanning tree.

For example, given the network in Figure 3.1A, if we assume the given pressure at node 1 is 350 psia, and the pressure guess at node 4 is 300 psia, the spanning tree can give an estimate for the other two nodes. Assuming each branch is 4000 ft, this results in a pressure gradient of $0.004\frac{psia}{ft}$. This can then be used to calculate the pressures at nodes 2 and 3.Figure 3.1: Sample graph (A) and its minimum-weighted spanning tree (B)

Initial guesses for the velocities in the branches is set as the average of the two external flow rates at the nodes connecting the branch. If both are zero, then the average of all external flow rates for the entire network. The direction of flow is determine by the adjoining node's flow rates, and when both are zero, the direction given by the incidence matrix is assumed.

In highly looped networks, it is also possible that these initial guesses are not adequate. For this case, the proposed method is to solve the spanning tree of the given network. While the additional branches in the looped network will, of course, cause

changes when compared to the analogous unlooped network, the solution found in the unlooped case results in a far better initial guess in the looped case.

Chapter 4: Multiphase Network Solver Validation and Benchmarking

In order to validate the formulation presented in Chapter 3, it is important to compare the results obtained from the model with published data sets and solution sets. While there are numerous examples of fluid flow in single conduits, experiments on networks is scarce. Despite this lack of network data, other published solutions exist to verify existing models, especially in single-phase flow. To validate multiphase, looped network cases, comparisons are made to existing software. For additional instructions on how to execute the program, see Appendix B. Instructions on how to properly create an input file are found in B.1, and an explanation of the output file can be found in B.2.

4.1 Incompressible Single-Phase Pipe

As any modeler is aware, model validation works best when testing a model against the most simplistic cases first. After the model has been properly validated against simple cases, additional complications can be considered with the confidence that the foundation is validated.

With this in mind, the multiphase network solver presented in this work is first tested in the simplest case: incompressible single-phase flow in a single conduit. While this may seem trivial, it serves as the basis for more complicated cases.

An exhaustive set of experiments on multiphase flow are performed in Sunil Kokal's PhD thesis from the University of Calgary in 1989 (Kokal, 1989). As it is common in multiphase flow literature, the experimenters calibrated and validated their experimental rig using single-phase flow at first. This allows the experimenters to match their

experimental values against published data and existing correlations.

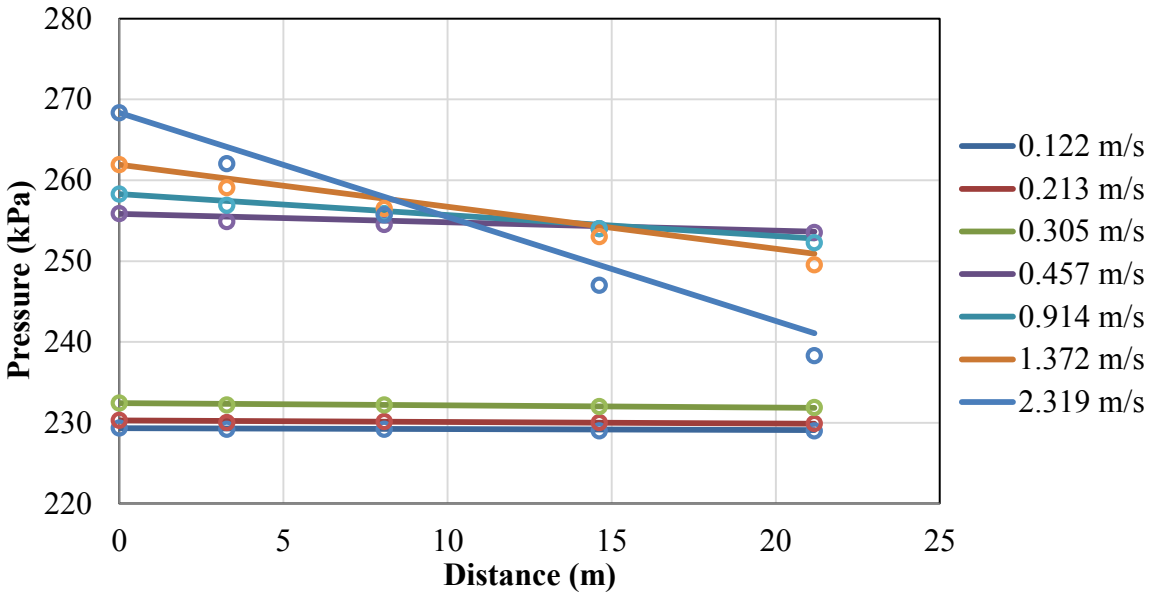

Figure 4.1: Incompressible, single-phase pipe calculated (lines) versus experimental (points) at different distances for increasing fluid velocity. Data from *An Experimental Study of Two-Phase Flow in Inclined Pipes* (Kokal, 1989).

Figure 4.1 presents data from Kokal's thesis against results obtained from the multiphase network solver. These data are obtained from oil ($\rho_o = 858\frac{kg}{m^3}, \mu_o = 7mPa \cdot s$) flowing through a circular pipe of 1" diameter and 25m length and no inclination. The average temperature is $23°C$ and the pressure ranges from 230-270kPa. In this scenario, only the wall shear transfer coefficient is being tested against the data as the hydrostatic term is nil.

As seen in Figure 4.1, the solver correctly explains the pressure decline due to wall shear along the length of the pipe (as displayed by the x-axis). Furthermore, it can be seen as the oil velocity is increased, that there is a marked change in the pressure gradient as the

fluid flow transitions from laminar to turbulent, which occurs from $0.305\,m/s$ to $2.319\,m/s$.

4.2 Incompressible Single-Phase Fluid Flow in a Network

Next, the multiphase network solver is tested against a base case for incompressible fluid flow in a network. While the first test validates the pressure drop equation in single-phase cases, this test is intended to test the model against Kirchhoff's first and second laws. A case is presented in Jeppson's 1976 textbook on pipe networks (Jeppson, 1976). This network can be seen below:

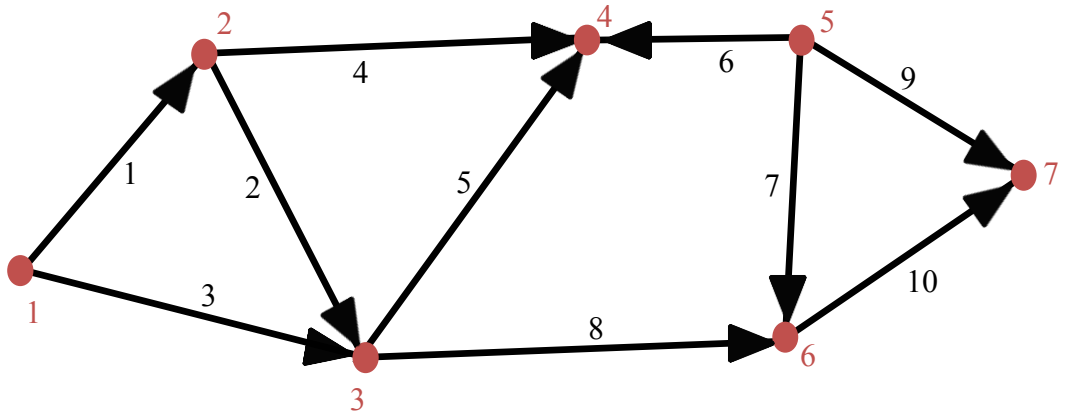

Figure 4.2: Single-phase pipe network used in Jeppson (Jeppson, 1976).

Additionally, the following boundary conditions are specified:

Junction	Demand (gal/min)
1	2000
2	-300
3	-900
4	-500
5	1500
6	-800
7	1000

Table 4.1: Junction demands

Branch	Length (ft.)	Diameter (in.)	Hydraulic Roughness (in.)
1	1600	18	0.0102
2	2000	15	0.0102
3	2400	18	0.0102
4	1800	12	0.0102
5	1900	12	0.0102
6	1300	10	0.009
7	1700	15	0.0102
8	2000	18	0.009
9	1200	24	0.0102
10	1800	15	0.0102

Table 4.2: Branch parameters

Table 4.1 and Table 4.2 give the parameters necessary to specify the system. The simulation also assumes that the fluid is water at $68°F$ and that there is no inclination in the system.

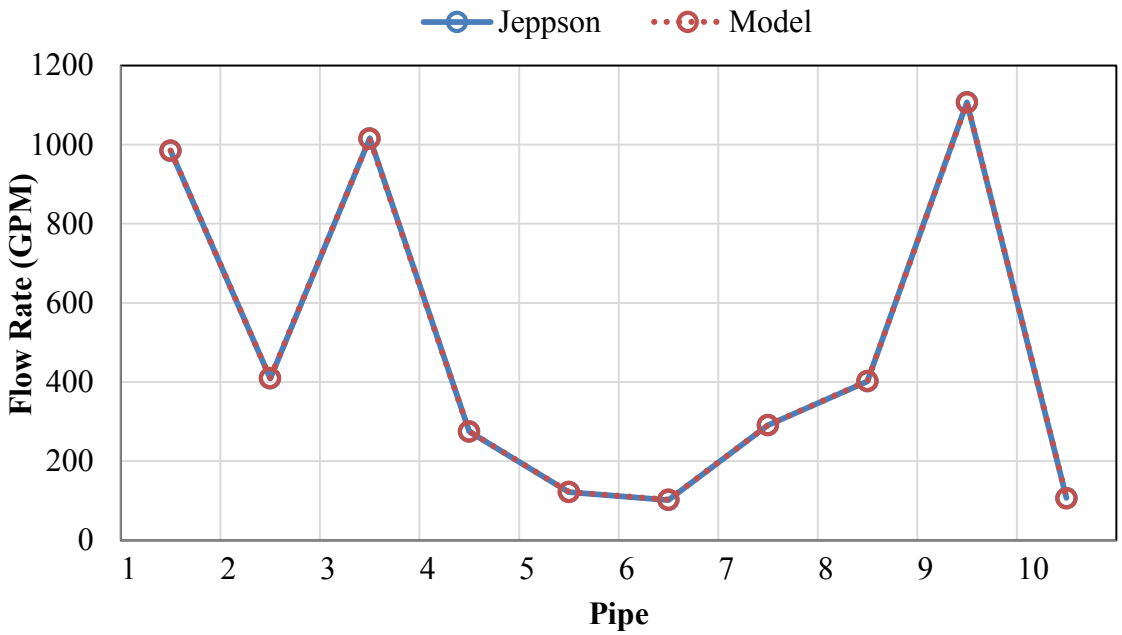

Figure 4.3: Calculated vs. reference (from Jeppson) flow rates in branches of the network in Jeppson (Jeppson, 1976).

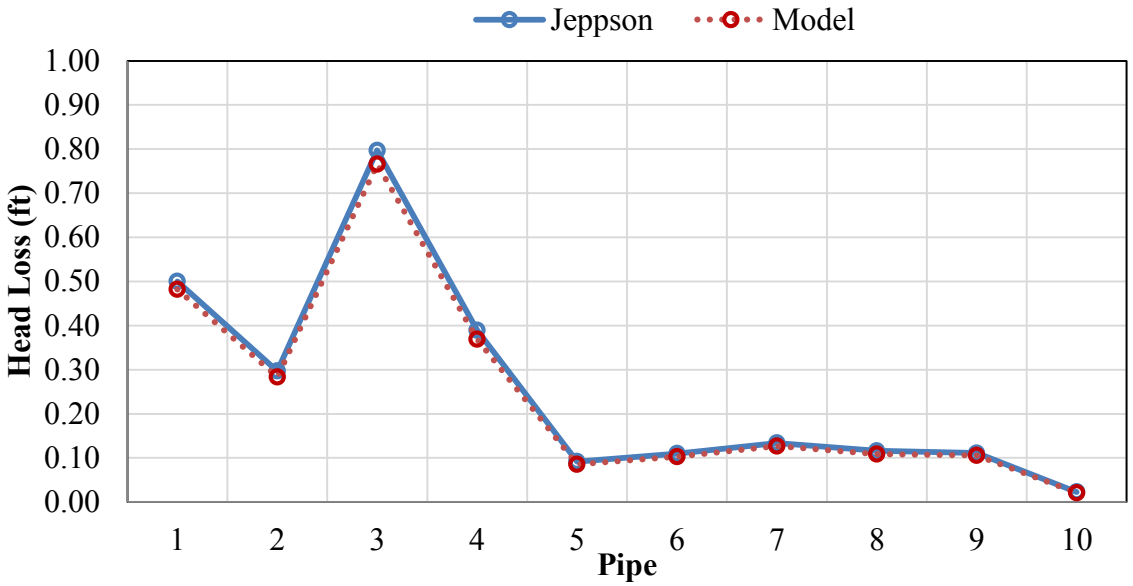

Figure 4.4: Calculated vs. reference (from Jeppson) pressure drops in branches of the network in Jeppson (Jeppson, 1976).

Figure 4.3 and Figure 4.4 show the calculated results against the reported results in Jeppson's textbook. It is evident that the results from our simulations do not appreciably differ from the published values, and indeed, the average error is 0.2 percent in the branch flow rates, and 6 percent in the head losses. While 6 percent may seem quite large, the magnitude of the actual pressure drops are low—on the order of thousandths of a psi, which is well within engineering precision. Additionally, the results obtained in Jeppson's example were obtained using LTM, whereas the model presented here is solved using a Newton-Raphson technique. As stated earlier, these results can only be compared to themselves—there are no ground truth measurements—as experimental results for network flow are uncommon.

4.3 COMPRESSIBLE SINGLE-PHASE PIPE

Continuing with model validation, the next step taken is compressible single-phase flow in single conduits. When compared to incompressible fluids, compressible fluids have the added complication of having the density be a function of pressure. This validation will, of course, test the actual density calculations in the solver and also the solving scheme. In the case of incompressible flow, branch values, such as flow rates and pressure drops, can be solved without considering node values, namely pressure. As the absolute pressure is inconsequential in incompressible calculations, it is paramount in compressible flow. Two cases were considered here: hydrostatically-dominated flows and friction-dominated flows. A hydrostatically-dominated flow was first considered as the hydrostatic term aids in the solver stability (Nagoo A. , 2013).

4.3.1 HYDROSTATICALLY DOMINATED

A gas well belonging to Marathon Oil Co. in the Camacho field is reported in a 1970 paper (Camacho). In the paper, the authors present data on how the bottom-hole pressure and wellhead pressure change with an increasing gas flow rate. The internal diameter is 2 inches, the depth, or in solver terms branch length, is 5790 feet, the specific gravity is 0.604, and the hydraulic roughness is 0.000 045 inches.

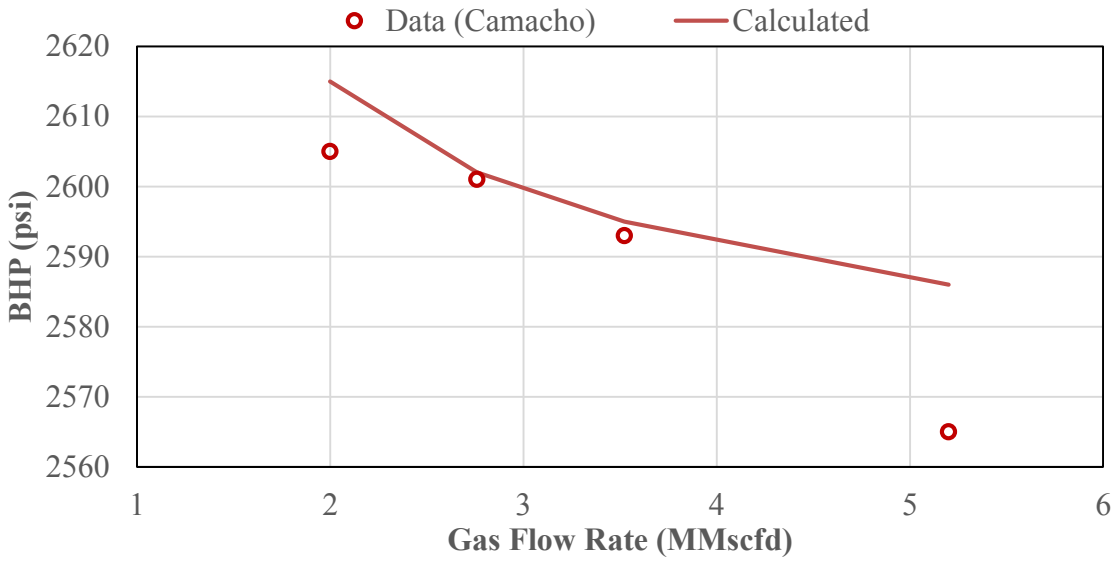

Figure 4.5: Calculated vs. experimental (from Camacho) bottom-hole pressures (BHP) at different flow rates (Camacho).

Figure 4.5 shows calculated pressures with measured pressures, and the average error found is 0.3 percent. As the data presented in the article is field data, it should also be noted that the data are not as well controlled as in a laboratory experiment.

This test also validates how the solver handles boundary conditions. It is commonplace in many commercial solvers to specify where a given boundary condition must be given, such as at a flow entrance. However, this is often not known *a priori*. This is the case in many oil & gas applications, where wellhead pressure is known and bottom-hole pressure is desired. Instead of using a solver iteratively to solve for BHP, the solver presented in this work can solve for it implicitly, which is simpler and more efficient.

4.3.2 Friction Dominated

Another work presented in 1964 gives a large diameter, cross-country pipeline (Hannah, 1964). Similar to the hydrostatic case in 4.3.1, the pressure-dependence of the

density—and the z-factor calculation—and its effects on the convergence are tested. While this case has minor elevation changes, it is readily seen that the frictional pressure gradient is much greater than the hydrostatic pressure gradient.

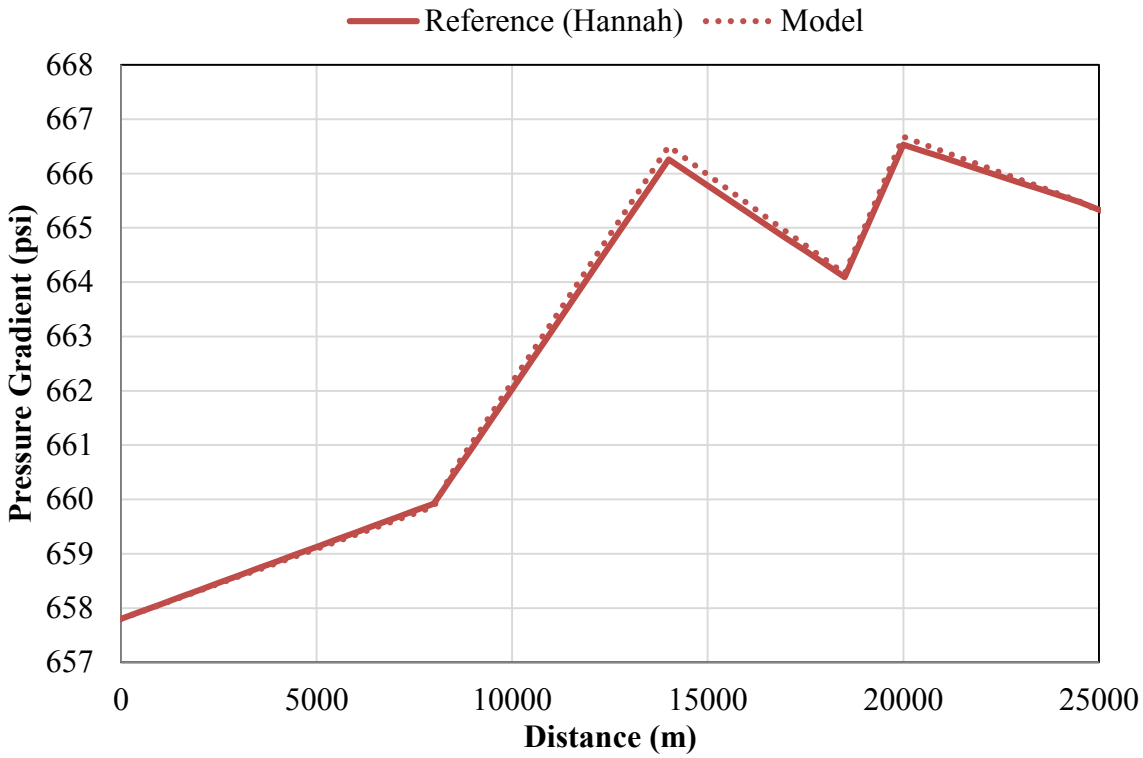

Figure 4.6: Calculated versus reference pressure profile in Hannah's paper on the NX-37 pipeline at varying distances from the outlet (Hannah, 1964).

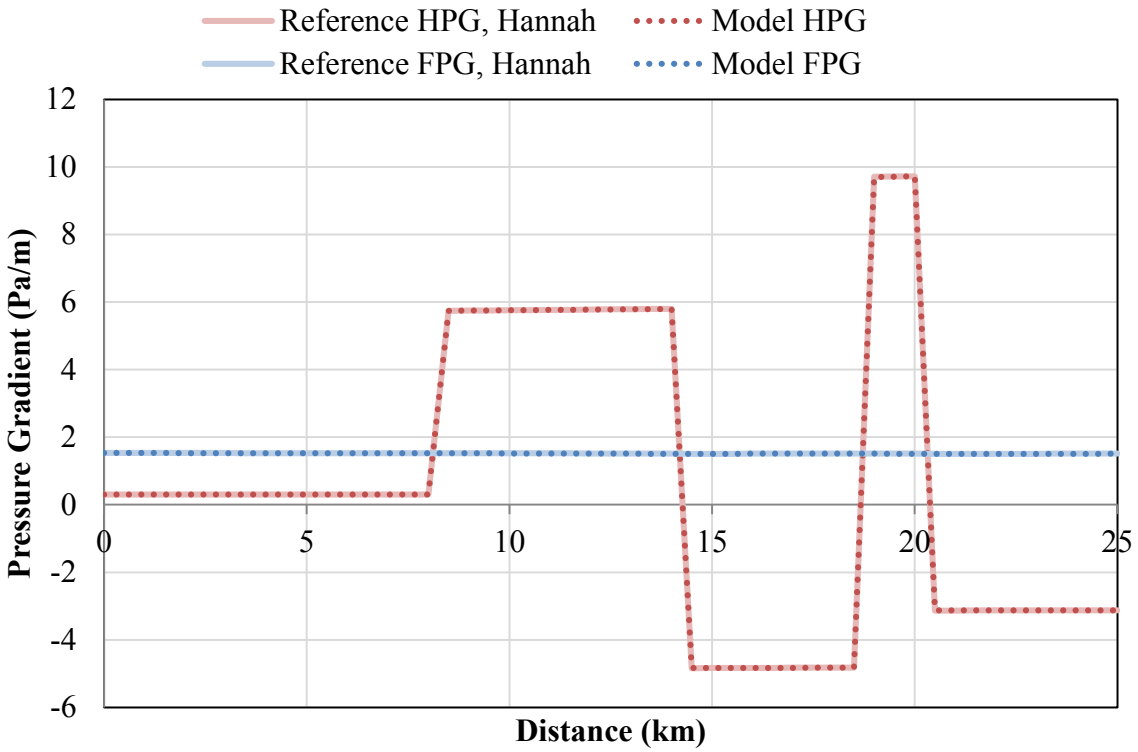

Figure 4.7: Calculated vs. reference frictional pressure gradient (FPG) and hydrostatic pressure gradient (HPG) in Hannah's paper on the NX-37 pipeline at varying distances from outlet (Hannah, 1964).

Figure 4.6 and Figure 4.7 show the multiphase network solver's results against the reported values. The maximum error calculated between the reported and modeled pressures along the pipeline is 1.6 percent, and the maximum error in the frictional pressure gradient is 0.5 percent.

4.4 Compressible Single-Phase Fluid Flow in a Network

The next step in validating the multiphase network solver is to examine a case of compressible flow in looped networks. While experimental data on the topic is limited, a paper written by Greyvenstein and Laurie presents a solution to the network in Figure 4.8,

below. The authors arrived at their solution by using a CFD approach to solve the Navier-Stokes equations. The authors assumed the ideal gas law, and a constant temperature of $15°C$. A pressure of 6 bars is assumed at junction 1, and hydraulic roughness is assumed to be 0 for all branches.

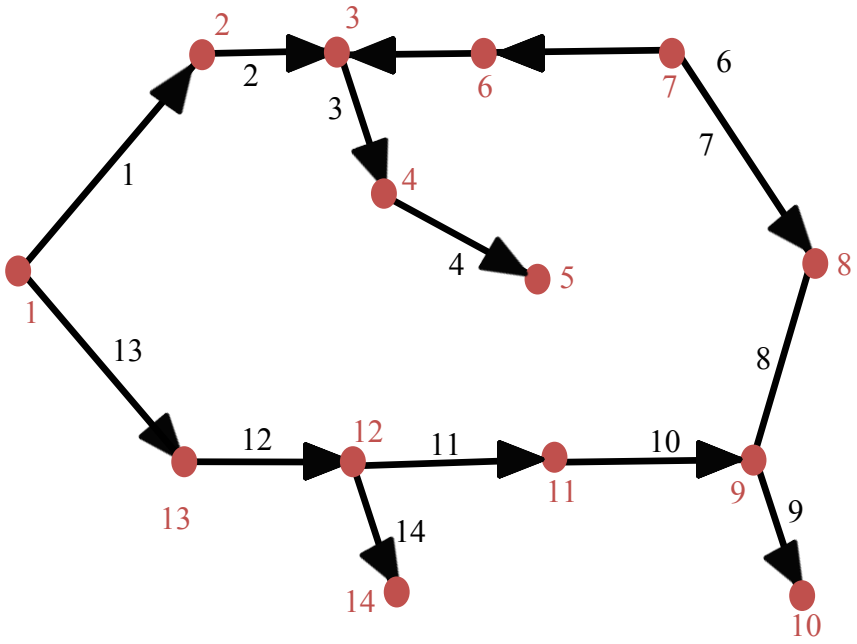

Figure 4.8: Network for compressible network validation (Greyvenstein & Laurie, 1994)

In obtaining the results, the authors used the following external demands:

Junction	Demand (kg/s)
1	0.016461
2	-0.00444
3	-0.00382
4	-0.00178
5	-0.00159
6	-0.00444
7	0.016461
8	-0.00414
9	0
10	-0.0028
11	-0.00299
12	0
13	-0.00414
14	-0.0028

Table 4.3: External demands specified in Greyvenstein and Laurie

Additionally the following lengths and diameters are assumed:

Branch	Diameter (m)	Length (m)
1	0.01588	400
2	0.01588	400
3	0.01	100
4	0.01	100
5	0.01588	400
6	0.01588	400
7	0.01588	400
8	0.01588	400
9	0.01	100
10	0.01588	400
11	0.01588	400
12	0.01588	400
13	0.01588	400
14	0.01	100

Table 4.4: Branch diameters and lengths used in CFD simulation

The authors compared their results to results obtained using the Hardy Cross method and LTM, which all converged to the same solution, albeit at a different number of iterations. The results obtained from our multiphase network solver can be compared to the reported values in Figure 4.9 and Figure 4.10.

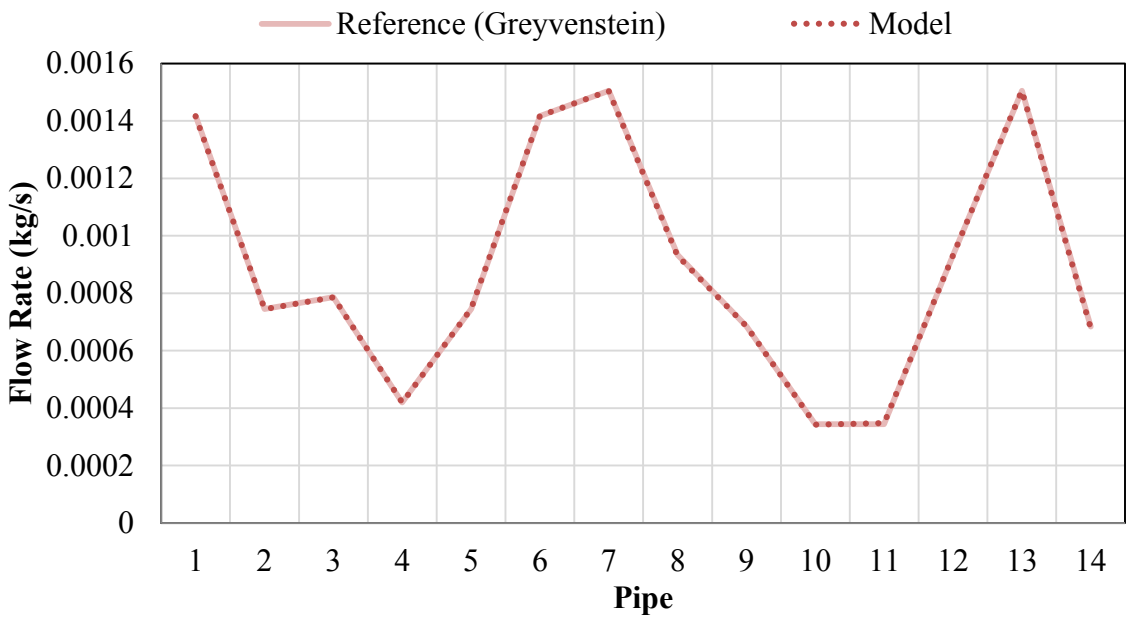

Figure 4.9: Calculated vs. reference mass flow rates (from Greyvenstein and Laurie) in different pipes from network in Figure 4.8 (Greyvenstein & Laurie, 1994).

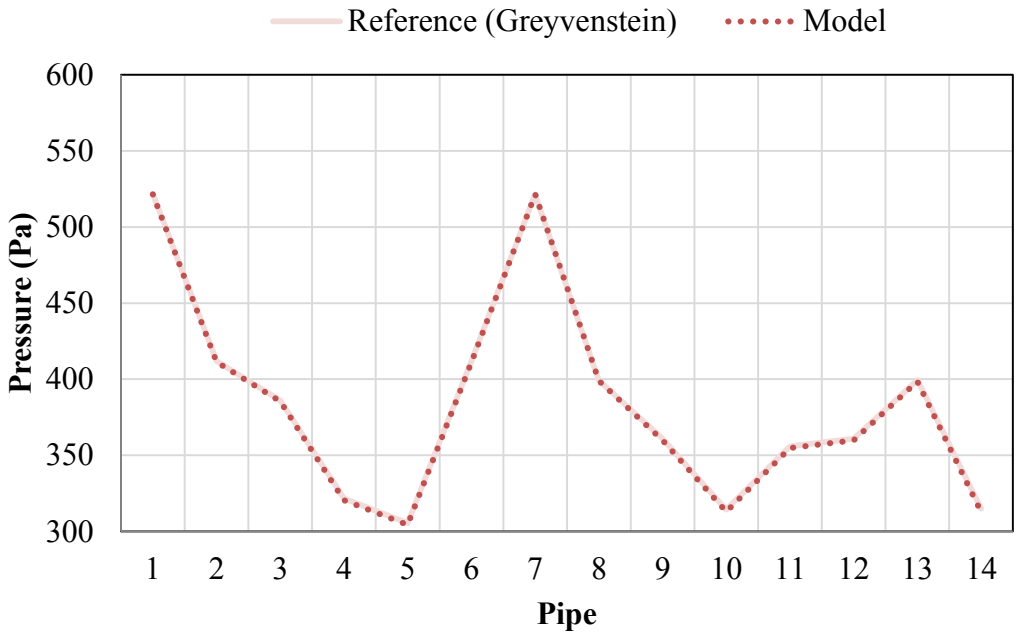

Figure 4.10: Calculated vs. reference pressures (from Greyvenstein and Laurie) in different nodes from network in Figure 4.8 (Greyvenstein & Laurie, 1994).

4.5 Multiphase Flow in Pipes

The addition of a second phase poses a challenge both in terms of physics and convergence. Additional equations need to be taken into account in order to fully describe the system at hand, and additional parameters need to be specified by the user. In order to properly validate these equations, first a single conduit is considered. This tests the additional physics—void fraction relationships in this formulation—and the nonlinearities present from density calculations in compressible phases. Of course, this phase of validation could be exhaustibly long. A large discipline of multiphase flow is to capture the physics present in one dimensional flow. Instead, the goal of this phase is to properly calculate existing relationships in the context of the large system of equations.

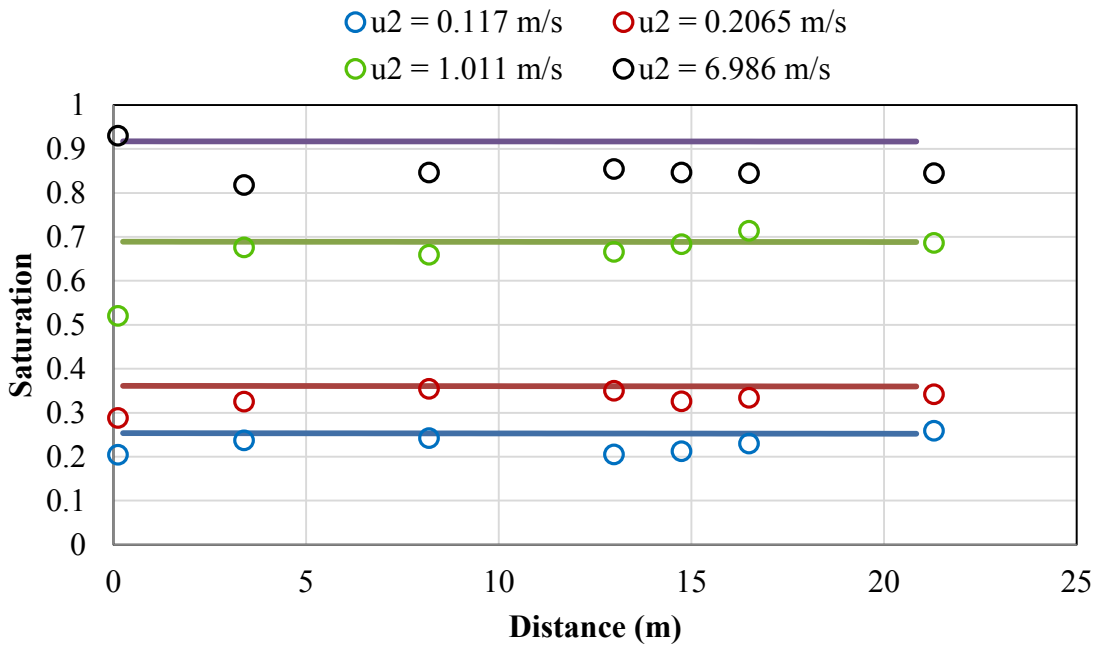

Figure 4.11: Calculated (lines) and experimental (points) gas saturation versus distance at different gas volume fluxes. Lines result from Woldesmayat and Ghajar void fraction relationship (Woldesemayat & Ghajar, 2007) coupled with the multiphase network solver, and points are data from Sunil Kokal's work in multiphase flow in inclined pipes (Kokal, 1989).

As can be seen in Figure 4.11, the void fraction relationship used accurately scales with the increase of gas volume flux. As the fractional flow of gas increases, an increase in the gas saturation is observed.

4.6 Multiphase Flow in Pipe Networks

The final validation is to look at multiphase flow in looped networks. The other validation steps are routinely handled by commercial solvers on the market. Incompressible flows in networks are often evaluated for municipal water distribution systems using EPANET, which is a public-domain solver developed by the Environmental Protection Agency. Compressible flow in networks is commonly evaluated in gas distribution systems. Systems like GASWorkS and Synergi are two commercial packages intended to handle gas distribution systems. To evaluate multiphase networks, more sophisticated software is necessary. Currently, Schlumberger's PIPESIM and LedaFlow have modules to solve for multiphase flow in looped networks. Petroleum Experts has a module called GAP intended for networks, but its solver does not work for looped systems.

4.6.1 Solution Validity and Uniqueness

Due to the scant data on reported solutions to multiphase flow in networks, results obtained from the multiphase network solver are compared to commercial solvers and a more rigorous inspection of the solution is required. One common measure of the validity of the solution obtained is the latest iteration's variable value compared to the previous iteration's value. A large discrepancy indicates that the solution is unstable, but not necessarily indicative of an inaccurate solution. This can occur when the chosen step size

is too large, and while the search direction (gradient) is correct, the distance travelled to the next iteration is not.

Another measure of a solution's validity is the residuals of the equations. It may seem trivial to say that the solution, or more precisely *a solution*, to a given system occurs when the variables satisfy the equations to within a certain tolerance. It is true that a solution exists when all equations are satisfied, but a mathematical solution is not always a physical one. An example would be the van der Waals equation.

$$Pv^3 - (RT + Pb)v^2 + av - ab = 0 \tag{4.1}$$

Equation (4.1) has three roots. When $T > T_c$, there is one real root, and two roots containing negative or imaginary numbers (Koretsky, 2004). These other two roots are mathematical artifacts with no physical basis.

Moreover, a solution can be an artifact of the function itself used to describe the phenomena at hand. Looking at the van der Waals example again, this occurs when $T < T_c$. Here, three real, positive roots exist (Koretsky, 2004). The lowest root is assumed to be the molar volume of the liquid phase, the highest root is assumed to be the gas phase. The middle root is excluded when $\frac{dP}{dv} > 0$ (Koretsky, 2004). Such a root violates Boyle's law, which states that pressure and volume are inversely proportional. When this is the case, the discontinuity eludes description by the van der Waals equation (Koretsky, 2004).

Other times a solution could be physically possible but not the steady state solution. In production engineering, a vertical lift performance curve can intersect the inflow performance curve twice—once at a higher pressure and once at a lower pressure. The

higher pressure solution is often said to be the solution during a transient period. As a well is being drawn down, the bottom-hole pressure decreases until the lower, constant pressure is seen.

Given these limitations, it is important to be mindful of any solution given for multiphase flow in looped networks. Indeed, more work needs to be done in this problem, especially research into the problem's solution space. While the author has not done work into this directly, it is suspected that looped networks add a degree of non-uniqueness to the solutions that is unseen in networks without loops. This insight also adds value to the manifold problem. If non-unique solutions are present in loops networks due to mathematical or functional artifacts, having a physically-based solution adds confidence to a solution found by the solver.

4.6.2 EXAMPLE

To illustrate the issues present in multiphase flow in looped networks, consider the familiar network in Figure 2.1. The elevation of each node is assumed to be equal, which results in a friction-dominated system. Often in multiphase flow, horizontal orientation can cause discontinuities in the void fraction profile and create numerical instabilities (Nagoo A. S., 2003). This is used to illustrate issues in solutions found from the multiphase network solver. For this example, all branch lengths are assumed to be 100ft., and all branch diameters are assumed to be 12 inches. Hydraulic roughness is assumed to be 0.000 045 inches. The gas specific gravity is 0.604 (natural gas), and the inlet mass fraction is 23 percent gas. The Woldesmayat and Ghajar void fraction relationship is assumed, the inlet pressure is 350 psia and the system temperature is 323 K.

The nodal demands are:

Junction	Demand (kg/s)
1	8.0
2	-2.0
3	-4.0
4	-2.0

Table 4.5: Nodal demands for multiphase network example

From this example, various solutions were obtained by varying the initial guesses.

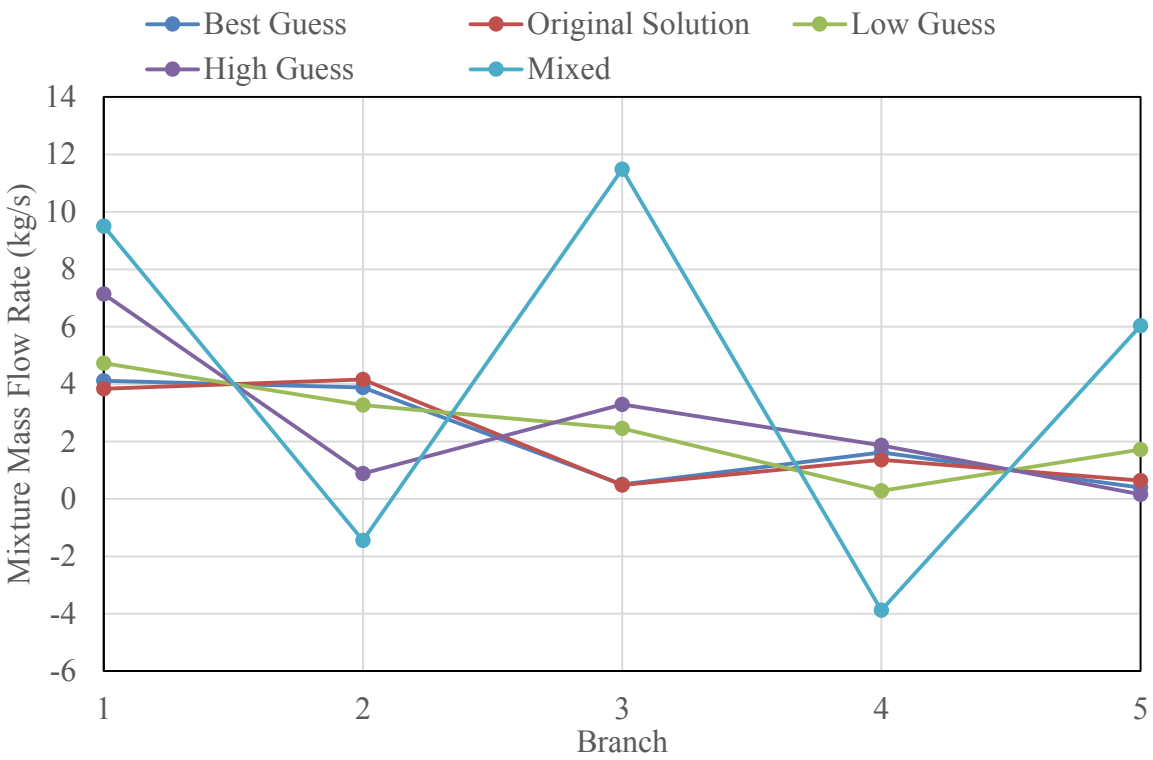

Figure 4.12: Mixture flow rates at branches for different initial guesses

Figure 4.12 gives the flow rates in the different branches for the problem presented here. The original solution is the solution obtained by the algorithm described in Section

3.3, and the best solution is found by manually adjusting the initial guess based on the results found in the original solution to find the lowest average equation residual (show below in Figure 4.13). The high guess and the low guess solutions were obtained by multiplying and dividing the initial guesses in the original algorithm by 10, respectively. The "mixed" solution was found by multiplying the initial guess of the water phase's velocity by 10 and dividing the initial guess of the gas phase's velocity by 10. To see the full output files, see Appendix C. The solutions found with the largest residuals are also overstated from an engineering perspective, as the only function residuals larger than 0.1 are pressure equations, and as all residuals are reported in SI units, a 1 Pa discrepancy is trivial in most engineering applications.

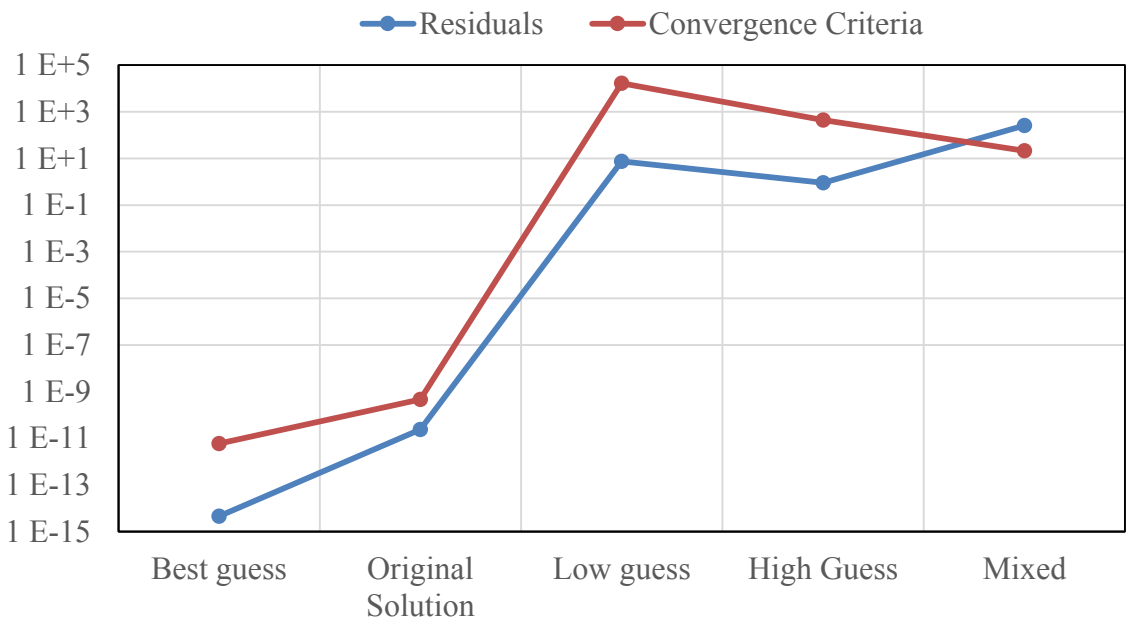

Figure 4.13: Function residuals and convergence criteria for solutions presented in Figure 4.12.

Figure 4.13 reports the functional residuals and convergence criteria for the solutions presented above. An important distinction should be made between the functional residuals and the convergence criteria. While the residuals quantify the accuracy of a solution, the convergence criteria, which is the average difference between the past iteration's solution and the current iteration's solution, can be said to describe the stability of the solution. A helpful analogy would be to consider a sewing pin standing vertically. While there exists an equilibrium for this state, the slightest perturbation can disrupt it. Similarly here, a stationary point may be found in a multiphase network that is a solution, but it may not be physically realizable because it is too unstable.

From this simple example it should be apparent that there does not exist a simple, cut-and-dry answer to looped multiphase networks. Inspection of a given solution is necessary in order to have the confidence necessary to rely upon it for engineering decisions. For example, one reason to discount the "mixed" solution is to consider the largest mixture flow rate found in the solution. While the solution has a mixture flow rate of almost $12\,\frac{kg}{s}$ in the 3rd branch, the only input into the network from the first node is $8\,\frac{kg}{s}$. It is suspect that one branch is flowing at a rate higher than the total supply into the network. This could be the result of transients from a higher supply into the network, but then that is the answer to a different question. In addition to the functional residuals, the suspicious flow rate in the third branch raises doubt about the physicality of the solution.

4.6.3 BENCHMARKING

Due to the scarcity of published results in multiphase fluid flow in networks, it is also important to consider the validity of the solutions obtained from the solver presented here with the results of other solvers. For single phase networks, EPANET and PIPESIM are used, and for multiphase networks, PIPESIM is used.

4.6.3.1 Single Phase Network

The network discussed in Section 4.2 is modeled using PIPESIM and EPANET. As EPANET can only model incompressible flows, water is assumed to be the fluid. Figure 4.14 and Figure 4.15 present the flow rates and pressure drops found by the various solvers, and Figure 4.16 presents the average equation residuals (mass balance and Kirchhoff's second law equations).

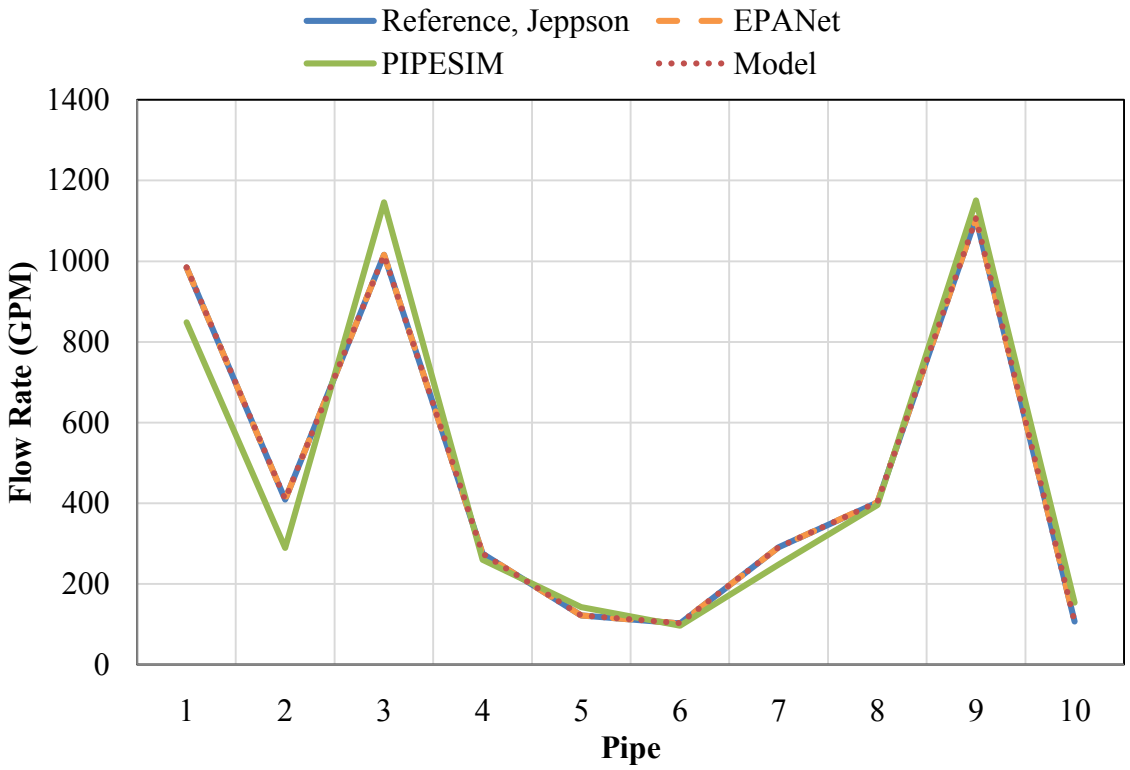

Figure 4.14: Simulated vs. reference (from Jeppson) flow rates in branches of the network in Jeppson (Jeppson, 1976).

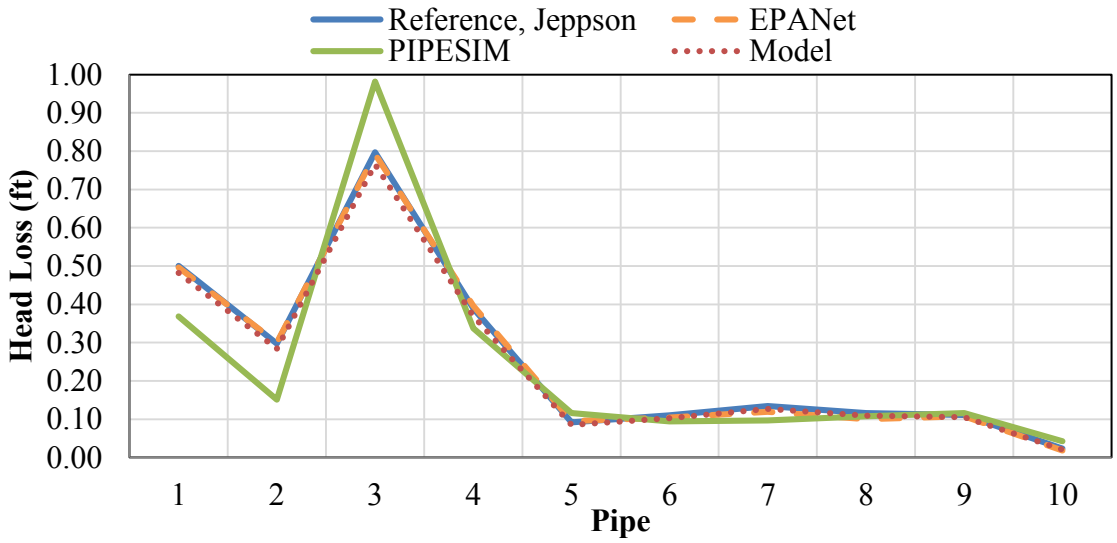

Figure 4.15: Simulated vs. reference (from Jeppson) head losses in branches of the network in Jeppson (Jeppson, 1976).

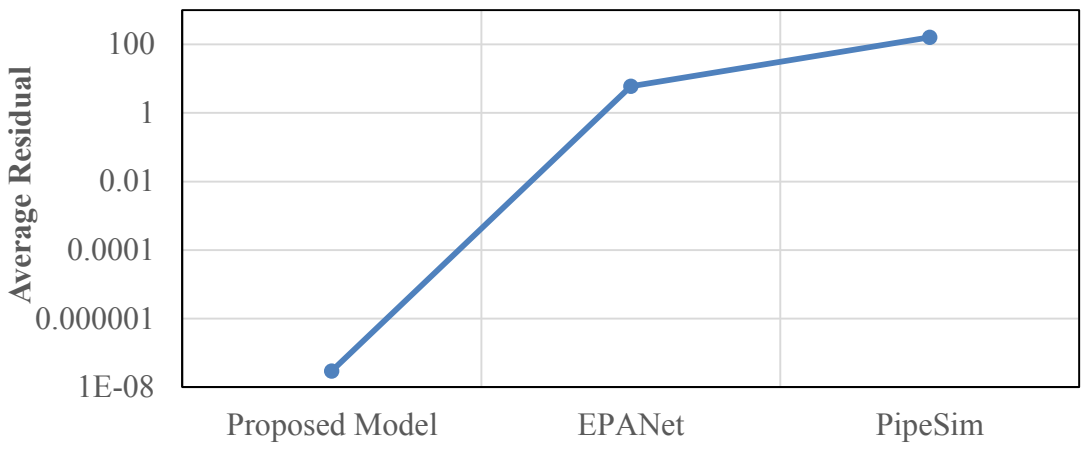

Figure 4.16: Average function residuals in simulations of Jeppson's network.

The first observation that is readily apparent is that the solution from PIPESIM is notably different from the reported values and the other solvers' solutions, and the residuals are orders of magnitude larger.

One reason this could occur is that the convergence criteria can differ from solver to solver. For example, the solution criteria for the pressures and flow rates in PIPESIM are:

$$P_{tol,i} = \sum_{b_i}^{b} \frac{P_{i,b_i} - P_{i,avg}}{P_{i,avg}} \tag{4.2}$$

$$m_{tol,i} = \frac{\frac{1}{b}\sum_{b_{in}}^{b} m_{i,b_{in}} - m_{i,avg}}{m_{i,avg}} \tag{4.3}$$

where $P_{tol,i}$ is the pressure tolerance at node i, P_{i,b_i} is the pressure at the end of branch b_i connected to node i, $P_{i,avg}$ is the average pressure at the node. $m_{tol,i}$ is the mass flow rate

tolerance at node i, $m_{i,avg}$ is the average flow rate at node i, and $m_{i,b_{in}}$ is the mass flow rate into node i from branch b.

A result of using equations (4.2) and (4.3) is that Kirchhoff's laws are not explicitly being conserved, and the residuals from PIPESIM are higher than if they were conserved. While the criteria used in PIPESIM may result in a correct solution, the solution needs to be further vetted.

4.6.3.2 Multiphase Network

Figure 4.17 and Figure 4.18 compare the results from our multiphase solver and PIPESIM assuming no slip occurs between phases. This allows one to compare the results directly, as both options are available in both programs. Figure 4.19 gives the equation residuals for both. While the average residual for PIPESIM is orders of magnitude higher than in this work, it is still relatively small. While the mass balances are satisfied in this case for PIPESIM, Kirchhoff's second law is not fully satisfied. The pressure drops are small, but it can be seen that the error in Kirchhoff's second law propagates into flow rates that are appreciably different.

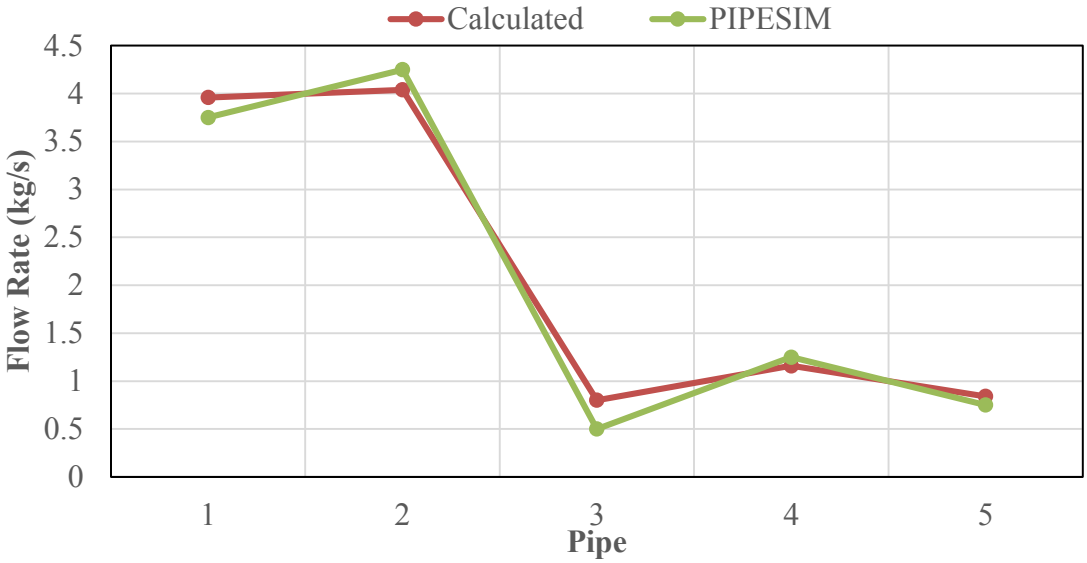

Figure 4.17: Calculated vs. PIPESIM flow rates at pipes in the network presented in Figure 2.1 using no slip assumption.

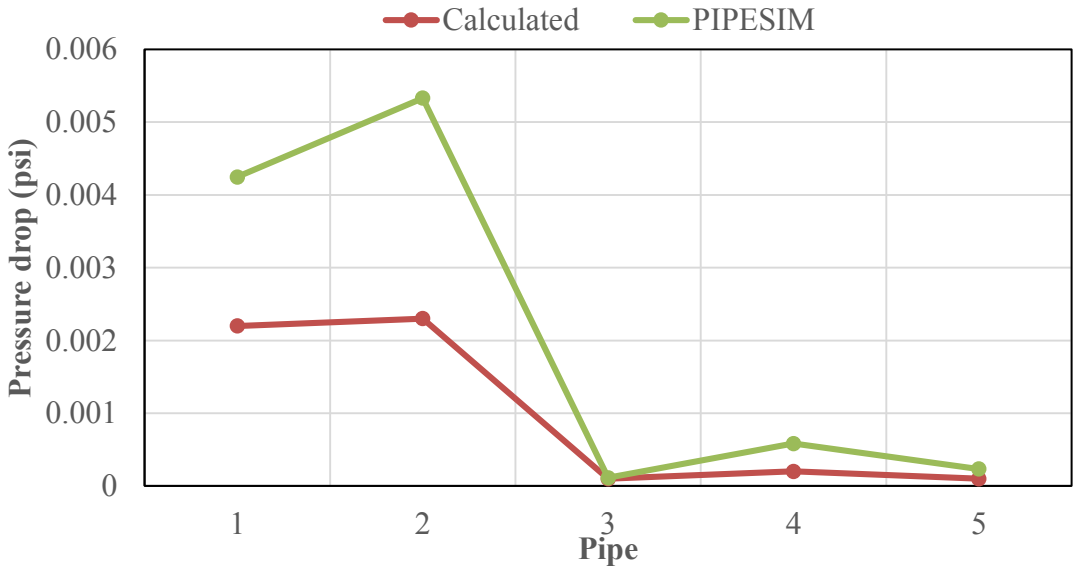

Figure 4.18: Calculated vs. PIPESIM pressure drops at pipes in the network presented in Figure 2.1 using no slip assumption.

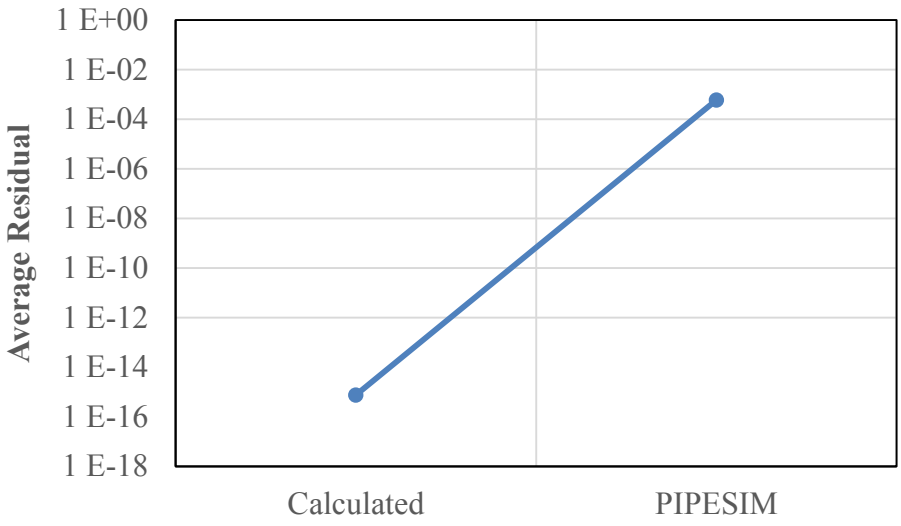

Figure 4.19: Our model versus PIPESIM average equation residual using no slip assumption

Next, it is worth comparing the results, but with slip considered between the phases. The results obtained from our multiphase solver and PIPESIM are much more in agreement here. Although the residual is lower in the calculations done in this work, the flow rates and pressure drops are within practical engineering tolerances.

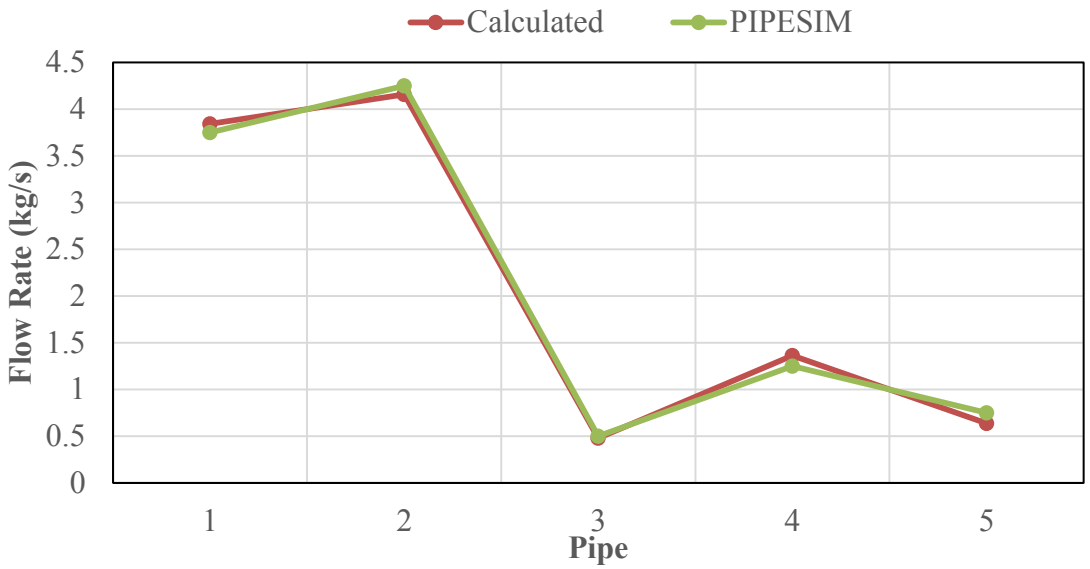

Figure 4.20: Calculated versus PIPESIM flow rates using Woldesmayat & Ghajar fractional flow relationship (for calculated values), and Beggs and Brill correlations for PIPESIM in Jeppson's network (Jeppson, 1976).

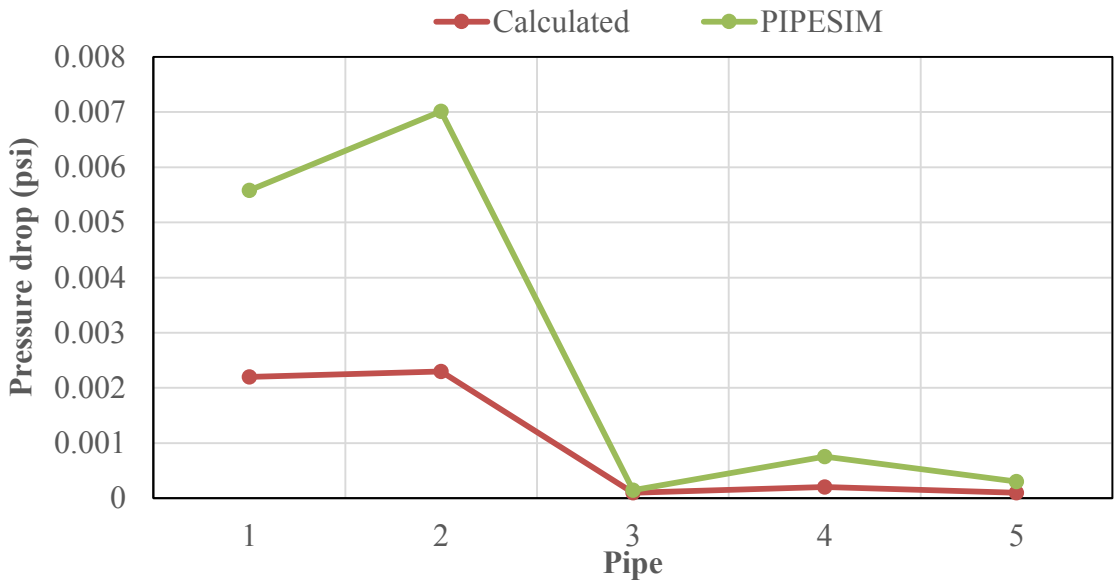

Figure 4.21: Calculated versus PIPESIM pressure drops at branches using Woldesmayat & Ghajar fractional flow relationship (for calculated values), and Beggs and Brill correlations for PIPESIM in Jeppson's network (Jeppson, 1976).

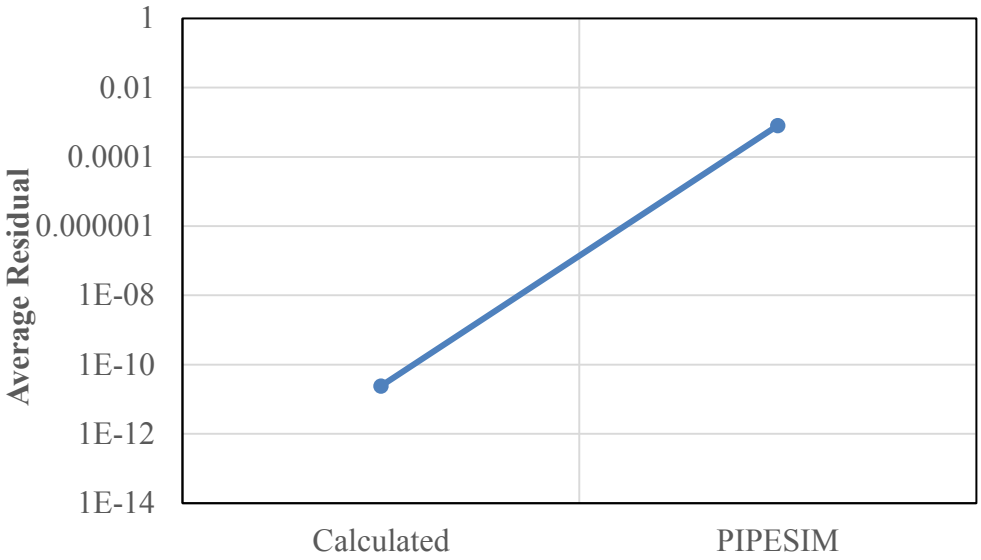

Figure 4.22: Our model versus PIPESIM average equation residuals using Woldesmayat & Ghajar fractional flow relationship (for calculated values), and Beggs and Brill correlations for PIPESIM.

Chapter 5: Phase Splitting Model Formulation and Validation

Before discussing the phase splitting problem in more detail, it is important to understand the data analysis used in literature to better understand the phenomena at play in the manifold problem.

5.1 Data Visualization

In branched flow literature, there are typically two ways to present phase-splitting data. Figure 5.1 plots an individual phase's takeoff against the other phase. In this case, the line bisecting the xy-axes is the equal split line, and total phase separation occurs along the x- and y-axis. All data points above the equal split line represent preferential splitting of that phase at the junction.

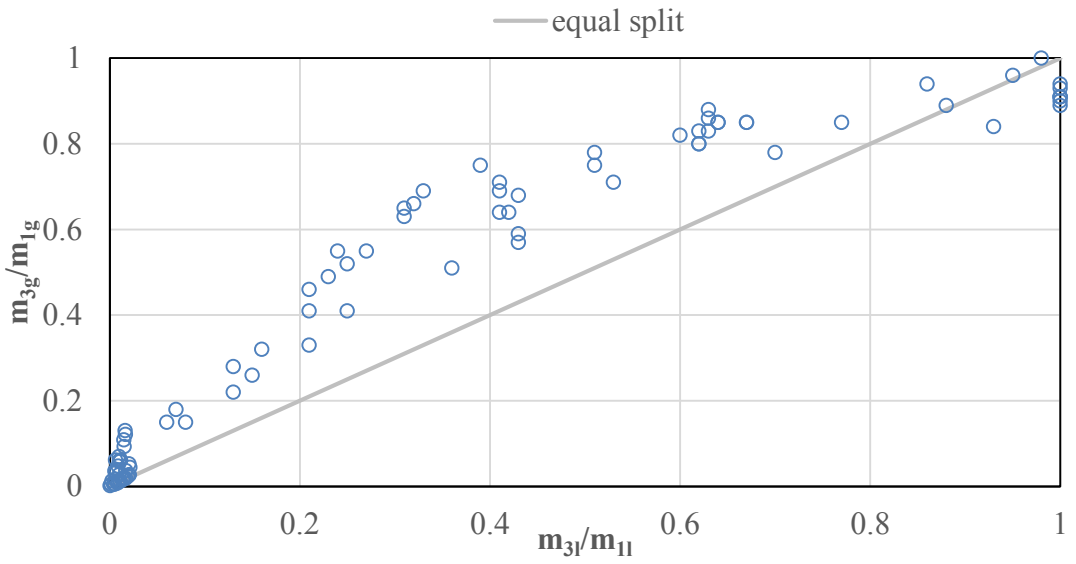

Figure 5.1: Phase 1 mass takeoff vs. phase 2 mass takeoff. Data points shown were artificially generated for illustrative purposes.

The other common method to present branched flow data is seen in Figure 5.2. Here, the total mass takeoff is plotted against the ratio of the mass fractions at the branch and inlet.

The equal split line is represented as the horizontal line at $\frac{x_3}{x_1} = 1$, and the total separation line is represented as the curve $\frac{x_3}{x_1} = \left(\frac{m_3}{m_1}\right)^{-1}$. The total separation line can be derived from the lighter phase mass balance with $m_2 = 0$.

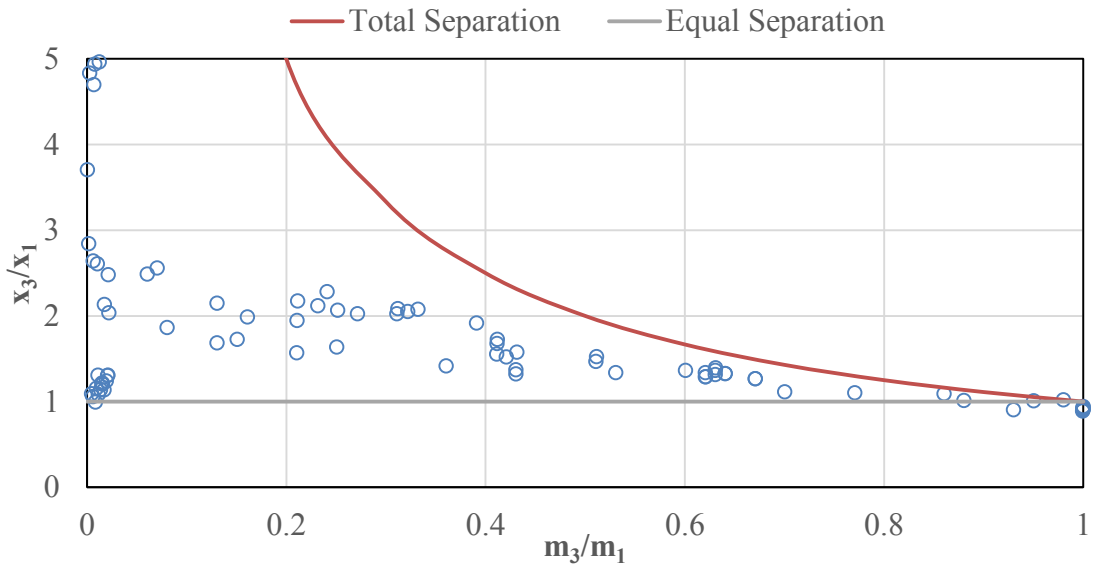

Figure 5.2: Total mass takeoff vs. branch-inlet quality ratio. Data points shown were artificially generated for illustrative purposes.

While these representation capture the relevant variables, it is often of practical concern to know what the branch quality or fractional flow is for a given inlet quality. This is the data representation that we have used in this work.

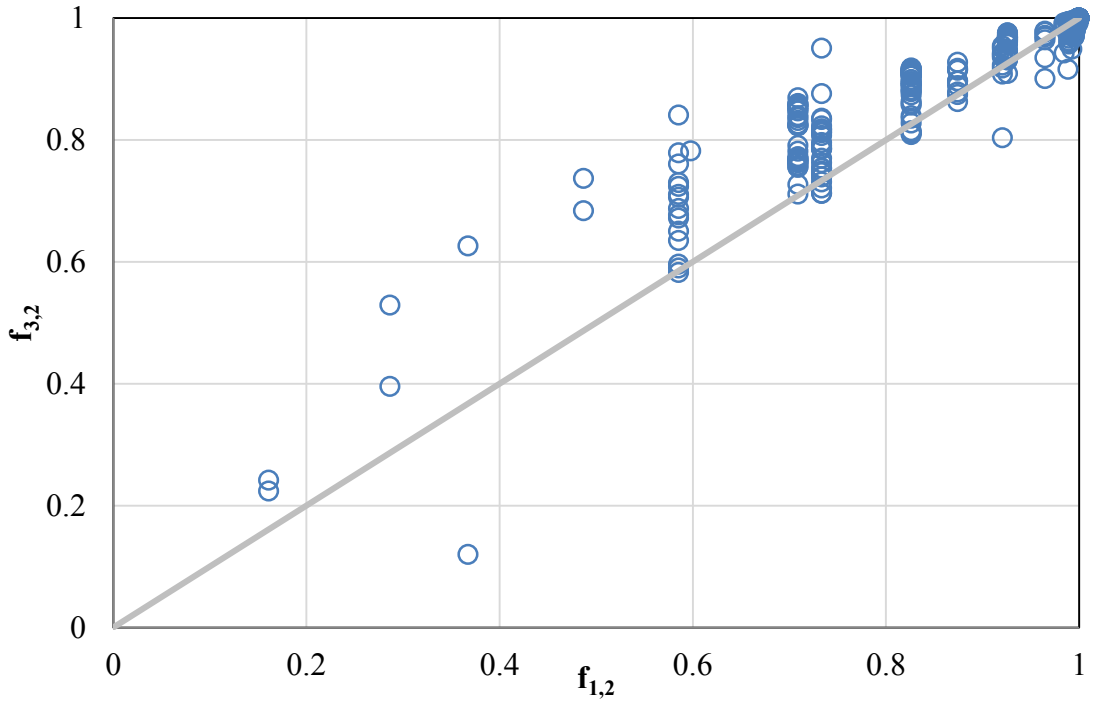

Figure 5.3: Fractional flow at inlet versus branch, with example data taken from vertical inlet, horizontal side-branch junctions. Experimental data collected from published articles (Conte, 2001) (Mak, Omebere-Iyari, & Azzopardi, 2006) (Azzopardi, The Split of Vertical Annualar Flow at a Large Diameter T Junction, 1994) (Davis & Fungtamasan, 1990). Columns of data represent data at different mass takeoffs.

Figure 5.3 shows data for vertical branches, with the fractional flow at the inlet plotted against the fractional flow at the branch. The unit slope line represents the equal phase split line. Different takeoffs are visualized by distinct curves from the origin to $f_{3,2} = f_{1,2} = 1$.

5.2 Popular Models

An Achilles' heel of current phase splitting models is the tradeoff between applicability and accuracy. While models such as Azzopardi's region-of-influence model can predict the phase split well for annular flow with vertical inlets and side-branch configuration, it is not extensible to other flow regimes or branch configurations. Similarly,

empirical models like Zetzmann's might be able to handle a variety of side-branch configurations, yet the results can be inaccurate. Figure 5.5 shows the measured fractional flows versus calculated values for Azzopardi's model. While there is little scatter in the data, it is also only applicable to annular flow, and consequently it is restricted to high-gas flow rates. Conversely, Figure 5.7 shows the measured fractional flow values versus calculated values for Zetzmann's correlation. While it is applicable for the range of inlet fractional flows, the calculated values are often inaccurate.

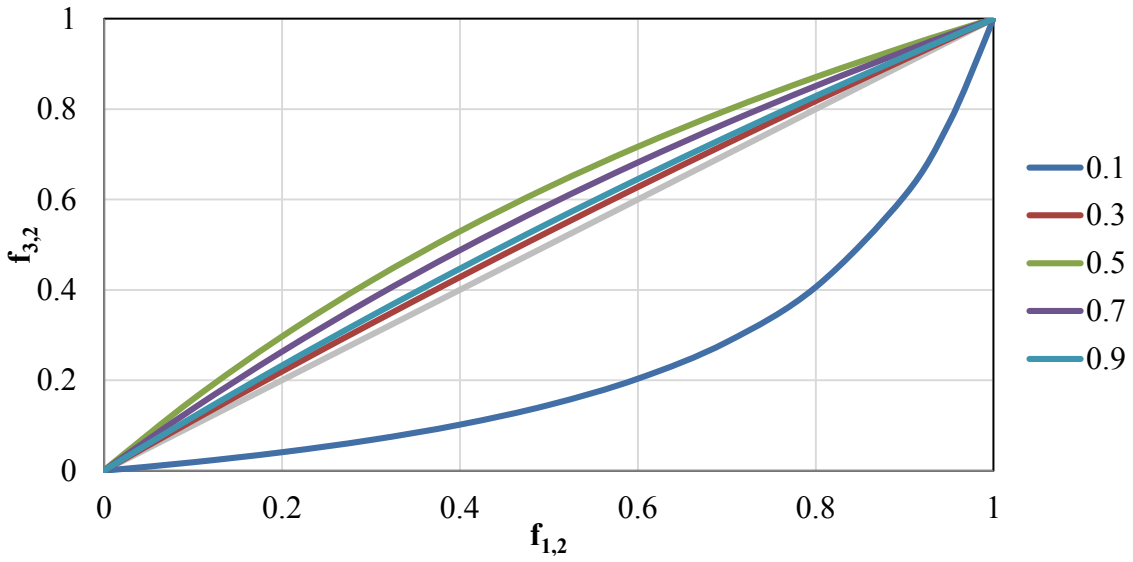

Figure 5.4: Type-curves at different takeoffs for Azzopardi's "region of influence" model

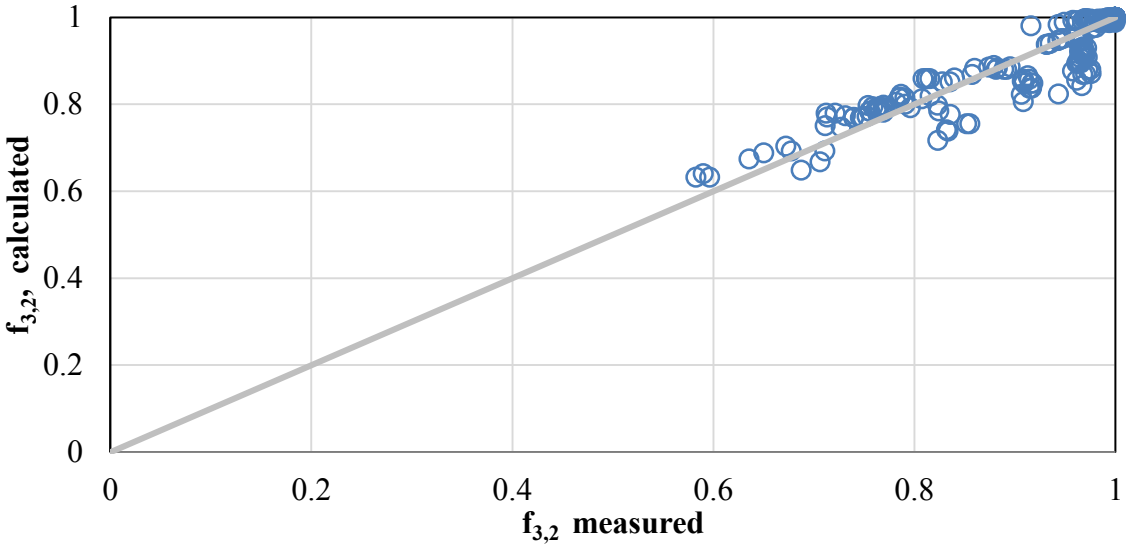

Figure 5.5: Measured versus calculated branch fractional flows for Azzopardi's "zone of influence" model

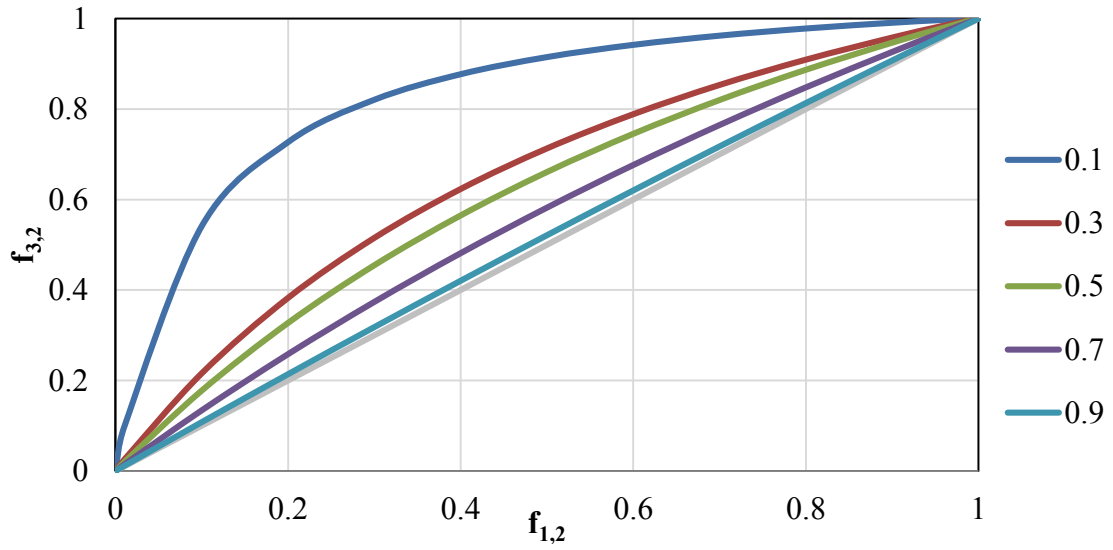

Figure 5.6: Type-curves at different takeoffs for Zetzmann's correlation

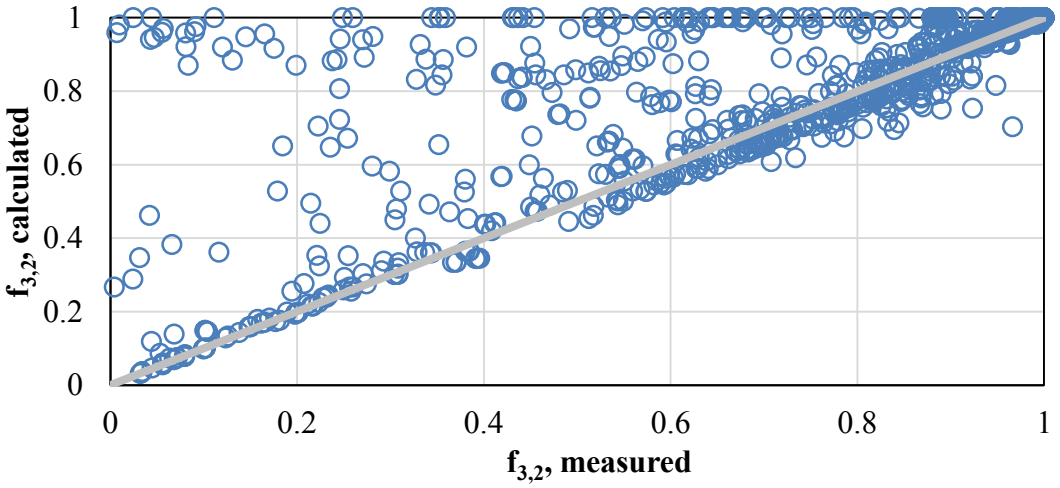

Figure 5.7: Measured versus calculated branch fractional flows for Zetzmann's correlation.

For any model to be extensible to a variety branch configuration, phases, takeoff, and flow conditions, there needs to be a physical basis for the model. Extrapolating empirical models is not the ideal case. Much like Saba and Lahey surmised, only another conservation equation can provide such a physical basis. With this in mind, and knowing that the conservation-of-mass equations and mixture conservation-of-momentum equations have already been specified, there are few choices on the remaining quantities to be conserved.

In line with the averaged-flow approach, the next logical equation to explore would be the mixture conservation-of-energy equation:

$$\frac{\delta Q}{dt} - \frac{\delta W_s}{dt} = \iint_{c.s.} \left(e + \frac{P}{\rho}\right) \rho (v \cdot n) dA + \frac{\partial}{\partial t} \iiint_{c.v.} e \rho dV + \frac{\delta W_\mu}{dt} \tag{5.1}$$

Assuming steady state and no shaft work, equation (5.1) becomes:

$$\iint_{c.s.} \left(e + \frac{P}{\rho}\right) \rho (v \cdot n) dA = \frac{\delta Q}{dt} - \frac{\delta W_\mu}{dt} \tag{5.2}$$

While this may seem like an attractive option, a closure relationship must be assumed for $\frac{\delta W_{\mu}}{dt}$, which is the work rate in overcoming viscous effects at the control surface (in this case, the pipe wall). While some work has been done to propose such a relationship, especially in the University of Tulsa's fluid flow project, their derivation relies on thermodynamic relationships determined with bodies at rest, which extrapolates poorly to moving bodies (Nagoo A. , 2013). Moreover, internal energy needs to be quantified for the mixture at the inlet and outlets, which can be troublesome. Heat transfer also needs to be quantified. With these reasons in mind, the conservation-of-energy approach is not ideal.

One of the governing properties in the manifold problem is often cited as the lighter phase's inertia (Lahey, Current Understanding of Phase Separation Mechanisms in Branching Conduits, 1986). This makes sense as the lighter phase's inertia will be lower than the heavier phase, which should allow it to decelerate at the branch and accelerate past it. Since the mixture conservation-of-momentum equation has already been specified in the pressure drop equation, therefore a single phase's momentum equation should be considered.

5.3 BRANCHED FLOW DATABASE

In developing such an equation, data sets on branched flow have been gathered, standardized and collated. The database has over 5000 data points from over a dozen laboratories.

Parameter	Values
Branch Inclination	$-90, 0, 90°$
Branch Azimuth	$0, 45, 90, 135°$
Inlet Pressure	$0 - 10\ bar$
Inlet Fractional Flow	$0.03 - 0.99995$
Branch Takeoff	$0 - 100\%$
Diameter	$0 - 5\ in.$
Mixtures	Air-Water, Air-Kerosene Kerosene-Water, Water-Silica

Table 5.1: Parameters of interest in the branched flow database

Table 5.1 gives the main parameters of interest in the database. In addition to being used to calibrate the proposed model, below, the branched flow data gathered was also used to test the model. More explanation is given in Section 5.5. Raw data has been graphed in Appendix E.

5.4 Model Development

Similar to the Saba-Lahey model, a phase-*i* momentum balance is considered. The control volume is considered to be the pipe junction.

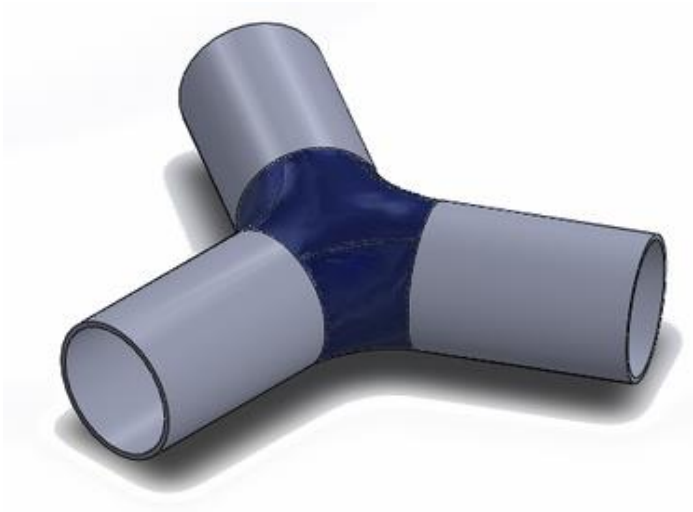

Figure 5.8: Control Volume (shaded) of the phase conservation-of-momentum equation

In the phase conservation equation, the conductive viscous momentum flux is neglected in favor of more dominant conductive (pressure) and convective (inertial) momentum fluxes (Nagoo A. S., 2003):

$$s_i\left(\frac{D\vec{v_i}}{Dt}\right) = \frac{\vec{\nabla}(s_i P)}{\rho_i} + s_i\vec{g} + \sum_{f=1}^{N_f}\frac{\Gamma_{totf\to i}}{\rho_i} \tag{5.3}$$

In equation (5.3), s_i is the saturation of phase *i*, $\vec{v_i}$ is the local *in-situ* velocity of phase *i*, *P* is the Pressure, ρ_i is the phase's density, and $\sum_{f=1}^{N_f}\frac{\Gamma_{totf\to i}}{\rho_i}$ is the sum of the interfacial forces between phase *i* and the other phases. This equation is an extension of the single-phase Euler equation.

Next, as shown in Nagoo's work, the Gauss-Ostrogradskii Divergence theorem can be applied to equation (5.3) to arrive at a macroscopic balance equation:

$$\overbrace{\int_V \rho_i s_i \left(\frac{D\vec{v_i}}{Dt}\right) dV}^{\substack{Spatial\ and\ temporal\ momentum \\ accumulation\ term}}$$

$$= -\overbrace{\int_A \vec{n} \cdot (s_i P) dA}^{Pressure\ force\ at\ faces} + \overbrace{\int_V (s_i \vec{g}) dV}^{\substack{Gravity\ force\ on \\ control\ volume}} \tag{5.4}$$

$$+ \overbrace{\int_V \left(\sum_{f=1}^{N_f} \Gamma_{totf \to i}\right) dV}^{\substack{momentum\ transfer\ through \\ other\ phases\ within\ control\ volume}} + \overbrace{\vec{F}_{w-i}}^{\substack{Momentum\ transfer \\ with\ wall\ (friction)}}$$

Where V is the control volume being inspected (the junction), A is the face's area (typically the conduit's cross-sectional area), and $\vec{n}$ is the unit vector normal to the face A.

Equation (5.4) deserves further inspection because the control volume in this case is the junction, and instead of two faces where momentum flux can occur (the inlet and the outlet of the conduit), there are three (the inlet, branch, and outlet). This can cause confusion, especially as the Saba-Lahey model only considers the inlet and branch.

As explained in Transport Phenomena by Bird, Stewart, and Lightfoot, inertial and pressure forces must be considered at all planes adjacent to the control volume (Bird, Stewart, & Lightfoot, 2007). Evaluating equation (5.4):

$$\overbrace{M_i\langle s_i\rangle\left(\frac{\Delta_t\left(\langle\langle v_{1,i}\rangle\rangle\,\vec{e}\right)}{\Delta t}\right)}^{\substack{Temporal\ momentum\\ accumulation}}$$

$$= -\overbrace{\left(s_{3,i}P_3A_3\vec{e} + s_{2,i}P_2A_2\vec{e} - s_{1,i}P_1A_1\vec{e}\right)}^{Pressure\ force\ at\ faces} + \overbrace{M_i s_i \vec{g}}^{\substack{Gravity\ force\ on\\ control\ volume}} \tag{5.5}$$

$$- \overbrace{M_i\langle s_i v_i\rangle\left(\frac{\left(\langle\langle v_{3,i}\rangle\rangle\,\vec{e} + \langle\langle v_{2,i}\rangle\rangle\,\vec{e} - \langle\langle v_{1,i}\rangle\rangle\,\vec{e}\right)}{\mathrm{L}}\right)}^{Convective\ momentum\ transfer} \overbrace{\vec{F}_{totf-i}}^{\substack{Momentum\ transfer\\ through\ other\ phases\\ within\ control\ volume}}$$

$$+ \overbrace{\vec{F}_{w-i}}^{\substack{Momentum\ transfer\\ with\ wall\ (friction)}}$$

In equation (5.5), the acceleration term has been broken into a spatial and temporal acceleration terms. This presents a complication as the control volume being considered, and the faces at which momentum transfer is occurring, is neither truly one-dimensional nor two-dimensional. The manifold being considered is most accurately described as 1.5-dimensional as three faces are present for momentum transfer.

$$\left(s_{3,i}P_3A_3 + s_{2,i}P_2A_2 - s_{1,i}P_1A_1\right)\frac{1}{V_{ctrl}}$$

$$= \rho_i s_i g sin(\theta) - \frac{G_{1,i}}{L}\left(\frac{G_{3,i}}{\rho_{3,i}s_{3,i}} + \frac{G_{2,i}}{\rho_{2,i}s_{2,i}} - \frac{G_{1,i}}{\rho_{1,i}s_{1,i}}\right) \tag{5.6}$$

$$- \rho_i s_{1,i}\left(\frac{\Delta_t\left(\frac{G_{1,i}}{\rho_{1,i}s_{1,i}}\right)}{\Delta t}\right) + \frac{1}{V_{ctrl}}\vec{F}_{totf-i} + \frac{1}{Vctrl}\vec{F}_{w-i}$$

Here, *G* represents the phase's mass flux at a face. Moreover, since steady-state is assumed, equation (5.6) becomes:

$$\left(s_{3,i}P_3A_3 + s_{2,i}P_2A_2 - s_{1,i}P_1A_1\right)\frac{1}{V_{ctrl}}$$

$$= \rho_i s_i g sin(\theta) - \frac{G_{1,i}}{L}\left(\frac{G_{3,i}}{\rho_{3,i}s_{3,i}} + \frac{G_{2,i}}{\rho_{2,i}s_{2,i}} - \frac{G_{1,i}}{\rho_{1,i}s_{1,i}}\right) \qquad (5.7)$$

$$+ \frac{1}{V_{ctrl}}\vec{F}_{totf-i} + \frac{1}{V_{ctrl}}\vec{F}_{w-i}$$

Equation (5.7) represents the functional form of the phase-splitting equation used in this work. A few terms need to be explained. Firstly, a volume needs to be assumed for the control volume as it does not have a constant cross-sectional area. Additionally, a length scale needs to be assumed. As used in the Saba-Lahey model, the mean phase streamline is assumed. See equation (2.47), and a derivation can be found in Saba's dissertation (Saba & Lahey, Phase Separation Phenomena in Branching Conduits, 1981). This can be described as the average length travelled by the phase in the control volume. The volume of the control volume can then be assumed to be the average of the conduits meeting at the junction of interest (where the length scale is the diameter of the branch). Finally, an angle θ is also needed. This is the angle the mean phase streamline makes with the direction of gravity. As the streamline is always a dividing streamline, it will always bisect the angle formed by the branch and the outlet in side-branch configurations. Hence it is assumed to be the average of the inclinations of the branch and main outlet.

Next, the two non-fundamental terms in equation (5.7) need to be specified. As explained in Nagoo's work, the wall-shear term is assumed to be of the form (Nagoo A. , 2013):

$$\tau_w = \frac{\vec{F}_{w-i}}{A_1} = \left(\frac{K\langle v_i\rangle}{2}\right)\rho_i\langle v_i\rangle = \frac{1}{2}K\rho_i\left(\frac{G_{1,i}}{\rho_{1,i}s_{1,i}}\right)^2 \tag{5.8}$$

where $\left(\frac{K\langle v_i\rangle}{2}\right)$ is the momentum flux transfer coefficient, and K is an empirical coefficient. The empirical coefficient used in the Saba-Lahey model is used here with the empirical constants modified for the database assembled here:

$$K_{1,3} = [2.09 + \left(\frac{m_3}{m_1}\right)^{7.64} + 1.67\left(\frac{m_3}{m_1}\right)](\frac{A_1}{A_3}) \tag{5.9}$$

For the interfacial shear term, the following model is used:

$$\tau_i = \frac{\vec{F}_{totf-i}}{A_1} = \frac{3}{4}\rho_{1,i}u_{r1,1-2}^2 L\left(\frac{C_D}{d}\right) \tag{5.10}$$

This form is borrowed from the Saba-Lahey model for interfacial shear (Saba & Lahey, Phase Separation Phenomena in Branching Conduits, 1981). $u_{r1,1-2}$ is the slip velocity ($\langle\langle u_{1,2}\rangle\rangle - \langle\langle u_{1,1}\rangle\rangle$), L is the length of the mean phase streamline, and $\frac{C_D}{d}$ is the drag coefficient over a length scale. In practical purposes, the length scale manifests for dimensional similitude.

A variety of models for interfacial shear exists. One common form is:

$$\tau_i = s_2\tau + \frac{1}{2}\rho_2\left|\langle\langle u_2\rangle\rangle\right|\langle\langle u_2\rangle\rangle C_D \tag{5.11}$$

Here, there are two components: a shear term, which is dominant in separated flows (high slip), and a drag term, which is dominant in dispersed flows (low slip) (Brooks, Hibiki, & Ishii, 2012). Due to the difficulty in quantifying each term in equation (5.11), the shear term is often neglected and the modeling is attempted via the drag-coefficient approach.

Another form for interfacial shear is to assume a friction factor and treat interfacial momentum transfer as in equation (5.8):

$$\tau_i = \frac{\vec{F}_{totf-i}}{A_{inf,1-2}} = f\rho_2\langle v_2\rangle^2; f = 0.005(1 + 300\frac{\delta}{D}) \tag{5.12}$$

This is the form used often in annular flow due to the well-defined interface (Pan, He, Ju, Hibiki, & Ishii, 2015). In order to keep the phase-splitting model applicable to all flow conditions, such an approach proves difficult, especially as the phase interface becomes difficult to quantify.

For these reasons, a drag model is used in this phase-splitting model. According to Ishii, the interfacial drag term is heavily dependent on slip ratio, Reynold's number, and volume fraction (Brooks, Hibiki, & Ishii, 2012). The following are a few of the models proposed in literature:

Model	$\boldsymbol{C_D/\ell}$ $(\boldsymbol{m^{-1}})$
Lahey (Churn-turbulent) (presented in Saba-Lahey model)	$54.9(\frac{\rho_2}{\rho_1}s_2(1-s_2)^2 + (1-s_2)^3)$
Slug	$21.8\frac{r_D}{D}(1-s_2)^3$
Bubble	$\frac{24}{N_{Re,b}}(1 + 0.1{N_{Re,b}}^{0.75})$

Table 5.2: Common interfacial drag terms (Brooks, Hibiki, & Ishii, 2012)

Based on these observations, the follow drag coefficient model is proposed:

$$\frac{C_D}{d}(m^{-1}) = 3999N_{Re,1}^{2.238}N_{Re,2}^{-2.507}N_{Fr,2}^{0.823}(1-s_2)^{-3.121} \tag{5.13}$$

Where $N_{Re,1}$ and $N_{Re,1}$ are the Reynolds number for the two phases, and $N_{Fr,2}$ is the Froude number for the second phase. The phase Reynolds number can be defined as:

$$N_{Re,i} = \left(\frac{Inertial\ force}{Viscous\ force}\right)^{\frac{1}{2}} = \frac{\rho_i \langle\langle v_i \rangle\rangle D_H}{\mu_i} \tag{5.14}$$

And the phase Froude number can be defined as:

$$N_{Fr,i} = \left(\frac{Inertial\ force}{Buoyant\ force}\right)^{\frac{1}{2}} = \frac{\langle\langle v_i \rangle\rangle}{\sqrt{D_H \left(\frac{\Delta\rho}{\rho_i}\right) g}} \tag{5.15}$$

As described in Ishii's work, it is clear that the Reynolds number plays an important role—both in terms of drag and in the overall phase-splitting problem. A low Reynolds number would lead to more of the carrier phase entering the branch as it is more viscously coupled to the lighter phase. Moreover, the Froude number can play a large role in the phase-splitting problem. In a situation with a vertical branch, the Froude number can quantify how buoyancy effects the phase splitting. A low Froude number for the lighter phase would mean a more exaggerated phase split in a vertical branch as the buoyant force dominates.

5.5 Model Calibration and Results

To calibrate the phase-splitting model, 30 data points were selected from the database that represented the widest array of parameters possible. This included vertical tees, horizontal side-arms, vertical side-arms, and impacting tees. Moreover, air-water, air-kerosene, and kerosene-water mixtures were included, as well as small and large diameter datasets, high pressure data, and varying degrees of inlet conditions and takeoffs. While the model is theoretically based, the fitting parameters are found empirically by curve

fitting. This is one of the major drawbacks of the model. A better fit can always be found by adding additional fitting factors and more training data, yet overfitting is an opposing threat. Further improvements in this area are possible. The following graph shows the measured versus calculated values for fractional flow as the result of the model:

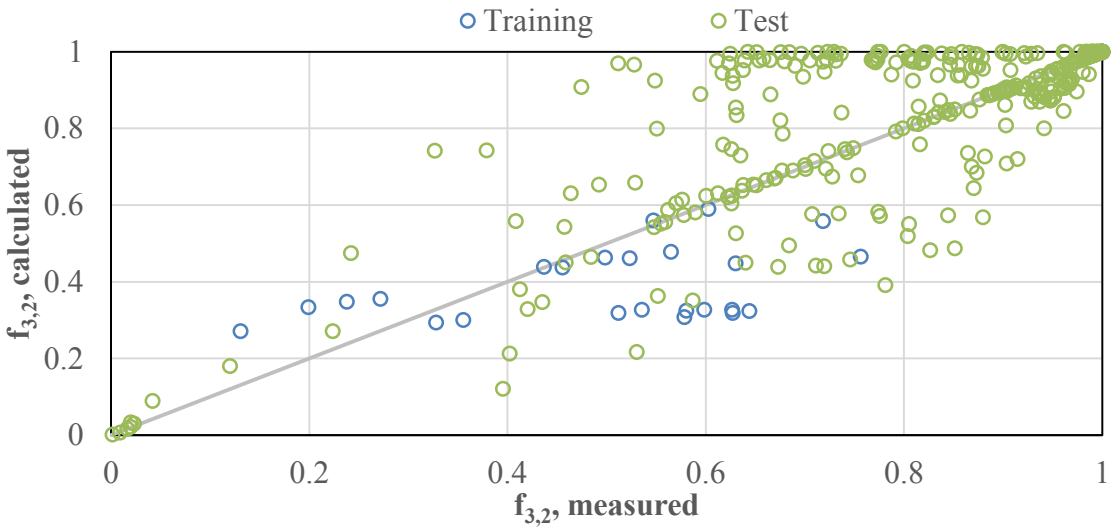

Figure 5.9: Measured versus calculated values of fractional flow at the branch of the lighter phase. Points closer to the unit-slope line represent better accuracy.

For a more thorough explanation of the data used to calibrate the model, see Appendix D. Also, Appendix E contains graphs of more raw data for different configurations.

Figure 5.10, Figure 5.11, and Figure 5.12 show the effect of mass takeoff with increasing inlet fractional flow. These were generated using an inlet mixture velocity of $2\ m/s$ and an inlet pressure of $1\ atm$. The mixture is assumed to be air-water, and all branches were set to be $1\ in.$ in diameter. A horizontal side-branch configuration is assumed. It should be noted that the model predicts a *lower* phase split of the lighter phase at the branch when the takeoff is low. This is seen for values $\frac{m_3}{m_1} < 0.6$. This can be seen as

a positive sign as overestimation of branch quality and fractional flow is commonplace in current models (see Figure 5.7). Moreover, the difference between the no-slip type curves and the slip type curves is striking. This reinforces the notion that slip and volume fraction are instrumental in determining phase split.

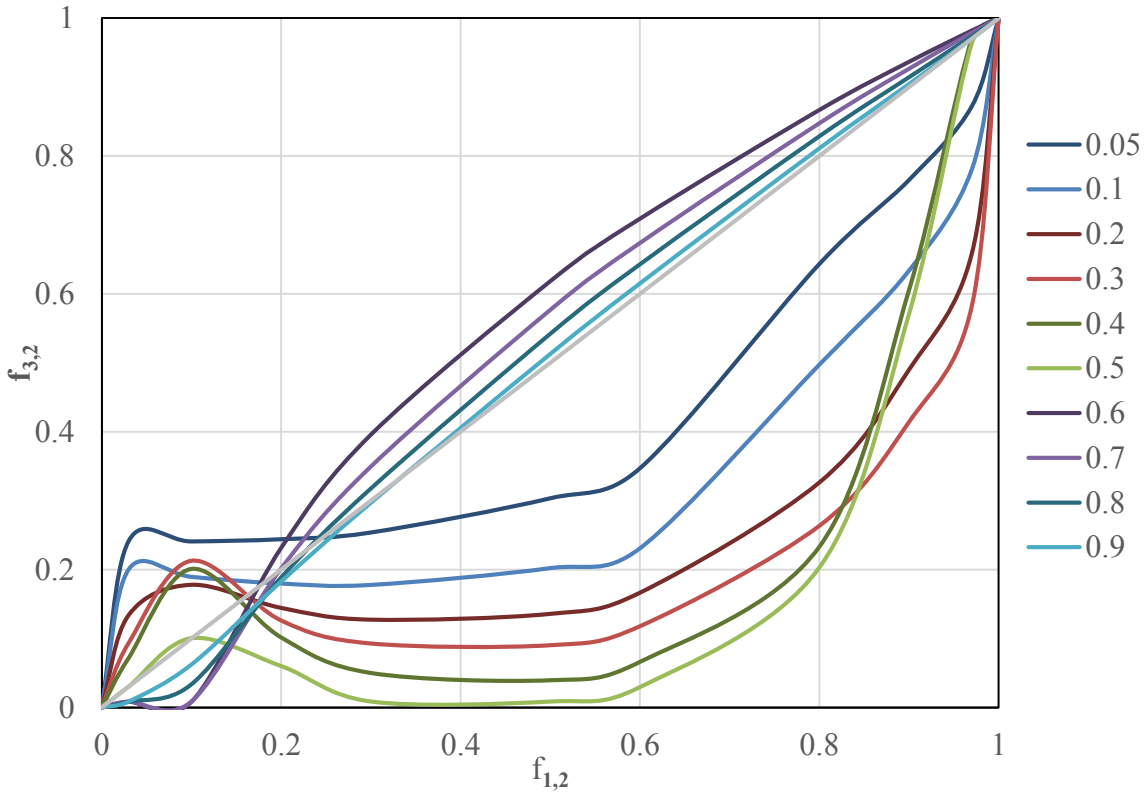

Figure 5.10: Fractional flow at inlet versus fractional flow at outlet using the Nicklin fractional flow relationship at different takeoffs.

Figure 5.13, below, shows the type curve of the proposed phase-splitting model with a vertical side branch with the Woldesmayat & Ghajar fractional flow relationship. Here it is readily seen that the branch fractional flow tends to be equal to and larger than the inlet fractional flow. This is again expected as data shows an increase phase split with

vertical side branches. Moreover, the difference between the type curves in Figure 5.11 and Figure 5.13 shows how inclination exaggerates phase split.

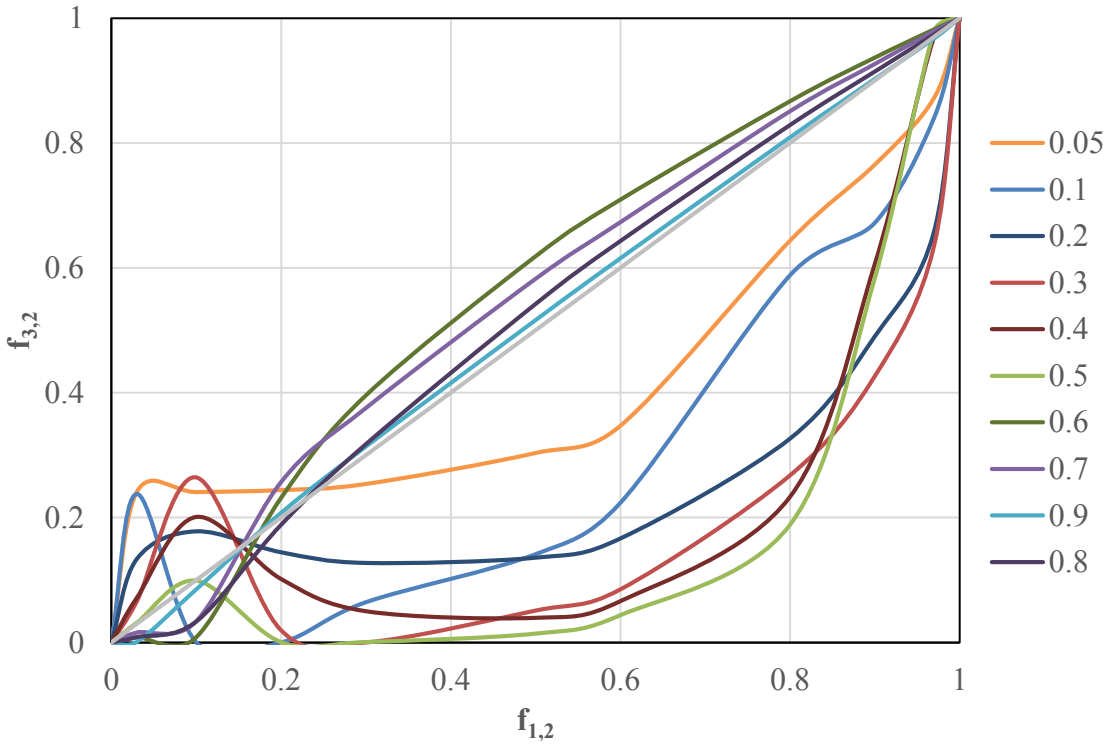

Figure 5.11: Fractional flow at inlet versus fractional flow at outlet using the Woldesmayat & Ghajar fractional flow relationship at different takeoffs

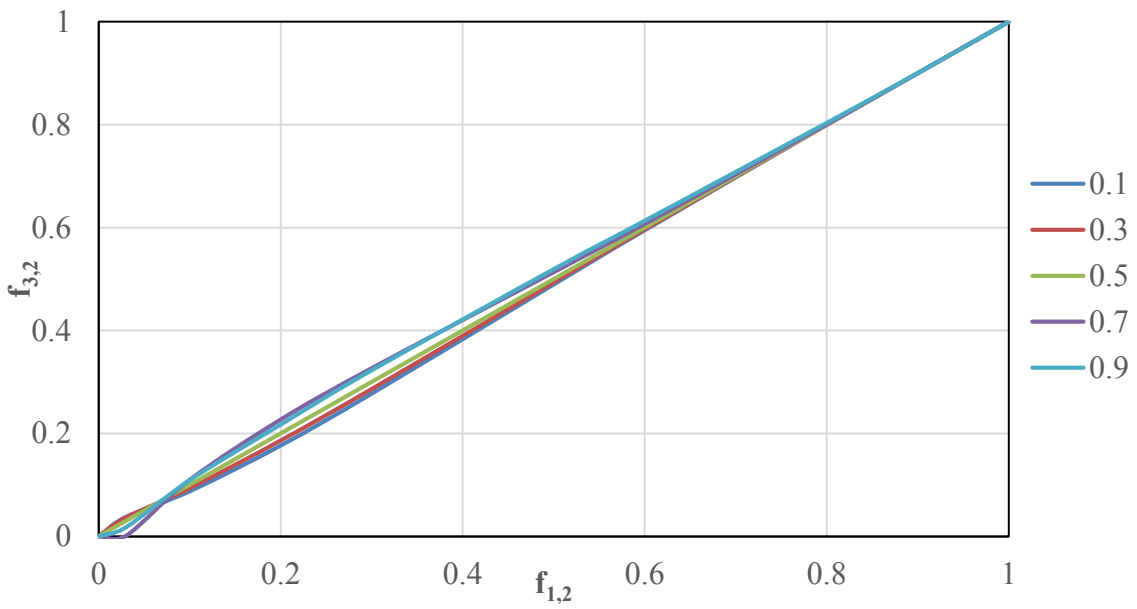

Figure 5.12: Fractional flow at inlet versus fractional flow at outlet assuming no-slip fractional flow relationship at different takeoffs.

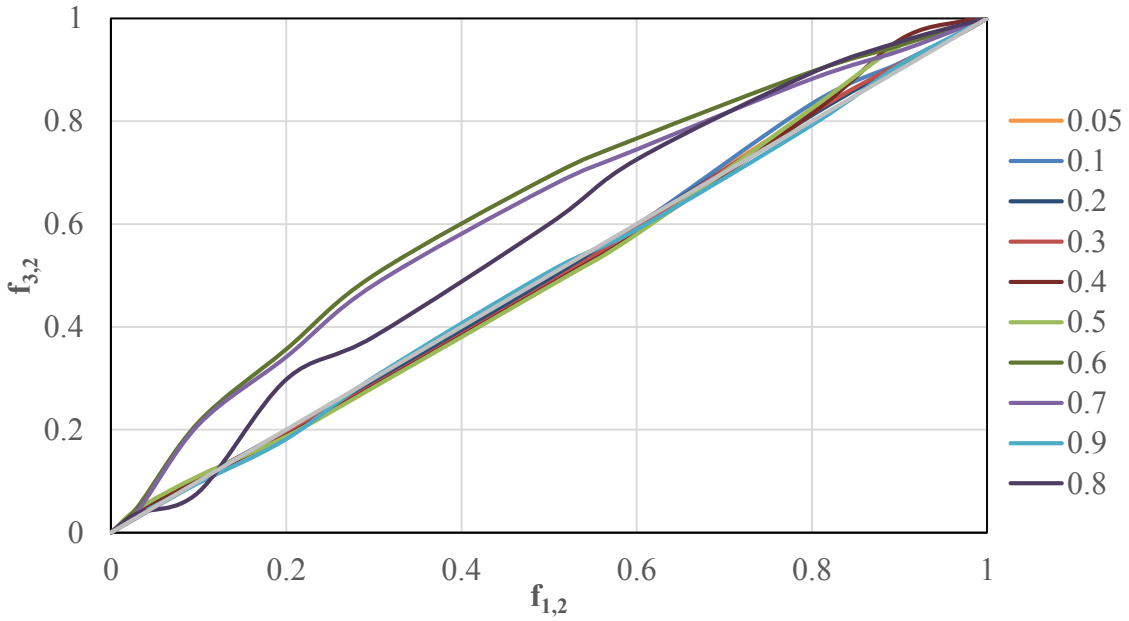

Figure 5.13: Fractional flow at inlet versus fractional flow at outlet using the Woldesmayat & Ghajar fractional flow relationship at different takeoffs with a vertical side branch.

Figure 5.14, Figure 5.15, Figure 5.16, and Figure 5.17 show model results (curves) against published experimental data. These examples illustrate that despite the generally-held understanding that the lighter phase is preferentially withdrawn into the branch, the data shows that this is often not the case. Figure 5.14 shows the case of a vertical inlet tee with a horizontal outlet. One data point stands out in that it is below the equal split line whereas the rest are about. This shows that while conventional wisdom is that inertial forces are the primary forces, the entire momentum balance needs to be considered.

Figure 5.15 and Figure 5.17 give two cases of a side-branch configuration with Figure 5.15 having a horizontal side branch and Figure 5.17 having a vertical side branch. These data show the branch fractional flow being greater than the inlet fractional flow, and the vertical case having an exaggerated branch fractional flow due to the effect of gravity. Figure 5.16 shows an impacting tee at two different mass take offs. These data show higher takeoffs corresponding to more equal splitting.

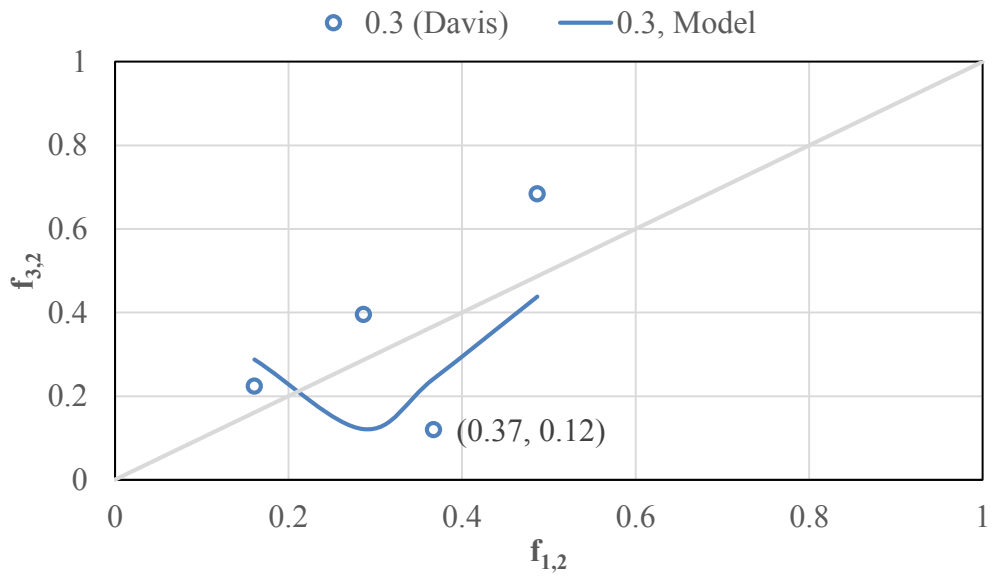

Figure 5.14: Fractional flow at inlet versus fractional flow at outlet using the Woldesmayat & Ghajar fractional flow relationship. $\frac{m_3}{m_1} = 0.3$. Points are experimental data taken from Davis & Fungtamasan (Davis & Fungtamasan, 1990). Branch configuration is a vertical inlet, horizontal side-branch. Unit slope line represents line of equal splitting.

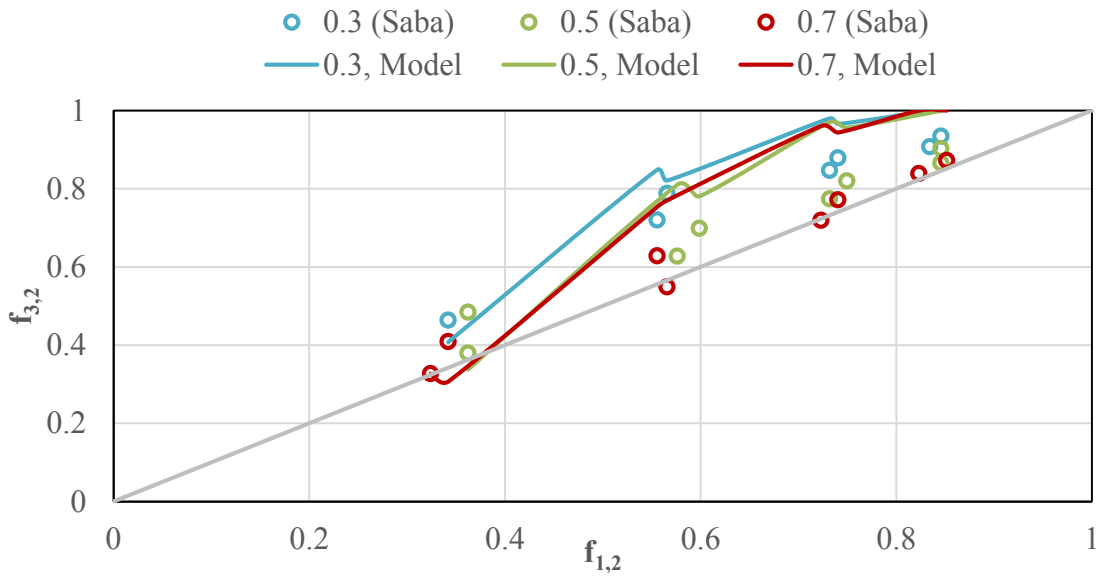

Figure 5.15: Fractional flow at inlet versus fractional flow at outlet using the Woldesmayat & Ghajar fractional flow relationship at varying takeoffs. Points are experimental data taken from Saba (Saba & Lahey, Phase Separation Phenomena in

Branching Conduits, 1981). Branch configuration is a horizontal inlet, horizontal side-branch. Unit slope line represents line of equal splitting.

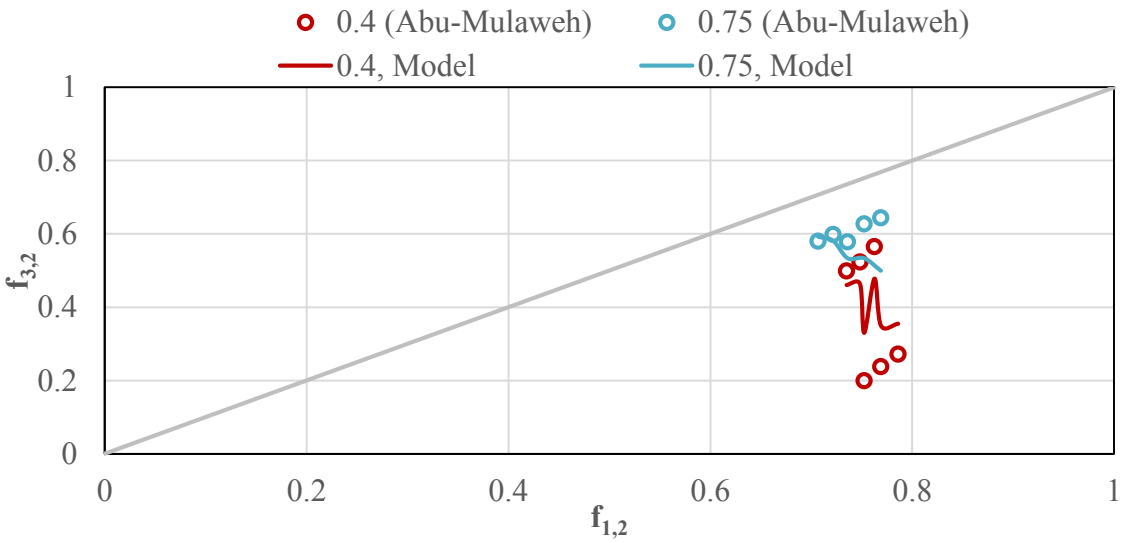

Figure 5.16: Fractional flow at inlet versus fractional flow at outlet using the Woldesmayat & Ghajar fractional flow relationship at different mass takeoffs. Points are experimental data taken from Abu-Mulaweh (Abu-Mulaweh, Al-Halhouli, Hammad, & al., 2008). Branch configuration is a horizontal impacting tee. Unit slope line represents line of equal splitting.

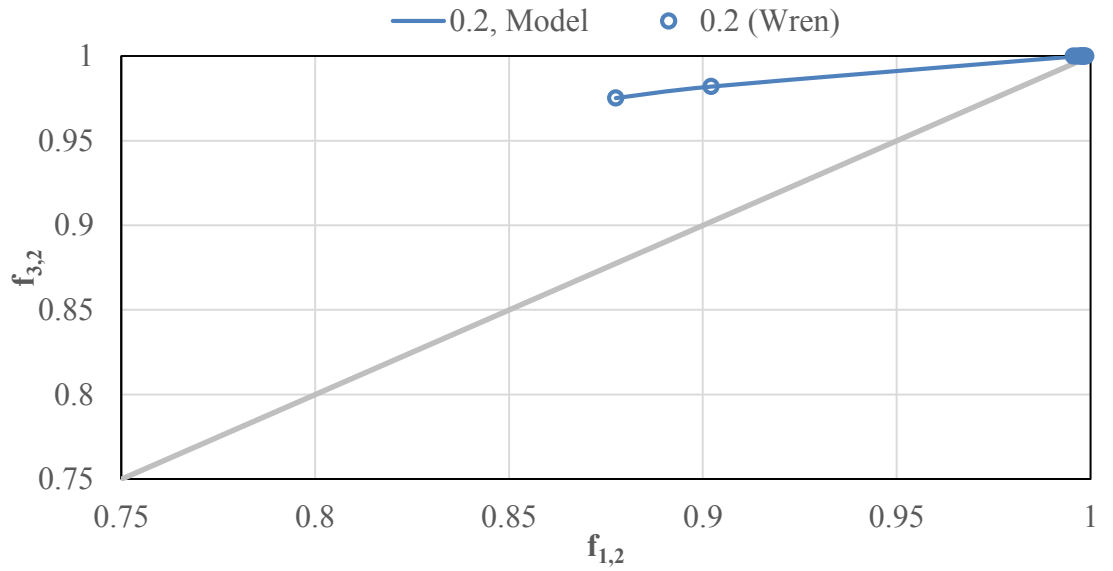

Figure 5.17: Fractional flow at inlet versus fractional flow at outlet using the Woldesmayat & Ghajar fractional flow relationship. $\frac{m_3}{m_1} = 0.2$. Points are experimental

data taken from Wren (Wren, 2001). Branch configuration is a horizontal inlet, vertical side branch. Unit slope line represents line of equal splitting.

5.6 Model Limitations and Conclusions

Despite the general applicability of the model, one of the main limitations is downward side branches. This is due to limitations in single pipes to model such flows, and these fractional flow relationships are used in the model here. Also, as these relationships are designed for fully-developed flow in pipes, the issue of entry and exit effects further complicate the model. Finally, branch azimuth is not explicitly accounted for in the model. Future work should examine how to incorporate this.

The type curves presented here suggest that the best way to see an exaggerated phase split at the branch is to use the segregating effects of gravity in conjunction with higher ($\frac{m_3}{m_1} > 0.5$) takeoff. During operation, it may not always be possible to specify a mass takeoff at such levels, so ensuring the best branch configuration can be instrumental.

If the most even phase split is desired, in situations such as having two pumps or separators in parallel, using a simple tee or wye junction may not be the most effective way to evenly split flow. For instance, in impacting tees, upstream flow conditions can cause the mixture velocity profile to be asymmetric, which can lead to an uneven phase split. One way to avoid this is to place baffles in the upstream pipe to homogenize the flow (United States of America Patent No. US5709468 A, 1998). Another method is to only allow flow into one branch at any given time, and change the time a given branch is open. This would have an equal phase split, but could cause issues with surging.

Chapter 6: Summary, Conclusions and Recommendations

6.1 Summary and Conclusions

This study has investigated solving steady-state, multiphase flow in pipe networks, and has formulated a novel approach to the system of equations being solved, based on the averaged-flow approach. This approach satisfies both Kirchhoff's laws and honors the averaged-flow framework from which it was developed. The model has been validated against existing published data sets as well as published solutions to network problems, and the model has been compared to existing network solvers that are commercially available.

An examination of past experimental data on flow splitting indicate the following:

1. The extent of phase splitting at a junction is not just dependent on the inertial forces present. One must consider the entire momentum balance.
2. The highest degree of phase splitting occurs in vertical side branches. Downward branches work exaggerate phase splitting well but present modeling challenges.
3. Phase splitting tends to be exaggerated with increasing slip and increasing difference in the two phase's inertias.

These important trends have been incorporated into a quantitative relationship that includes flow rates, pressures, volume fractions, branch inclination, and inertias. This relationship acts as a closure relation for the general mass and momentum balance equations for pipe flow networks.

A phase splitting model has been developed based on a macroscopic momentum balance of the second phase, which is based on Nagoo's area-averaged approach, and borrows elements from Saba- and Lahey's mechanistic model, which is based on a momentum balance of the lighter phase (Saba & Lahey, Phase Separation Phenomena in Branching Conduits, 1981). While Saba and Lahey assume homogeneous flow, it has been shown in previous work that this is insufficient for a wide variety of circumstances, and which is a constant source of error noted in many other works (Nagoo A. , 2013). Additionally, this model is extensible to a wide variety of relevant pipe-junction configurations seen in industry, which is often a limitation of such models. The developed phase-splitting model can be used in network solvers as either additional information in place of unknown boundary conditions, or can be used as a tool to check the results of existing network solvers.

6.2 RECOMMENDATIONS

As the manifold problem is a subtopic within multiphase flow, the same limitations for non-branching systems apply to branching systems. As shown in Nagoo's work, one of the chief necessities is for better saturation-fractional flow closure relationships (Nagoo A. , 2013). This is especially relevant in the field of downward flow and in solids flow, where few relationships are able to accurately predict saturation.

The most important understanding that remains to be seen is the interplay been flow development and the manifold problem. The averaged-flow approach used in this work is robust, but the closure relationships used have the assumption of fully developed flow. The understanding of flow development, even in single-phase flow, is tenuous. Indeed, as

Geoffrey Hewitt states, “There will always be a pressure gradient, and under its influence the gas velocity will be constantly increasing.” (Nagoo A. , 2013). Indeed, in compressible flow there exists a time-independent acceleration, which suggests that the idea of a fully-developed flow may be looking at the issue from the wrong perspective. The right question to ask is under what conditions do entry and outlet effects become insignificant. Unfortunately, this is also a poorly understood topic. While Persen suggests that in single-phase flow a transition length of 60-80 diameters is present, estimates for multiphase flow are as high as 800 diameters (Nagoo A. , 2013).

Due to the lack of understanding of entry and exit effects on multiphase flow, it is difficult to separate those effects from phase-splitting effects at a junction, which acts as a *de facto* exit. Therefore it is of utmost important to have reliable measurements of flow conditions at many distances with respect to the junction. The work of Fungtamasan and Davis does a good job of this, but the six flow conditions tested are inadequate to draw conclusions. Of particular interest is having three branches with at least 800 diameters in length connected at a junction. Having reliable volume fraction, pressure, and flow rate data along these pipes would help to answer how flow development occurs before and after the junction, and how effects downstream affect upstream conditions. Hence, more fundamental research into entry and exit effects is important to separate those effects from junction effects.

Additionally, the development of a comprehensive phase-splitting model has been limited. Most attempts at a fully-applicable model start with a conservation equation, and in the instance of the Saba-Lahey model, a phase-momentum balance. Accurately modeling

interfacial shear is difficult due to constantly changing flow patterns, which can cause modeling difficulties. Moreover, the wall shear term can be a modeling challenge due to changing flow conditions. While in bubble flow the momentum transfer with the wall may occur primarily through the carrier phase, in slug flow, for instance, the lighter phase's contribution to wall shear may not be negligible. This can create a system of compensating deficiencies in the phase splitting model. Nevertheless, today's phase splitting models are useful as long as their limitations are kept in mind.

APPENDICES

Appendix A: Nomenclature

A.1 SUBSCRIPTS

Subscript	Meaning
b	Branch
i	Phase
1	Junction Inlet
2	Junction main outlet
3	Junction branch
n	Node
j	Junction
l	Liquid
g	Gas
m	Mixture
w	wall

A.2 SYMBOLS

Symbol	Meaning
N_b	Number of branches in network
N_n	Number of nodes in a network
N_ℓ	Number of independent lo
N_p	Number of phases
K_b	Hydraulic resistance
Q	Volumetric flow rate

d	Diameter
m	Mass flow rate
x	Quality (mass fraction)
G	Mass flux
A	Area
ΔP	Pressure change
h_f	Hydraulic Head
u	Volume flux (superficial velocity)
v	*In situ* velocity
X_{tt}	Martinelli parameter
$K_{1,2}$	Friction coefficient for main run momentum balance in Saba and Lahey model
$K_{1,3}$	Friction coefficient for branch momentum balance in Saba and Lahey model
C_D	Drag coefficient
u_r	Slip velocity
s	Saturation (volume fraction)
f	Fractional flow
S_G	Specific gravity
L	Length
L_j	Streamline line in Saba and Lahey model
Z	Gas deviation factor
T	Temperature

R	Universal gas constant
M_w	Molecular weight
D_H	Hydraulic diameter

A.3 GREEK SYMBOLS

Symbol	Meaning
ρ	Density
μ	Viscosity
σ	Interfacial tension
θ	Inclination with respect to horizontal
ϕ	Azimuth with respect to inlet branch
τ	Shear (τ_w is wall shear, τ_i is interfacial shear)

Appendix B: Solver User Manual

Appendix B provides a sample input file as well as instructions on how to create a new file if necessary. The input file is divided into six sections: junctions, pipes, phases, parameters, report, and options. It should be noted that all titles are written in brackets ([]) and the semicolon character (;) denotes commenting, so anything on a line written after a semicolon is considered to be a comment. The length of spaces between entries is irrelevant. The program allows for entering multiple unit types and boundary conditions.

B.1 Input File

B.1.1 Junctions

```
[JUNCTIONS]
;ID                 Elev            Demand          Pressure        MassFrac2       PressureGuess
 1                  0               3.041           37              0.0026586       37              ;
 2                  5               0               -               1               36              ;
 3                  10              0               -               1               36              ;
 4                  15              0               -               1               36              ;
 5                  20              0               -               1               36              ;
 6                  25              0               -               1               36              ;
 7                  30              0               -               1               36              ;
 8                  35              0               -               1               36              ;
 9                  40              0               -               1               36              ;
 10                 50              0               -               1               36              ;
 11                 60              0               -               1               36              ;
 12                 65              0               -               1               36              ;
 13                 70              0               -               1               36              ;
 14                 75              0               -               1               36              ;
 15                 80              0               -               1               36              ;
 16                 85              0               -               1               36              ;
 17                 90              0               -               1               36              ;
 18                 95              0               -               1               36              ;
 19                 100             -1.7028         -               0.0010445       36              ;
 20                 50              0               -               1               34              ;
 21                 50              0               -               1               34              ;
 22                 50              0               -               1               34              ;
 23                 50              0               -               1               34              ;
 24                 50              0               -               1               34              ;
 25                 50              0               -               1               34              ;
 26                 50              0               -               1               34              ;
 27                 50              0               -               1               34              ;
 28                 50              -1.33791        -               0.004713        34              ;
```

Figure B.1: Junction section

Figure B.1 shows the section of a sample input file for inputting junction information.

The first column is for the junction's ID. This is used in the program to identify the node and to identify it in the graph. It is also the location of the node in the incidence matrix.

The second column is elevation. This is used to calculate the inclination of the pipe connecting two nodes.

The third column is the demand. This is the flow external to the junction, either entering or leaving the network. For multiphase flow, this is a mixture quantity, and can be entered by specifying a mass flow rate, a reference-condition volumetric flow rate, or a standard-conditions volumetric flow rate. The type of demand specified to be specified is denoted in the options section.

The fourth column is the pressure boundary condition. One pressure at one node should be specified. This may be a separator pressure, or it could be at the location of a meter where the pressure is known. Generally speaking, the most downstream pressure, if applicable, should be specified.

The fifth column is the mass fraction or fractional flow of the external flow. Either the mass fraction or the fractional flow may be entered here. It should be noted that the fractional value entered here is for the *lighter* phase.

The sixth column is the pressure guess. Only one pressure guess is needed to populate the network's initial values, but the user may enter pressures at every node if they choose. This override's the program's pressure initialization via the spanning tree.

The following columns are optional and are intended to be used for when the phase-splitting equations are being specified in cases where external boundary conditions are

unknown. If no columns are present after the sixth column, the program assumes that the problem is well-conditioned, and the equations balance the unknowns. The seventh and eighth column (not shown) specifies the azimuth of the branches adjacent to the node. Two azimuths are supplied: the azimuth of the branch and run. These are specified as the azimuth of the 2nd highest and highest link IDs with respect to the link with the lowest ID. For instance, if the branches that are adjacent to a given node are 2, 3, and 5, the azimuths specified are between branches 2-3 and 2-5.

B.1.2 Pipes

```
[PIPES]
;ID    Node1           Node2   Length          Diameter        Roughness       U1Guess         U2Guess         Ph2SatGuess
 1     1               2       5               5               0.00025         1.54            1.4             0.2             ;
 2     2               3       5               5               0.00025         1.54            1.4             0.2             ;
 3     3               4       5               5               0.00025         1.54            1.4             0.2             ;
 4     4               5       5               5               0.00025         1.54            1.4             0.2             ;
 5     5               6       5               5               0.00025         1.54            1.4             0.2             ;
 6     6               7       5               5               0.00025         1.54            1.4             0.2             ;
 7     7               8       5               5               0.00025         1.54            1.4             0.2             ;
 8     8               9       5               5               0.00025         1.54            1.4             0.2             ;
 9     9               10      10              5               0.00025         1.54            1.4             0.2             ;
 10    10              11      10              5               0.00025         1               0.2             0.2             ;
 11    11              12      5               5               0.00025         1               0.2             0.2             ;
 12    12              13      5               5               0.00025         1               0.2             0.2             ;
 13    13              14      5               5               0.00025         1               0.2             0.2             ;
 14    14              15      5               5               0.00025         1               0.2             0.2             ;
 15    15              16      5               5               0.00025         1               0.2             0.2             ;
 16    16              17      5               5               0.00025         1               0.2             0.2             ;
 17    17              18      5               5               0.00025         1               0.2             0.2             ;
 18    18              19      5               5               0.00025         1               0.2             0.2             ;
 19    10              20      10              5               0.00025         1.6             1.6             0.35            ;
 20    20              21      5               5               0.00025         1.6             1.6             0.35            ;
 21    21              22      5               5               0.00025         1.6             1.6             0.35            ;
 22    22              23      5               5               0.00025         1.6             1.6             0.35            ;
 23    23              24      5               5               0.00025         1.6             1.6             0.35            ;
 24    24              25      5               5               0.00025         1.6             1.6             0.35            ;
 25    25              26      5               5               0.00025         1.6             1.6             0.35            ;
 26    26              27      5               5               0.00025         1.6             1.6             0.35            ;
 27    27              28      5               5               0.00025         1.6             1.6             0.35            ;
```

Figure B.2: Pipes section of input file

Figure B.2 shows the pipes section of a sample input file. Here, all relevant pipe parameters are input.

The first column is the pipe's ID. This is used to identify the pipe in the network and to properly place the branch in the incidence matrix.

The second column is the originating node for the branch. As the incidence matrix used in the program is directed, the "Node1" column is the originating node for the pipe.

The third column is the terminating node for the branch. “Node2” is the other node that is connected to the pipe. The first three columns are used to set up the entire incidence matrix and identify the loops in the network.

The fourth column is the length of the pipe.

The fifth column is the pipe’s hydraulic diameter.

The sixth column is the pipe’s hydraulic roughness. This is used to determine the wall shear coefficient (friction factor).

The last three columns are optional, and are used to specify the initial guess when the user wants to explicitly specify the initial guess for certain parameters.

The seventh column is the initial guess for heavier phase’s volume flux (superficial velocity).

The eighth column is the initial guess for lighter phase’s volume flux (superficial velocity).

The ninth column is the initial guess for the lighter phase’s volume fraction.

The tenth column (not pictured) gives the inclination of the branch. This term is optional and the default value of the branch’s inclination is determined from each node’s elevation.

B.1.3 Phases

```
[PHASES]
;ID             Tag             Density         Gravity         Compressibility     Viscosity
 1              WATER           998             1               1E-10               0.000072;
 2              AIR             10              1               1E-7                0.00000012;
```

Figure B.3: Phase section of input file

Figure B.3 gives the phase section of the input file.

The first column identifies the phase. The standard notation is for the first phase to be the heavier one and the second phase to be the lighter.

The second column specifies what kind of phase is identified. Tags can be water, air, oil, gas, and solid.

The third column is the reference density of the phase. For slightly compressible fluids (oil), this is the density at standard conditions. For compressible fluids where an equation of state is used to calculate density. This is the initialized value of density for that phase in the model.

The fourth column specifies the gravity of the phase. For liquids and solids, the reference is water, and for gas, the reference is air. This is mainly used in calculating the gas deviation factor.

The fifth column specifies the compressibility for slightly compressible fluids. Note that this term is only active when the compressibility flag is activated.

The sixth column is the viscosity.

B.1.4 Parameters

```
[PARAMETERS]
 Temperature(K)                294
 yN2(molefrac)                 0.0
 yCO2(molefrac)                0.0
 yH2S(molefrac)                0.0
```

Figure B.4: Parameters section of input file

Figure B.4 gives system parameters of the network. The first line gives the temperature to be used in the gas density calculation. The next three lines give mole fractions of impurities in the gas. These are used in the gas deviation factor calculations.

B.1.5 Report

```
REPORT]
Status                  No
Summary                 Yes
Page                    1
```

Figure B.5: Report section of input file

Figure B.5 gives a sample report section of the input file. The options that can be specified in the report section are:

Report Tag	Options	Explanation
Page	1-255	Optional. Lines per page in output file
Status	No/Yes	Optional. Status updates printed to output file
Summary	No/Yes	Summary of network and parameters printed to output file
Messages	No/Yes	Solver messages printed to output file
Nodes	None/All/<Node#>	Outputs node data to output file. Individual nodes can be output by specifying with numbers separated by commas.
Links	None/All/<Link#>	Outputs branch data to output file. Individual branches can be output by specifying with numbers separated by commas.
File	<filename>	Specifies the output file name.
<Variable>	Below/above/precision <number>	Variable is output to specified to given decimal places. Eg: Pressure above 4 Pressure is output to a minimum 4 decimal points.

Table B.1: Report options in input file

B.1.6 Options

```
[OPTIONS]
 Headloss                D-W
 Trials                  40
 Accuracy                0.001
 CHECKFREQ               2
 MAXCHECK                10
 DAMPLIMIT               0
 Unbalanced              Continue 10
 FFmodel                 WOLGHA
 Compmodel               INCOMP
 GasModel                REAL
 BCReference             MASS

 IUVolflow               GPM
 IUVFlux                 MPS
 IUMassFlow              KGS
 IUPres                  PSI
 IUElev                  CM
 IULength                CM
 IUDiam                  CM
 IURough                 CM
 IUDens                  KGCM
 IUVis                   PAS
 OUMassFlow              KGS
 OUPres                  PSI
 OUVolflow               CMS
 OUVFlux                 MPS
 OUPGradient             psi/ft
 ConvAccel               NO
 ;DontInclude            1
 Phasespliteqn           NO
```

Figure B.6: Options section of input file

Figure B.6 gives a sample options section of the input file.

Report Tag	Options	Explanation
Headloss	D-W	Darcy-Weisbach friction factor used.
Trials	>1	Maximum number of NR iterations
Accuracy	1E-16 - 1E16	Convergence criteria to use.
CHECKFREQ	1-Trials	How often to check for convergence.
MaxCheck	Deprecated	
DampLimit	Deprecated	
Unbalanced	Stop Continue <number>	If maximum trials are exceeded, specifies whether to stop or continue if the convergence criteria is too large. Eg:

		Continue 15

Table B.2: Numerical options

Report Tag	Options	Explanation
FFmodel	Noslip/Wolgha/Butter /Nicklin/SLIPRATIO	Volume fraction – fractional flow relationship to be used. See (Nagoo A. , 2013).
Compmodel	Incompressible/Compressible	Liquid density model to use
Gasmodel	Ideal/Real	Gas model to use
BCreference	Mass/Standard/Reference	External flow rate type. Mass flow rate, standard conditions volumetric flow, reference conditions volumetric flow

Table B.3: Network flow and thermodynamic Options

Report Tag	Options	Explanation
IUVolflow	CMS	Cubic meters per second, m^3/s
	CFS	Cubic feet per second, ft^3/s
	GPM	Gallons per minute, gal/m
	AFD	Acre-feet per day, $acre-ft/d$
	MGD	Million US gallons per day, $MMUSgal/d$
	IMGD	Million imperial gallons per day, $MMIgal/d$
	LPS	Liters per second, ℓ/s
	LPM	Liters per minute, ℓ/m
	CMH	Cubic meters per hour, m^3/h
	CMD	Cubic meters per day, m^3/d
	MLD	Megaliters per day, $M\ell/d$
IUMassflow	KGS	Kilograms per second, kg/s
	KGM	Kilograms per minute, kg/m
	KGD	Kilograms per day, kg/d

	LBS	Pounds per second, lb/s
	LBM	Pounds per minute, lb/m
	LBD	Pounds per day, lb/d
IUPres	PSI	Psi
	KPA	KiloPascals
	PAS	Pascals
	METERS	m
	BAR	bar
IUVFlux	MPS	Meters per second, m/s
	MPM	Meters per minute, m/m
	MPD	Meters per day, m/d
	FPS	Feet per second, ft/s
	FPM	Feet per minute, ft/m
	FPD	Feet per day, ft/d
IUElev	FEET	Feet
	METERS	Meters
	MILES	Miles
	KMS	Kilometers
	INCH	Inches
	CM	centimeters
IUViscos	PAS	Pascal-seconds, $Pa-s$
	CP	Centipoise, cP
IUDensity	KGCM	Kilograms per cubic meter, kg/m^3
	LBCF	Pounds per cubic foot, lb/ft^3
OUPGradient	PSI/FT	Psi per ft, psi/ft
	PA/M	Pascals per meter, Pa/m
	KPA/M	Kilopascals per meter, kPa/m
IULength	Same as IUElev	
IUDiameter	Same as IUElev	
IURough	Same as IUElev	
OUMassFlow	Same as IUMassFlow	
OUPres	Same as IUPres	
OUVolflow	Same as IUVolflow	
OUVFlux	Same as IUVFlux	

Table B.4: Units options

Report Tag	Options	Explanation

ConvAccel	No/Yes	Should convective acceleration be considered?
DontInclude	<LinkID>	Troubleshooting term; only used when loops are present. If solver doesn't converge with default values, enter the branches that you would like to use to select the loops. These branches will be considered the chords in the spanning tree.EG: 1,2,5
Phasespliteqn	No/Yes	Should the phase splitting equation be solve with the other equations present?
MakeInitialGuess	No/Yes	Should solver generate initial guesses (yes) or are initial guesses supplied by the user (no)?
Inclination	Elevation/Inclination	Specifies if branch inclination should be specified from the elevation or inclination.
Nodespliteqn	<NodeID>	Specifies which nodes should have the phase splitting equation specified. Exceptions are thrown when more than three branches are adjacent to a node. EG: 1,2,3

Table B.5: Troubleshooting/Misc. options

B.2 Output File

B.2.1 Output Parameters

```
Page 1                                          Thu Jul 09 09:52:58 2015

**********************************************************************
*                    Branched Fractional Flow                        *
*                      Hydrodynamic Analysis                         *
*                                                                    *
*                         Version 1.1                                *
**********************************************************************


    Input Data File ................... C:\Users\Jeff Stewart\BFF\n
    Number of Junctions................ 4
    Number of Pipes ................... 5
    Headloss Formula .................. Darcy-Weisbach
    Fractional Flow Model.............. Wolgha
    Liquid Density..................... Incomp
    Gas Density Model.................. Real
    Convective Acceleration............ Not included
    Reporting Criteria:
       All Nodes
       All Links

Analysis begun Thu Jul 09 09:52:58 2015

    Maximum Trials .................... 162
    Convergence Error.................. 4.361e+002
```

Figure B.7: Output file parameters

Figure B.7 shows a summary of the output parameters in a given simulation run.

The Headloss option specifies how wall shear to determined (Darcy-Weisbach vs. Hazen Williams). The convective acceleration term says whether or not convective acceleration is included in the simulation.

The maximum trials row tells how many iterations the Newton-Raphson method used in order to solve the system of equations. The convergence error tells the magnitude of the convergence error in the solver. The convergence error is the sum of the differences between the latest iteration and past iteration variable values.

B.2.2 Node Results

Node Results:

Node	Demand kg/s	Pressure psi	MassFrac	Saturation	FracFlow
1	8.0000	350.0000	0.2300	0.9000	0.8817
2	-2.0000	349.9876	0.2300	0.9333	0.8817
3	-4.0000	349.9881	0.2300	0.9333	0.8817
4	-2.0000	349.9876	0.2300	0.9000	0.8817

Figure B.8: Node Results

Figure B.8 shows the results for the nodes in the network simulation. This gives the demand and pressure at each node, as wells as the quality, saturation and fractional flow if there is a demand at a given node.

B.2.3 Link Results

Link Results:

Link	Mass FR kg/s	Pres Loss psi	FricP Loss psi	HydroP Loss psi	ConvP Loss psi	TotalP Grad psi/ft
1	4.7338	0.0124	0.0132	0.0000	-0.0008	0.0001
2	3.2668	0.0119	0.0119	0.0000	-0.0000	0.0001
3	2.4523	-0.0005	0.0011	0.0000	-0.0017	-0.0000
4	0.2817	-0.0000	0.0018	0.0000	-0.0018	-0.0000
5	1.7189	0.0005	0.0011	0.0000	-0.0006	0.0000

Figure B.9: Link Results

Figure B.9 shows the simulation results for all links in the network.

B.2.4 Equation Residuals

Residuals:

Equation	Equation Type	Residual Value
1	"Pressure drop"	-5.5727
2	"Pressure drop"	-0.0879
3	"Pressure drop"	-11.4482
4	"Pressure drop"	-12.4385
5	"Pressure drop"	-4.2485
6	"Phase 1 Density"	0.00e+000
7	"Phase 1 Density"	0.00e+000
8	"Phase 1 Density"	0.00e+000
9	"Phase 1 Density"	0.00e+000
10	"Phase 1 Density"	0.00e+000
11	"Friction factor"	-2.20e-009
12	"Friction factor"	-1.14e-010
13	"Friction factor"	-4.58e-008
14	"Friction factor"	-2.81e-008
15	"Friction factor"	-2.59e-008
16	"Phase 1 MB"	-7.24e-008
17	"Phase 1 MB"	7.18e-007
18	"Phase 1 MB"	2.02e-007

Figure B.10: Equation Residual Results

Figure B.10 gives the equation residuals. Values further away from 0 have more error than values closer to 0. Each equation is in sequential order according to the link and node indices. For example, the fourth pressure drop equation represents the fourth link's pressure drop equation, and the second mass balance equation represents the second node's mass balance equation.

Appendix C: Output Files

C.1 MULTIPHASE NETWORK EXAMPLE

C.1.1 Original Guess

```
**************************************************************
*              Branched Fractional Flow                      *
*               Hydrodynamic Analysis                        *
*                                                            *
*                  Version 1.1                               *
**************************************************************
```

Input Data File ..... C:\Users\Jeff Stewart\BFF\n4b5-2ph_original_guess.inp
Number of Junctions..... 4
Number of Pipes 5
Headloss Formula ..... Darcy-Weisbach
Fractional Flow Model..... Wolgha
Liquid Density..... Incomp
Gas Density Model..... Real
Convective Acceleration..... Not included
Reporting Criteria:
All Nodes
All Links

Maximum Trials 15
Convergence Error..... 4.657e-010

Node Results:

Node	Demand kg/s	Pressure psi	MassFrac	Saturation	FracFlow
1	8.0000	350.0000	0.2300	0.7000	0.8817
2	-2.0000	349.9800	0.2300	0.8000	0.8817
3	-4.0000	349.9787	0.2300	0.8000	0.8817
4	-2.0000	349.9773	0.2300	0.7000	0.8817

Link Results:

Mass FR	Pres Loss	FricP Loss	HydroP Loss	ConvP Loss	TotalP Grad	FricP Grad

Link	kg/s	psi	psi	psi	psi	psi/ft	psi/ft
1	3.8424	0.02	0.02	0	0	0.0061	0.0061
2	4.1576	0.0213	0.0213	0	0	0.0065	0.0065
3	0.4797	0.0013	0.0013	0	0	0.0004	0.0004
4	1.3628	0.0027	0.0027	0	0	0.0008	0.0008
5	0.6372	0.0014	0.0014	0	0	0.0004	0.0004

HydroP Grad psi/ft	ConvP Grad psi/ft	Reynolds #	Ph1 VolFlux m/s	Ph1 Vel m/s	Ph1 Dens kg/m3	Ph2 VolFlux m/s
0	0	9.31E+11	0.2594	1.5777	998	4.9187
0	0	9.49E+11	0.2864	1.6853	998	4.9717
0	0	2.06E+11	0.0256	0.099	998	1.0269
0	0	2.99E+11	0.0973	0.3687	998	1.4193
0	0	2.16E+11	0.0391	0.1453	998	1.0534

Ph2 Vel m/s	Ph2 Dens kg/m3	Mix Dens kg/m3	Slip ratio	Ph2 Sat	Ph2 FracFlow	F-Factor
5.8863	16.4495	177.8038	3.731	0.8356	0.9499	0.007
5.9895	16.4494	183.2509	3.5539	0.8301	0.9455	0.007
1.3846	16.4489	270.0634	13.9898	0.7416	0.9757	0.007
1.9284	16.4489	275.5629	5.2296	0.736	0.9358	0.007
1.441	16.4489	280.4773	9.9142	0.731	0.9642	0.007

Residuals:

Equation	Equation Type	Residual Value
1	"Pressure drop"	4.83e-013
2	"Pressure drop"	9.95e-013
3	"Pressure drop"	1.04e-012
4	"Pressure drop"	7.11e-015
5	"Phase 1 Density"	-8.88e-015
6	"Phase 1 Density"	0.00e+000
7	"Phase 1 Density"	0.00e+000
8	"Phase 1 Density"	0.00e+000
9	"Phase 1 Density"	0.00e+000
10	"Friction factor"	0.00e+000
11	"Friction factor"	-6.07e-018
12	"Friction factor"	4.16e-017

13	"Friction factor"	-1.10e-016
14	"Friction factor"	1.39e-017
15	"Phase 1 MB"	-4.77e-017
16	"Phase 1 MB"	1.78e-015
17	"Phase 1 MB"	-1.62e-014
18	"delP definition"	1.73e-014
19	"delP definition"	0.00e+000
20	"delP definition"	4.66e-010
21	"Given Pressure"	4.66e-010
22	"Loop"	0.00e+000
23	"Loop"	1.78e-014
24	"Phase 2 Loop"	-1.60e-014
25	"Phase 2 Loop"	5.33e-014
26	"Phase 2 Density"	-2.84e-014
27	"Phase 2 Density"	7.11e-015
28	"Phase 2 Density"	0.00e+000
29	"Phase 2 Density"	-7.11e-015
30	"Phase 2 Density"	-3.55e-015
31	"Phase 2 MB"	3.55e-015
32	"Phase 2 MB"	1.33e-015
33	"Phase 2 MB"	2.78e-016
34	"Saturation"	-1.11e-015
35	"Saturation"	-7.77e-016
36	"Saturation"	0.00e+000
37	"Saturation"	-2.63e-014
38	"Saturation"	2.22e-016
39	"Saturation"	-2.55e-015

C.1.2 Low Guess

```
**********************************************************************
*                Branched Fractional Flow                            *
*                 Hydrodynamic Analysis                              *
*                                        *
*                   Version 1.1                  *

**********************************************************************
```

Input Data File ..... C:\Users\Jeff Stewart\BFF\n4b5-2ph_low_guess.inp

Number of Junctions..... 4

Number of Pipes 5

Headloss Formula ..... Darcy-Weisbach
Fractional Flow Model..... Wolgha
Liquid Density..... Incomp
Gas Density Model..... Real
Convective Acceleration..... Not included
Reporting Criteria:
All Nodes
All Links

Maximum Trials 141
Convergence Error..... 1.691e+004

Node Results:

Node	Demand kg/s	Pressure psi	MassFrac	Saturation	FracFlow
1	8.0000	350.0000	0.2300	0.9000	0.8817
2	-2.0000	349.9843	0.2300	0.9333	0.8817
3	-4.0000	349.9924	0.2300	0.9333	0.8817
4	-2.0000	350.0004	0.2300	0.9000	0.8817

Link	Mass FR kg/s	Pres Loss psi	FricP Loss psi	HydroP Loss psi	ConvP Loss psi	TotalP Grad psi/ft	FricP Grad psi/ft
1	7.1358	0.0157	0.0165	0	-0.0008	0.0002	0.0002
2	0.8843	0.0076	0.0079	0	-0.0002	0.0001	0.0001
3	3.2884	-0.0081	0.002	0	-0.01	-0.0001	0
4	1.8583	-0.016	0.0026	0	-0.0186	-0.0002	0
5	0.1627	-0.008	0.0005	0	-0.0085	-0.0001	0

HydroP Grad psi/ft	ConvP Grad psi/ft	Reynolds #	Ph1 VolFlux m/s	Ph1 Vel m/s	Ph1 Dens kg/m3	Ph2 VolFlux m/s
0	0	5.32E+11	0.0838	0.2363	998	0.8625
0	0	3.68E+11	0.0008	0.0026	998	0.6872
0	-0.0001	2.09E+11	0.0415	0.0756	998	0.2232
0	-0.0002	2.69E+11	0.0211	0.0341	998	0.2652
0	-0.0001	1.12E+11	0	0	998	0.1356

Ph2 Vel	Ph2 Dens	Mix Dens	Slip ratio	Ph2 Sat	Ph2 FracFlow	F-Factor

m/s	kg/m3	kg/m3				
1.3364	16.4496	364.4949	5.6563	0.6454	0.9115	0.007
1.0091	16.4498	329.4861	394.1765	0.6811	0.9988	0.007
0.4947	16.4494	555.201	6.5467	0.4511	0.8433	0.007
0.6998	16.4496	625.9956	20.5491	0.379	0.9262	0.007
0.3135	16.4498	573.506	5.04E+15	0.4325	1	0.007

Residuals:

Equation	Equation Type	Residual Value
1	"Pressure drop"	-5.3317
2	"Pressure drop"	-1.6274
3	"Pressure drop"	-69.1099
4	"Pressure drop"	-128.4517
5	"Pressure drop"	-58.6803
6	"Phase 1 Density"	0.00e+000
7	"Phase 1 Density"	0.00e+000
8	"Phase 1 Density"	0.00e+000
9	"Phase 1 Density"	0.00e+000
10	"Phase 1 Density"	0.00e+000
11	"Friction factor"	-5.92e-009
12	"Friction factor"	-8.46e-009
13	"Friction factor"	-5.98e-008
14	"Friction factor"	-5.20e-008
15	"Friction factor"	-1.70e-007
16	"Phase 1 MB"	1.22e-007
17	"Phase 1 MB"	-5.99e-007
18	"Phase 1 MB"	-1.63e-007
19	"delP definition"	0.0371
20	"delP definition"	0.0099
21	"delP definition"	0.0152
22	"Given Pressure"	0.00e+000
23	"Loop"	4.46e-008
24	"Loop"	-4.46e-008
25	"Phase 2 Loop"	8.9209
26	"Phase 2 Loop"	-15.8714
27	"Phase 2 Density"	-5.01e-006
28	"Phase 2 Density"	-4.79e-006
29	"Phase 2 Density"	-2.48e-006
30	"Phase 2 Density"	-3.01e-006
31	"Phase 2 Density"	-2.98e-006

32	"Phase 2 MB"	-0.0201
33	"Phase 2 MB"	-0.0110
34	"Phase 2 MB"	0.0100
35	"Saturation"	0.0231
36	"Saturation"	0.0170
37	"Saturation"	0.1002
38	"Saturation"	-0.0262
39	"Saturation"	0.1472

C.1.3 High Guess

```
**********************************************************************
*              Branched Fractional Flow              *
*               Hydrodynamic Analysis                *
*                                    *
*                Version 1.1                *

**********************************************************************
```

Input Data File ..... C:\Users\Jeff Stewart\BFF\n4b5-2ph_high_guess.inp
Number of Junctions..... 4
Number of Pipes 5
Headloss Formula ..... Darcy-Weisbach
Fractional Flow Model..... Wolgha
Liquid Density..... Incomp
Gas Density Model..... Real
Convective Acceleration..... Not included
Reporting Criteria:
All Nodes
All Links

Maximum Trials 162
Convergence Error..... 4.361e+002

Node Results:

Node	Demand kg/s	Pressure psi	MassFrac	Saturation	FracFlow
1	8.0000	350.0000	0.2300	0.9000	0.8817
2	-2.0000	349.9876	0.2300	0.9333	0.8817

3	-4.0000	349.9881	0.2300	0.9333	0.8817
4	-2.0000	349.9876	0.2300	0.9000	0.8817

Link	Mass FR kg/s	Pres Loss psi	FricP Loss psi	HydroP Loss psi	ConvP Loss psi	TotalP Grad psi/ft	FricP Grad psi/ft
1	4.7338	0.0124	0.0132	0	-0.0008	0.0001	0.0001
2	3.2668	0.0119	0.0119	0	0	0.0001	0.0001
3	2.4523	-0.0005	0.0011	0	-0.0017	0	0
4	0.2817	0	0.0018	0	-0.0018	0	0
5	1.7189	0.0005	0.0011	0	-0.0006	0	0

HydroP Grad psi/ft	ConvP Grad psi/ft	Reynolds #	Ph1 VolFlux m/s	Ph1 Vel m/s	Ph1 Dens kg/m3	Ph2 VolFlux m/s
0	0	4.79E+11	0.0524	0.1373	998	0.7671
0	0	4.53E+11	0.0322	0.0892	998	0.7663
0	0	2.09E+11	0.0312	0.045	998	0.1494
0	0	2.24E+11	0	0	998	0.2347
0	0	2.29E+11	0.0211	0.0287	998	0.149

Ph2 Vel m/s	Ph2 Dens kg/m3	Mix Dens kg/m3	Slip ratio	Ph2 Sat	Ph2 FracFlow	F-Factor
1.2402	16.4497	390.8635	9.035	0.6185	0.9361	0.007
1.1996	16.4497	371.0006	13.4447	0.6388	0.9596	0.007
0.4873	16.4494	696.9969	10.8245	0.3067	0.8272	0.007
0.6294	16.4494	631.9303	6.63E+14	0.373	1	0.007
0.5673	16.4494	740.1413	19.7771	0.2627	0.8757	0.007

Residuals:

Equation	Equation Type	Residual Value
1	"Pressure drop"	-5.5727
2	"Pressure drop"	-0.0879
3	"Pressure drop"	-11.4482
4	"Pressure drop"	-12.4385
5	"Pressure drop"	-4.2485
6	"Phase 1 Density"	0.00e+000
7	"Phase 1 Density"	0.00e+000

8	"Phase 1 Density"	0.00e+000
9	"Phase 1 Density"	0.00e+000
10	"Phase 1 Density"	0.00e+000
11	"Friction factor"	-2.20e-009
12	"Friction factor"	-1.14e-010
13	"Friction factor"	-4.58e-008
14	"Friction factor"	-2.81e-008
15	"Friction factor"	-2.59e-008
16	"Phase 1 MB"	-7.24e-008
17	"Phase 1 MB"	7.18e-007
18	"Phase 1 MB"	2.02e-007
19	"delP definition"	0.0037
20	"delP definition"	0.0015
21	"delP definition"	0.0156
22	"Given Pressure"	0.00e+000
23	"Loop"	1.49e-013
24	"Loop"	5.41e-009
25	"Phase 2 Loop"	-0.5615
26	"Phase 2 Loop"	0.4421
27	"Phase 2 Density"	-1.99e-007
28	"Phase 2 Density"	-1.70e-007
29	"Phase 2 Density"	-9.39e-008
30	"Phase 2 Density"	-1.04e-007
31	"Phase 2 Density"	-9.80e-008
32	"Phase 2 MB"	-0.0005
33	"Phase 2 MB"	-0.0003
34	"Phase 2 MB"	0.0003
35	"Saturation"	-0.0020
36	"Saturation"	3.00e-005
37	"Saturation"	0.0310
38	"Saturation"	-0.0357
39	"Saturation"	-0.0187

C.1.4 Mixed Guess

```
*****************************************************************
*              Branched Fractional Flow                 *
*               Hydrodynamic Analysis                   *
*                                    *
*               Version 1.1                  *

*****************************************************************
```

Input Data File ..... C:\Users\Jeff Stewart\BFF\n4b5-2ph_mixed_guess.inp
Number of Junctions..... 4
Number of Pipes 5
Headloss Formula ..... Darcy-Weisbach
Fractional Flow Model..... Wolgha
Liquid Density..... Incomp
Gas Density Model..... Real
Convective Acceleration..... Not included
Reporting Criteria:
All Nodes
All Links

Maximum Trials 33
Convergence Error..... 2.132e+001

Node Results:

Node	Demand kg/s	Pressure psi	MassFrac	Saturation	FracFlow
1	8.0000	350.0000	0.2300	0.9000	0.8817
2	-2.0000	350.1979	0.2300	0.9333	0.8817
3	-4.0000	350.3270	0.2300	0.9333	0.8817
4	-2.0000	350.5763	0.2300	0.9000	0.8817

Link	Mass FR kg/s	Pres Loss psi	FricP Loss psi	HydroP Loss psi	ConvP Loss psi	TotalP Grad psi/ft	FricP Grad psi/ft
1	9.5014	-0.1979	0.0505	0	-0.2484	-0.002	0.0005
2	-1.4526	-0.327	-0.0089	0	-0.3181	-0.0033	-0.0001
3	11.4814	-0.1291	0.1259	0	-0.2551	-0.0013	0.0013
4	-3.8777	-0.3784	-0.0331	0	-0.3453	-0.0038	-0.0003
5	6.0282	-0.2492	0.0438	0	-0.2931	-0.0025	0.0004

HydroP Grad psi/ft	ConvP Grad psi/ft	Reynolds #	Ph1 VolFlux m/s	Ph1 Vel m/s	Ph1 Dens kg/m3	Ph2 VolFlux m/s
0	-0.0025	1.29E+12	0.0846	0.7893	998	2.783
0	-0.0032	5.43E+11	0	0	998	-1.2096
0	-0.0026	2.27E+12	0.0764	0.9011	998	4.928

0	-0.0035	1.11E+12	-0.0129	-0.1374	998	-2.4433
0	-0.0029	1.36E+12	0.0341	0.4127	998	2.9508

Ph2 Vel m/s	Ph2 Dens kg/m3	Mix Dens kg/m3	Slip ratio	Ph2 Sat	Ph2 FracFlow	F-Factor
3.1171	16.4548	121.6544	3.9494	0.8928	0.9705	0.007
-1.3541	16.458	121.2157	1.87E+10	0.8933	1	0.007
5.3844	16.4629	99.6596	5.9756	0.9152	0.9847	0.007
-2.6971	16.4689	108.8299	19.6256	0.9059	0.9947	0.007
3.2164	16.4721	97.524	7.7934	0.9174	0.9886	0.007

Residuals:

Equation	Equation Type	Residual Value
1	"Pressure drop"	-1712.4343
2	"Pressure drop"	-2193.0831
3	"Pressure drop"	-1758.7259
4	"Pressure drop"	-2380.4285
5	"Pressure drop"	-2020.7457
6	"Phase 1 Density"	0.00e+000
7	"Phase 1 Density"	0.00e+000
8	"Phase 1 Density"	0.00e+000
9	"Phase 1 Density"	0.00e+000
10	"Phase 1 Density"	0.00e+000
11	"Friction factor"	-1.15e-008
12	"Friction factor"	-3.12e-008
13	"Friction factor"	-4.42e-009
14	"Friction factor"	6.87e-012
15	"Friction factor"	-1.04e-008
16	"Phase 1 MB"	1.78e-007
17	"Phase 1 MB"	4.58e-007
18	"Phase 1 MB"	-1.68e-007
19	"delP definition"	0.0117
20	"delP definition"	0.0019
21	"delP definition"	-0.0295
22	"Given Pressure"	0.00e+000
23	"Loop"	9.09e-013
24	"Loop"	-6.82e-013
25	"Phase 2 Loop"	-18.9446

26	"Phase 2 Loop"	-9.1688
27	"Phase 2 Density"	-2.28e-005
28	"Phase 2 Density"	-6.76e-005
29	"Phase 2 Density"	-3.18e-005
30	"Phase 2 Density"	-0.0001
31	"Phase 2 Density"	-8.19e-005
32	"Phase 2 MB"	-0.0489
33	"Phase 2 MB"	-0.1022
34	"Phase 2 MB"	0.0006
35	"Saturation"	0.0736
36	"Saturation"	-0.1067
37	"Saturation"	0.0318
38	"Saturation"	-0.0941
39	"Saturation"	0.0605

Appendix D: Model Training Set

					Inlet							
le Name (25 characters	Phase	Phase	rho1	rho2	u1	u2	sat2	diam	incl	pres	flow regime	
Abu.Exp.8	Liquid	Gas	995.9245	1.177892	0.602	1.998	NA	0.0254	0	202650	SLUG	
Abu.Exp.9	Liquid	Gas	995.6817	1.177401	0.657	1.985	NA	0.0254	0	202650	SLUG	
Abu.Exp.10	Liquid	Gas	995.4601	1.178579	0.712	1.979	NA	0.0254	0	202650	SLUG	
Bak.Sep.E1.5	Liquid	Gas	797	1.4	0.07	5.1	NA	0.0381	0	120000	Stratified	
Bak.Sep.E1.6	Liquid	Gas	797	1.4	0.07	5.1	NA	0.0381	0	120000	Stratified	
Bak.Sep.E2.20	Liquid	Gas	797	1.4	0.18	3.3	NA	0.0381	0	120000	Slug	
Els.Two.S4-1	Liquid	Gas	998	1.787	0.0403	0.5	NA	0.0378	0	252325	Stratified	
Els.Two.S4-2	Liquid	Gas	998	1.787	0.0404	0.5	NA	0.0378	0	252325	Stratified	
Els.Two.W2-7	Liquid	Gas	998	1.787	0.0403	10.04	NA	0.0378	0	252325	Wavy	
Els.Two.A1-1	Liquid	Gas	998	1.787	0.0027	40.01	NA	0.0378	0	252325	Annular	
Wre.Geo.B1-44	Liquid	Gas	998	1.17	0.31	4	NA	0.127	0	206325	Stratified	
Sim.Two.5-5	Liquid	Gas	998	1.787	0.0095	4.4	NA	0.0381	0	252325	Stratified-wavy	
Sim.Two.23-4	Liquid	Gas	998	1.787	0.0095	18.3	NA	0.0381	0	251325	Semi-annular	
Sim.Two.24-1	Liquid	Gas	998	1.787	0.002	40.2	NA	0.0381	0	251325	Annular	
Sab.Pha.D1-45	Liquid	Gas	998	2.001844	2.717621	13.68529	NA	0.0381	0	170762.5	Slug	
Hwa.Stu.E1-46	Liquid	Gas	998	1.650253	1.326494	1.966198	0.54233	0.0381	0	141000	Stratified	
Azz.Spl.A2-1	Liquid	Gas	998	1.198343	0.02	21	NA	0.125	90	253312.5	Annular	
Azz.Spl.A2-2	Liquid	Gas	998	1.198343	0.02	21	NA	0.125	90	253312.5	Annular	
Mak.Spl.R1-1	Liquid	Gas	998	1.692937	0.11	10.8	NA	0.005	90	140000	Annular-Churn	
Mak.Spl.R6-8	Liquid	Gas	998	1.692738	0.02	17.27	NA	0.005	90	140000	Annular-Churn	
Mak.Spl.R7-1	Liquid	Gas	998	1.685945	0.25	2.9	NA	0.005	90	140000	Slug	
Pand.Liq.Std.2-9	Liquid	Liquid	1000	787	0.17	0.05	NA	0.0254	0	115100	Stratified	
Pand.Liq.Std.5-13	Liquid	Liquid	1000	787	0.56	0.71	NA	0.0254	0	115100	Stratified-Wavy	
Pand.Liq.Std.8-7	Liquid	Liquid	1000	787	0.9	0.05	NA	0.0254	0	115100	Plug	
Pand.Liq.Pres.1-15	Liquid	Liquid	1000	787	0.07	0.05	NA	0.0254	0	115100	Stratified	
Pand.Liq.Pres.1-16	Liquid	Liquid	1000	787	0.07	0.05	NA	0.0254	0	135800	Stratified	
Pand.Liq.Pres.2-27	Liquid	Liquid	1000	787	0.28	0.05	NA	0.0254	0	135800	Stratified-Wavy	
Fun.Two.Slip-1	Liquid	Gas	998	1.697653	6.836	1.308	0.153	0.05	90	264779.6	0	
Fun.Two.Slip-2	Liquid	Gas	998	1.697653	3.445	1.382	0.276	0.05	90	264779.6	0	
Fun.Two.Slip-3	Liquid	Gas	998	1.697653	3.057	1.774	0.347	0.05	90	264779.6	0	
Fun.Two.Slip-4	Liquid	Gas	998	1.697653	2.569	2.437	0.442	0.05	90	264779.6	0	
Fun.Two.Slip-5	Liquid	Gas	998	1.697653	1.926	2.862	0.548	0.05	90	264779.6	0	
Fun.Two.Slip-6	Liquid	Gas	998	1.697653	6.836	1.308	0.153	0.05	90	264779.6	0	
Fun.Two.Slip-7	Liquid	Gas	998	1.697653	3.445	1.382	0.276	0.05	90	264779.6	0	
Fun.Two.Slip-8	Liquid	Gas	998	1.697653	3.057	1.774	0.347	0.05	90	264779.6	0	
Fun.Two.Slip-9	Liquid	Gas	998	1.697653	2.569	2.437	0.442	0.05	90	264779.6	0	
Fun.Two.Slip-10	Liquid	Gas	998	1.697653	1.926	2.862	0.548	0.05	90	264779.6	0	
Rie.Two.Run-186-85	Liquid	Gas	996.3772	12.06427	1.03	14.73	NA	0.05	0	1000000	0	
Rie.Two.Run-187-86	Liquid	Gas	998.6272	11.86622	1.1	15.07	NA	0.05	0	990000	0	
Rie.Two.Run-37-129	Liquid	Gas	996.0458	9.971322	4.22	10.41	NA	0.05	0	826000	0	

				Branch						Outlet				
	u1	u2	sat2	diam	incl	az	pres_r	u1	u2	sat2	diam	incl	az	pres_rev
	0.3507	0.367986	NA	0.0254	0	90	202210	0.251303	1.627443	NA	0.0254	0	-90	201410
	0.361746	0.199427	NA	0.0254	0	90	202417	0.295256	1.784203	NA	0.0254	0	-90	202155
	0.394804	0.192612	NA	0.0254	0	90	202537	0.317199	1.784264	NA	0.0254	0	-90	202175
	0.001321	0.877122	NA	0.0381	90	90	120000	0.065151	3.94705	NA	0.0381	90	90	120000
	0.00055	4.448263	NA	0.0381	90	90	120000	0.066802	0.501213	NA	0.0381	90	90	120000
	0.134595	2.819322	NA	0.0381	90	90	120000	0.053046	0.563864	NA	0.0381	90	90	120000
	0.0403	0.5	NA	0.0378	-90	90	252325	0	0	NA	0.0378	0	90	252325
	0.021156	0.5	NA	0.0378	-90	90	252325	0.019244	0	NA	0.0378	0	90	252325
	0.014481	8.087272	NA	0.0378	-90	90	251352.7	0.014656	8.184929	NA	0.0378	0	90	251352.1
	0.0027	40.01	NA	0.0378	-90	90	249742	0	0	NA	0.0378	0	90	251929.2
	0.017222	1.2	NA	0.0762	0	90	206325	0.3038	3.568	NA	0.127	0	0	206325
	0.027182	17.58513	NA	0.01905	0	90	251945	0.002704	0.003717	NA	0.0381	0	0	252325
	0.018183	92.75348	NA	0.00785	0	90	241261	0.008728	14.36391	NA	0.0381	0	0	251451
	0.003721	22.26253	NA	0.00785	0	90	250705	0.001842	39.25527	NA	0.0381	0	0	251425
	0.802192	7.832788	NA	0.0381	0	90	170762.5	1.916746	2.531013	NA	0.0381	0	0	170762.5
	0.250321	1.65319	NA	0.0381	0	90	140800	1.076174	0.312689	NA	0.0381	0	0	141000
	0.004	8.4	NA	0.125	0	90	253312.5	0.016	12.6	0	0.125	90	0	253312.5
	0.0062	9.45	NA	0.125	0	90	253312.5	0.0138	11.55	0	0.125	90	0	253312.5
	0.045316	3.820613	NA	0.005	0	90	140000	0.07022	6.798886	0	0.005	90	0	140000
	0.019596	9.327003	NA	0.005	0	90	140000	0	7.912909	0	0.005	90	0	140000
	0.257965	2.9	NA	0.005	0	90	140000	0	0	0	0.005	90	0	140000
	0.169573	0.05	NA	0.0254	0	90	115100	0.000427	0	0	0.0254	0	0	115100
	0.486797	0.529696	NA	0.0254	0	90	115100	0.073203	0.180304	0	0.0254	0	0	115100
	0.840001	0.049938	NA	0.0254	0	90	115100	0.059999	6.21E-05	0	0.0254	0	0	115100
	0.066048	0.046174	NA	0.0254	0	90	115100	0.003952	0.003826	0	0.0254	0	0	115100
	0.069088	0.046239	NA	0.0254	0	90	135800	0.000912	0.003761	0	0.0254	0	0	135800
	0.27851	0.04928	NA	0.0254	0	90	135800	0.00149	0.00072	0	0.0254	0	0	135800
	2.047	0.59	0.218	0.05	0	90	264779.6	4.79	0.745	0.13	0.05	90	0	264779.6
	1.053	0.689	0.386	0.05	0	90	264779.6	2.414	0.636	0.213	0.05	90	0	264779.6
	0.95	0.1296	0.537	0.05	0	90	264779.6	2.107	0.516	0.196	0.05	90	0	264779.6
	0.875	1.895	0.65	0.05	0	90	264779.6	1.681	0.503	0.211	0.05	90	0	264779.6
	0.588	2.112	0.737	0.05	0	90	264779.6	1.338	0.837	0.354	0.05	90	0	264779.6
	4.149	1.325	0.23	0.025	0	90	264779.6	5.799	1.047	0.154	0.05	90	0	264779.6
	1.821	2.044	0.498	0.025	0	90	264779.6	2.989	0.855	0.23	0.05	90	0	264779.6
	1.837	3.075	0.582	0.025	0	90	264779.6	2.598	1.086	0.281	0.05	90	0	264779.6
	1.705	4.777	0.685	0.025	0	90	264779.6	2.129	1.256	0.348	0.05	90	0	264779.6
	1.13	5.777	0.764	0.025	0	90	264779.6	1.643	1.611	0.468	0.05	90	0	264779.6
	0.188109	4.474238	NA	0.05	0	90	1000000	0.841832	10.26057	0	0.05	0	0	1000000
	0.228983	5.537066	NA	0.05	0	90	990000	0.871099	9.526049	0	0.05	0	0	990000
	1.017179	8.15535	NA	0.05	0	90	826000	3.202306	2.254957	0	0.05	0	0	826000

Appendix E: Raw Data

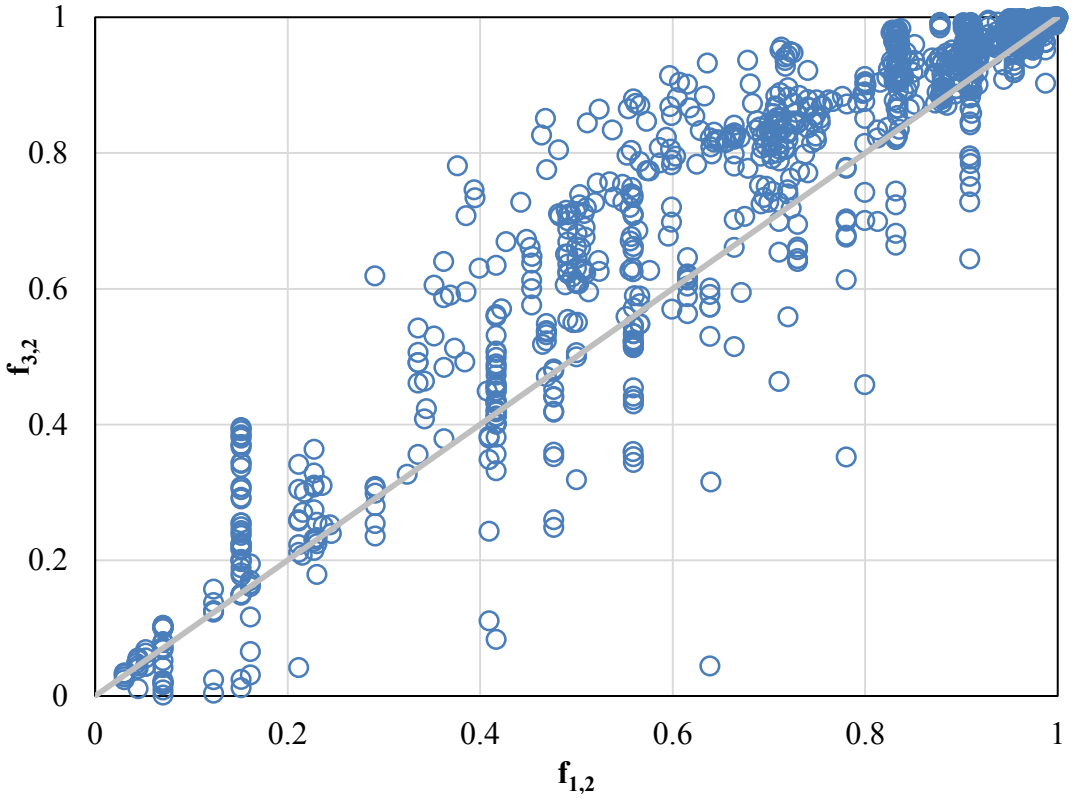

Figure E.1: Fractional flow at inlet versus fractional flow at branch for a horizontal side-branch configuration. Points are experimental data from various studies (Riemann, Brinkmann, & Domanski, 1988) (Lahey & Hwang, A Study on Phase Separation Phenomena in Branching Conduits, 1986) (Pandey, Gupta, Chakrabarti, Das, & Ray, 2006) (Nasr-El-Din, Masliyah, & Afacan, 1989) (Conte, 2001) (Wren, 2001) (Walters, Soliman, & Sims, 1998) (Saba & Lahey, Phase Separation Phenomena in Branching Conduits, 1981) . The unit slope line is the equal splitting line.

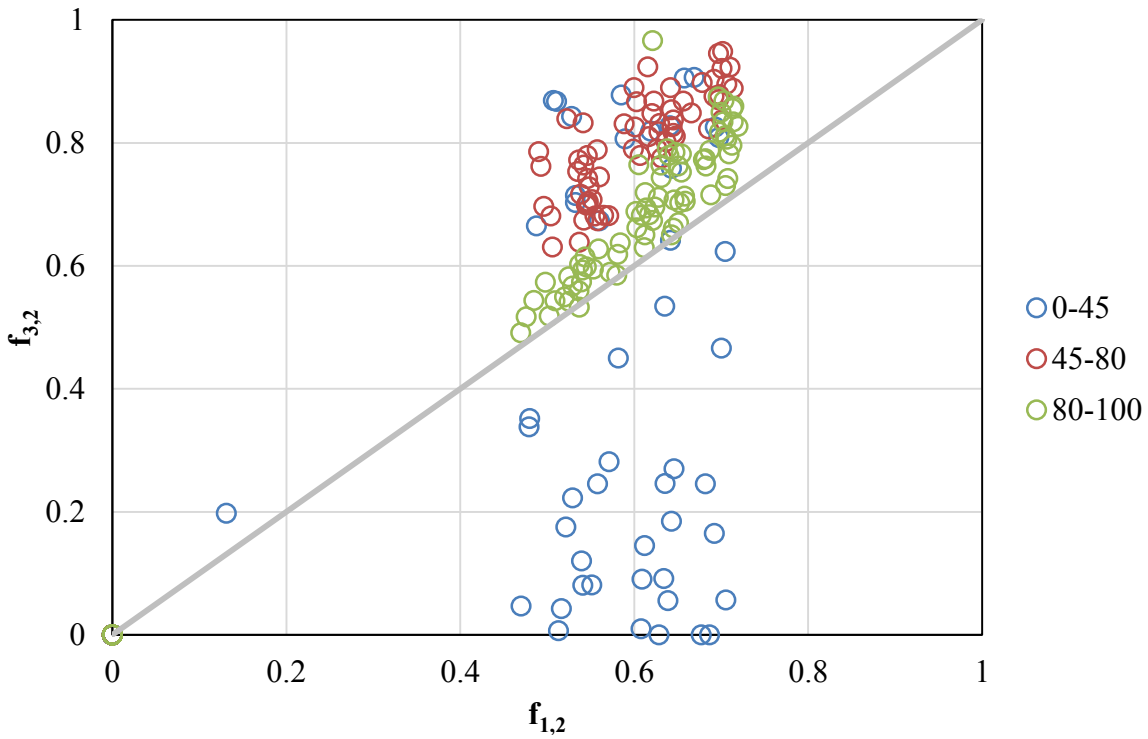

Figure E.2: Fractional flow at inlet versus fractional flow at branch for a horizontal side-branch configuration with a 45° azimuth. Points are experimental data from Lahey & Hwang at different takeoffs (Lahey & Hwang, A Study on Phase Separation Phenomena in Branching Conduits, 1986). The unit slope line is the equal splitting line.

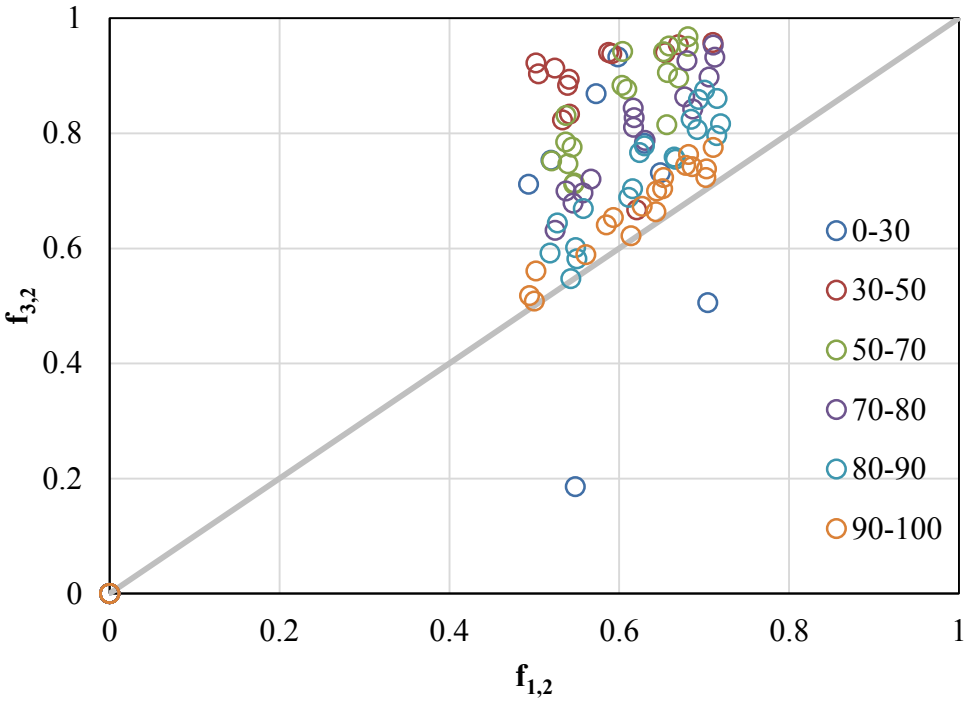

Figure E.3: Fractional flow at inlet versus fractional flow at branch for a horizontal side-branch configuration with a 135° azimuth. Points are experimental data from Lahey & Hwang at different takeoffs (Lahey & Hwang, A Study on Phase Separation Phenomena in Branching Conduits, 1986). The unit slope line is the equal splitting line.

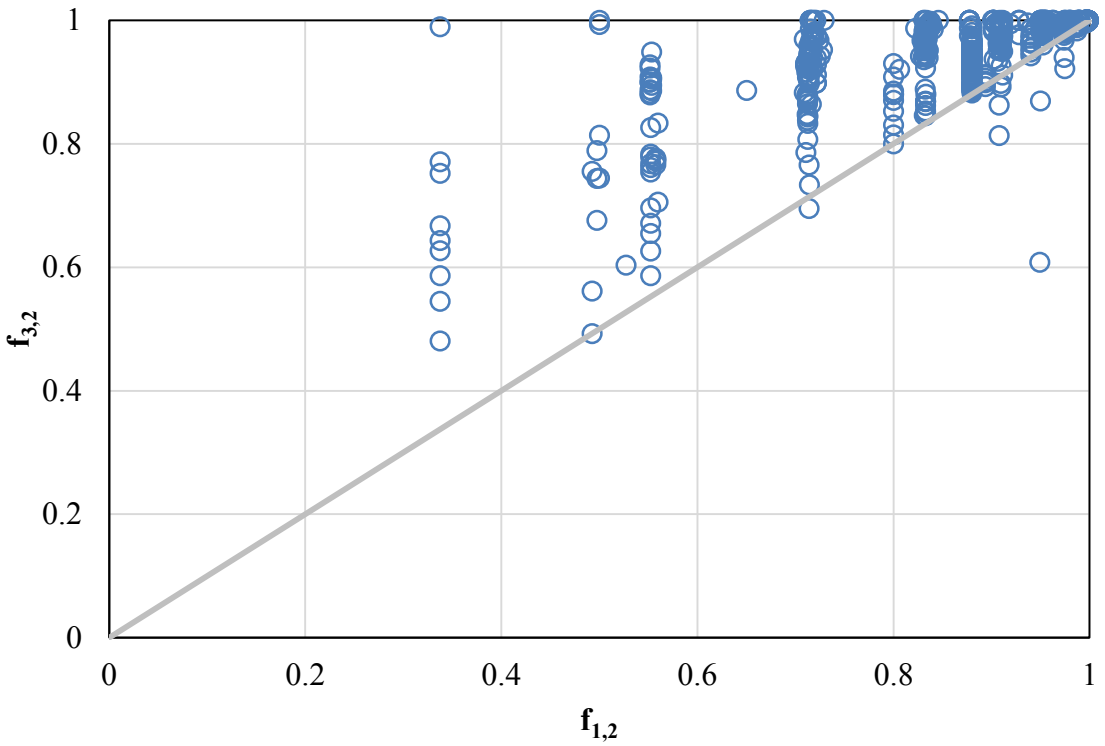

Figure E.4: Fractional flow at inlet versus fractional flow at branch for a vertical side-branch configuration. Points are experimental data from various studies (Riemann, Brinkmann, & Domanski, 1988) (Nasr-El-Din, Masliyah, & Afacan, 1989) (Wren, 2001) . The unit slope line is the equal splitting line.

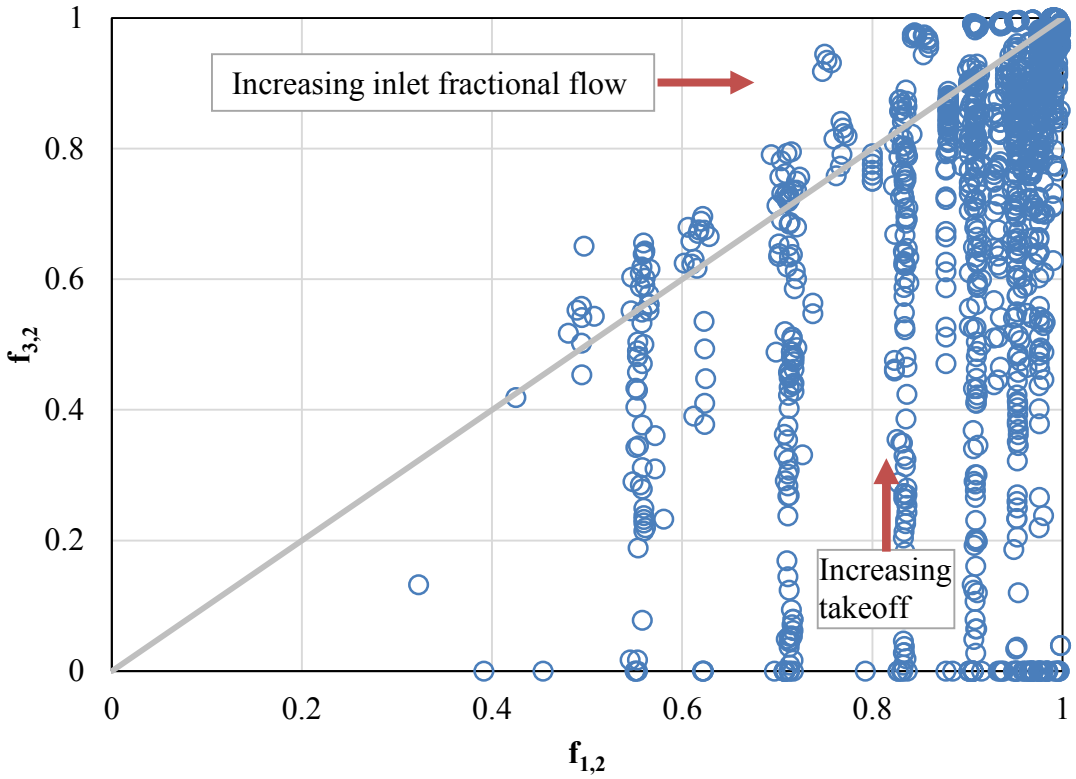

Figure E.5: Fractional flow at inlet versus fractional flow at branch for a downward vertical side-branch configuration. Points are experimental data from various studies (Riemann, Brinkmann, & Domanski, 1988) (Wren, 2001) (Baker, 2003). The unit slope line is the equal splitting line. The scatter seen in the data below the equal split line are due to other differences in the inlet conditions (flow rates, pressures, etc.) and takeoff.

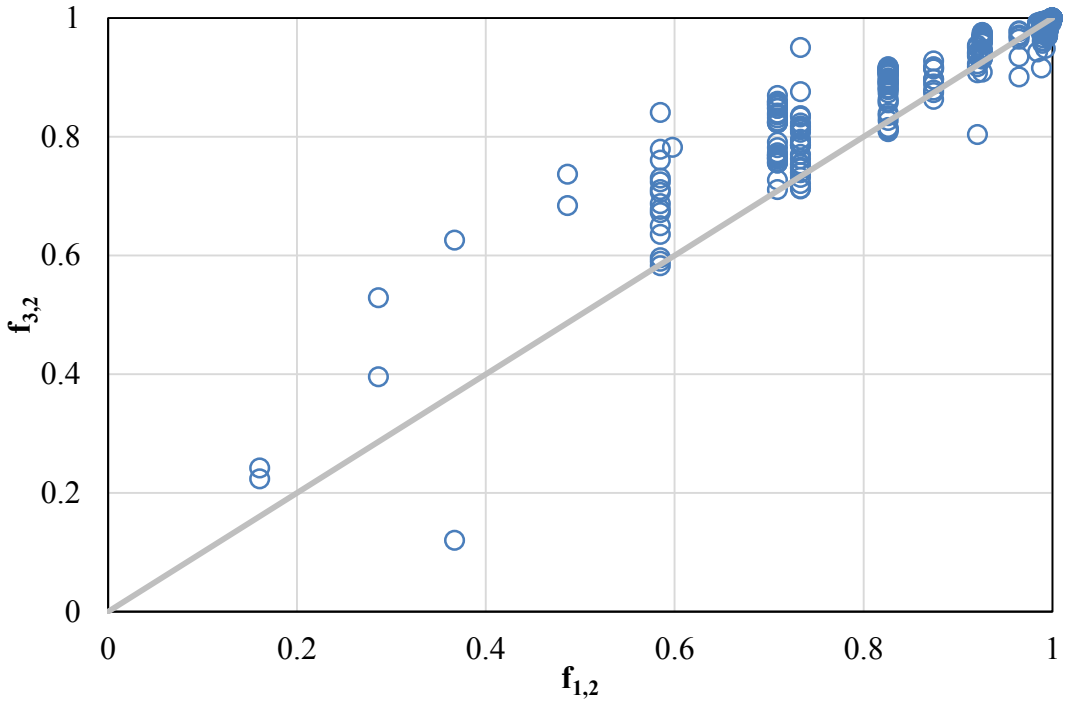

Figure E.6: Fractional flow at inlet versus branch, with example data taken from vertical inlet, horizontal side-branch junctions. Experimental data collected from published articles (Conte, 2001) (Mak, Omebere-Iyari, & Azzopardi, 2006) (Azzopardi, The Split of Vertical Annualar Flow at a Large Diameter T Junction, 1994) (Davis & Fungtamasan, 1990). Columns of data represent data at different mass takeoffs.

References

Abbeel, P. (2012, August). *Nonlinear Optimization for Optimal Control*. Retrieved May 19, 2015, from UC Berkeley EECS: http://www.cs.berkeley.edu/~pabbeel/cs287-fa12/slides/NonlinearOptimizationForOptimalControl.pdf

Abu-Mulaweh, H., Al-Halhouli, A., Hammad, H., & al., e. (2008). Experimental apparatus for measurements of two-phase slug flow pressure drop in a T-junction. *International Journal of Mechanical Engineering Education, 36*(3), 184-192.

Arirachakaran, S. (1990). Two-Phase flow splitting phenomenon at a regular horizontal side-arm tee. *PhD Thesis*.

Armijo, L. (1966). Minimization of functions having Lipschitz continuous first partial derivatives. *Pacific J. Math., 16*(1), 1-3.

Azzopardi, B. (1986). Two Phase Flow in Junctions. *Encyclopedia of Fluid Mechanics*, 677-713.

Azzopardi, B. (1994). The Split of Vertical Annualar Flow at a Large Diameter T Junction. *International Journal of Multiphase Flow, 20*(6), 1071-1083.

Azzopardi, B. (2000). Phase Separation at T Junctions. *Multphase Science and Technology, 11*, 229-329.

Azzopardi, B., & Baker, S. (1981). Two-phase flow in a 'T' junction. The effect of flow pattern in vertical upflow. *Atomic Energy Research Establishment*, 10174.

Azzopardi, B., & Hervieu, E. (1994). Phase Separation at Junctions. *Multiphase Science and Technology, 8*, 645-714.

Azzopardi, B., & Whalley, P. (1982). The Effect of Flow Patterns on Two-Phase Flow in a 'T' Junction. *International Journal of Multiphase Flow, 8*(5).

Baker, G. (2003). *Separation and control of gas-liquid flows at horizontal T-junctions.* Nottingham: University of Nottingham.

Bird, R., Stewart, W., & Lightfoot, E. (2007). *Transport Phenomena: Second Edition.* New York: John Wiley & Sons, Inc.

Brooks, C., Hibiki, T., & Ishii, M. (2012). Interfacial drag force in one-dimensional two-fluid model. *Progress in Nuclear Energy*, 57-68.

Conte, G. (2001). *An experimental study for the characterisation of gas/liquid flow splitting at T-junctions.* Nottingham: University of Nottingham.

Davis, M., & Fungtamasan, B. (1990). Two-Phase Flow through Pipe Branch Junctions. *International Journal of Multiphase Flow, 16*(5), 799-817.

Dence, T. (1997). Cubics, chaos, and Newton's Method. *Mathematical Gazette, 81*, 403-408.

Dolan, A., & Aldous, J. (1993). *Networks and Algorithms: an introductory approach.* Chichester: John Wiley & Sons.

Dolan, A., & Aldous, J. (1993). *Networks and Algorithms: An Introductory Approach.* West Sussex: John Wiley & Sons.

Dranchuk, P., & Abu-Kassem, J. (1975). Calculation of Z-Factors for Natural Gases Using Equations of State. *Journal of Canadian Petroleum Technology*, 34-6.

El-Shaboury, Soliman, H., & Sims, G. (2007). Two-Phase flow in horizontal equal-sided imacting tee junction. *International Journal of Multiphase Flow, 33*, 411-31.

Greyvenstein, G., & Laurie, D. (1994). A Segregated CFD Approach to Pipe Network Analysis. *International Journal for Numerical Methods in Engineering*, 3685-705.

Hankinson, R., Thomas, L., & Phillips, K. (1969). Predict Natural Gas Properties. *Hydrocarbons Processing*, 106-8.

Hannah, K. (1964). Transient flow of gas; a special report on the pipeline research project NX-37. *American Gas Association*.

Issa, R., & Oliveira, P. (1993). Numerical Prediction of Phase Separation in Two-Phase Flow Through T-Junctions. *Computers Fluids*, 347-72.

Jeppson, R. W. (1976). *Analysis of Flow in Pipe Networks.* Ann Arbor: Ann Arbor Science Publishers, Inc.

Kalcach-Navarro, S., Lee, S., Lahey, R., & Drew, D. (1990). The prediction of phase separation in a branching conduit using a three-dimensional two-fluid model. *Multiphase Transport and Particulate Phenomena, 1*.

Katsaounis, A. (1987). Flow Pattern and Pressure Drop in Tees. *Chemical Engineering Communications, 54*, 119-38.

Kawahara, A., Sadatomi, M., Matsuo, H., & al., e. (2011). Investigation of Characteristics of Gas-Liquid Two-Phase Flows in a Rectangular Microchannel with Return Bends. *Joint Fluids Engineering Conference*, (pp. 1-11).

Kokal, S. (1989). *An experimental study of two-phase flow in slightly inclined pipes.* Calgary: University of Calgary.

Koretsky, M. (2004). *Engineering and Chemical Thermodynamics.* Hoboken: John Wiley & Sons, Inc.

Lahey, R. (1986). Current Understanding of Phase Separation Mechanisms in Branching Conduits. *Nuclear Engineering and Design, 95*, 145-161.

Lahey, R., & Hwang, S. (1986). A Study on Phase Separation Phenomena in Branching Conduits. *PhD Thesis*.

Lahey, R., Soliman, H., & Hwang, S. (1989). Phase separation in impacting wyes and tees. *International Journal of Multiphase Flow, 15*(6), 965-75.

Lemonnier, H., & Hervieu, E. (1991). Theoretical modeling and experimental investigation of single-phase and two-phase flow division at a tee-junction. *Nuclear Engineering and Design*, 201-13.

Lemonnier, H., & Hervieu, E. (1991). Theoretical modelling and experimental investigation of single-phase and two-phase flow division at a tee-junction. *Nuclear Engineering and Design, 125*, 201-213.

Mak, C., Omebere-Iyari, N., & Azzopardi, B. (2006). The split of vertical two-phase flow at a small diameter T-junction. *Chemical Engineering Science, 61*, 6261-6272.

Mucharam, Leksono, & Adewumi, M. (1990). A Compositional Two-Phase Flow Model for Analyzing and Designing Complex Pipeline Network Systems. *Society of Petroleum Engineers, 90*(18), 1-16.

Muller, U., & Riemann, J. (1991). Redistribution of Two-Phase Flow in Branching Conduits: A Survey. *1st International Conference on Multiphase Flows.* Tsukuba, Japan.

Nagoo, A. (2013). *Pipe Fractional Flow Theory - Principles and Applications.* The University of Texas at Austin.

Nagoo, A. S. (2003). *Analysis of Steady and Quasi-Steady Gas Flows in Complex Pipe Network Topology.* University Park: Pennsylvania State University.

Nasr-El-Din, H., Masliyah, J., & Afacan, A. (1989). Solids Segregation in Slurry Flow through a T-Junction With a Horizontal Approach. *International Journal of Multiphase Flow, 15*(4), 659-671.

Pan, L., He, H., Ju, P., Hibiki, T., & Ishii, M. (2015). The influences of gas–liquid interfacial properties on interfacial shear. *International Journal of Heat and Mass Transfer, 89*, 1172-83.

Pandey, S., Gupta, A., Chakrabarti, D., Das, G., & Ray, S. (2006). Liquid–Liquid Two Phase Flow Through a Horizontal T-Junction. *Chemical Engineering Research and Design, 84*(A10), 895-904.

Popp, M., & Sallet, D. (1983). Experimental investigation of one- and two-phase flow through a tee-junction. *International Conference on Physical Modeling of Multiphase Flow.* Coventry, England.

Press, W. H. (2002). *Numerical Recipes in C++, second edition.* Cambridge: Cambridge University Press.

Riemann, J., Brinkmann, H., & Domanski, R. (1988). Gas-Liquid Flow in Dividing Tee-Juncitons with a Horizontal Inlet and Different Branch Orientations and Diameters. *PhD Thesis*.

Riemann, J., Brinkmann, H., & Domanski, R. (1988). *Gas-Liquid Flow in Dividing Tee-Junctions with a Horizontal Inlet and Different Branch Orientations and Diameters.* Thesis, Technical University of Warsaw, Institut für Reaktorbauelemente, Warsaw.

Saba, N., & Lahey, R. (1981). Phase Separation Phenomena in Branching Conduits. *PhD Thesis*.

Saba, N., & Lahey, R. (1984). The Analysis of Phase Separation Phenomena in Branching Conduits. *International Journal of Multiphase Flow, 10*(1), 1-20.

Saleh, J. (2002). *Fluid Flow Handbook.* McGraw-Hill.

Seeger, W., Reimann, J., & Muller, U. (1985). Two-Phase Flow in a T-Junction with a Horizontal Inlet, Part I: Phase Separation. *International Journal of Multiphase Flow*, 575-585.

Shoham, O. B., & Taitel, Y. (1987). Two-Phase Flow Splitting in a Tee Junction--Experiment and Modeling. *Chemical Engineering Science, 42*(11), 2667-76.

Shoham, O., Ashton, P., & Penmatcha, V. (1996). Two-Phase Stratified Flow Splitting at a T-Junction with an Inclined Branch Arm. *International Journal of Multiphase Flow, 22*(6), 1105-22.

Smoglie, C., & Reimann, J. (1983). Flow Through a Small Pipe at the Top of a Large Pipe with Stratified Flow. *Annual Meeting of the European Two-Phase flow Group.* Zurich.

Smoglie, C., Reimann, J., & Muller, U. (1986). Two-Phase Flow Thorugh Small breaks in a Horizontal Pipe with Stratified Flow. *International Journal of Multiphase Flow, 12*, 609-26.

Walters, L., Soliman, H., & Sims, G. (1998). Two-phase pressure drop and phase distribution at reduced tee junctions. *International Journal of Multiphase Flow, 24*(5), 775-792.

Woerheide, E., & Stoy, J. R. (1998). *United States of America Patent No. US5709468 A.*

Woldesemayat, M., & Ghajar, A. (2007). Comparison of void fraction correlations for different flow patterns in horizontal and upward inclined pipes. *International Journal of Multiphase Flow, 33*, 347-70.

Wood, D., & Charles, C. (1972). Hydraulic Network Analysis Using Linear Theory. *J. Hydraulics Division*(HY7), 1157-1170.

Wren, E. (2001). *Geometric effects on phase split at a large diameter T-junction.* Nottingham: University of Nottingham.

Zetzmann, K. (1982). *Phasenseparation und Druckfall in Zweiphasen Durchstromten Vertikalen Rohrabzweigungen.* Hannover: University of Hannover.